ABSTRACT

Title of Document: IMPACTS OF SATELLITE-DERIVED FRACTIONAL SNOW-COVERED AREA OBSERVATIONS ON OPERATIONAL STREAMFLOW PREDICTIONS VIA DIRECT INSERTION

Stacie M. Bender, Master of Science, 2013

Directed By: Dr. Kaye L. Brubaker, Department of Civil and Environmental Engineering

Snowmelt is a primary driver of spring and early summer streamflow in the western United States. Improved predictions of snowmelt-driven streamflow benefit a wide variety of users. In this study, the snow model used in the National Weather Service's hydrologic operations, SNOW17, is run with and without consideration of fractional snow covered area (fSCA) observations from the National Aeronautics and Space Administration's MODerate Resolution Imaging Spectroradiometer (MODIS). Because computationally frugal methods are desirable in an operational environment, the updating scheme evaluated is a simple direct insertion method. Resulting predictions of snowmelt-driven streamflow for water years 2000 to 2010 are compared to observed flow and a control simulation (using the model without snow cover input). Results indicate that use of MODIS fSCA in SNOW17, with no adjustments, via direct insertion, degrades the streamflow predictions, compared to control simulations. Future research directions include advanced data assimilation and use of different snow models.

IMPACTS OF SATELLITE-DERIVED FRACTIONAL SNOW-COVERED AREA OBSERVATIONS ON OPERATIONAL STREAMFLOW PREDICTIONS VIA DIRECT INSERTION

By

Stacie M. Bender

Thesis submitted to the Faculty of the Graduate School of the
University of Maryland, College Park, in partial fulfillment
of the requirements for the degree of

Master of Science
2013

Advisory Committee:
Dr. Kaye L. Brubaker, Chair
Dr. Barton Forman
Dr. Richard McCuen

DEDICATION

To Mr. Swob and Mrs. Elliott, for their support of science education in public schools, and for being two of the people in my life who taught me to ask “Why?”.

ACKNOWLEDGEMENTS

Thank you to my family and friends, for their support and eternal patience while I worked full-time and pursued a graduate degree on a part-time basis. Your support during the entire process, especially during the most sleep-deprived moments, is a major reason why I survived the experience and lived to tell about it. I feel very fortunate that most people in my life have an astronomical amount of patience.

Thank you to the advisors, professors, and teachers who have encouraged me as a student (both as a kid and as an adult) and in the lifelong learning process. Your influence, input, encouragement, and flexibility were additional reasons that I finished this degree, despite juggling many (sometimes far too many) commitments at once.

Thank you to the curious scientists I have met throughout my career, for the privilege of collaboration, for enduring seemingly endless science and modeling questions, and for making sure I retained as much sanity as possible (often through therapeutic happy hour sessions) while I pursued a graduate degree on a part-time basis.

TABLE OF CONTENTS

LIST OF TABLES

LIST OF FIGURES

LIST OF ACRONYMS

ADC – Areal Depletion Curve

AESC – Areal Extent of Snow Cover (model estimate of snow cover extent)

AMSR-E - Advanced Microwave Scanning Radiometer for EOS

AOR – area of responsibility

CBRFC – Colorado Basin River Forecast Center, part of the NWS

CHPS – Community Hydrologic Prediction System

COOP – COoperative Observer Program (NWS)

CRB – Colorado River Basin

DA – Data Assimilation

DEM – Digital Elevation Model

EnKF – Ensemble Kalman Filter

EOS – Earth Observing System, a program of polar orbiters managed by NASA

ETM+ - Enhanced Thematic Mapper Plus

EUMETSAT - European Organisation for the Exploitation of Meteorological Satellites

fSCA – Fractional Snow Covered Area (observed snow cover extent)

GB – Great Basin

GDAL – Geospatial Data Abstraction Library

GOES - Geostationary Operational Environmental Satellite

IFOV – Instantaneous Field of View

JPL – Jet Propulsion Laboratory

JPSS – Joint Polar Satellite System

KF – Kalman Filter

LDCM – Landsat Data Continuity Mission

MAT – Mean Areal Temperature

MAP – Mean Areal Precipitation

MCM - Million Cubic Meters

ME – Mean Error

MODIS - Moderate Resolution Imaging Spectroradiometer

MODDRFS - MODIS Dust Radiative Forcing in Snow

MODSCAG - MODIS Snow-Covered Area and Grain size

MRLC - Multi-Resolution Land Characteristics Consortium

NASA - National Aeronautics and Space Administration

NDSI – normalized difference snow index

NDVI – normalized difference vegetation index

NIR – Near-infrared portion of the electromagnetic spectrum

NLCD – National Land Cover Database

NOAA - National Oceanic and Atmospheric Administration

NPOESS - National Polar-orbiting Operational Environmental Satellite System

NPP - NPOESS Preparatory Project

NRCS – National Resources Conservation Service

NWS – National Weather Service

OHD – Office of Hydrologic Development, part of the NWS

OLI – Operational Land Imager (instrument on LDCM satellite)

R&D – Research and Development

RFC – River Forecast Center, part of the NWS

RMSE – Root Mean Squared Error

RMSE-SS – Root Mean Squared Error Skill Score

Q_o – Observed Streamflow

Q_p – Predicted Streamflow

PB – Percent Bias

SAC-SMA – Sacramento Soil Moisture Accounting Model

SCA – Snow-Covered Area

SMADA - Snow Modeling and Data Assimilation Testbed

SS – Skill Score

SNOTEL – SNOpack TELemetry

SNOW17 – snow accumulation and ablation model used by NWS RFCs

SWE – Snow Water Equivalent

SWIR – Shortwave infrared portion of the electromagnetic spectrum

TM – Thematic Mapper

USGS – United States Geological Survey

VIIRS - Visible Infrared Imager Radiometer Suite

WBWCD - Weber Basin Water Conservancy District

WFO – Weather Forecast Office (part of the NWS)

VZ – Visible portion of the electromagnetic spectrum

CHAPTER 1: INTRODUCTION

1.1 PROBLEM STATEMENT

1.1.1 Importance of the Snowpack in Mountainous Regions

Snowmelt is vital to the hydrologic cycle of the mountainous western United States. Mountain snowpacks provide the majority of annual streamflow for many locations in the western U.S., where snowfall can make up 60% or more of the annual precipitation (Serreze et al., 1999). Snowmelt represents about two-thirds (60-70%) of the total annual runoff in the western U.S. (Daly et al., 2000). Snowpack meltwater serves as a water source for municipalities, agriculture interests, recreation interests, hydropower interests, and others.

As the snowfall accumulates and the snowpack builds throughout the winter, the snowpack acts as a reservoir, the contents of which are released in an uncontrolled fashion during the melt season. While the snowpack serves multiple uses and benefits many people in the semiarid regions of the western U.S., its uncontrolled melt can sometimes cause problems. The rapid melt of an abnormally extensive snowpack can easily cause high streamflow and flooding, threatening life and property. Seasonal runoff volumes, upon which many groups depend for domestic water, irrigation, and recreation, may impact reservoir operations and water deliveries. Informative snowmelt-driven streamflow prediction is a critical

component of the management of snowmelt-driven rivers, and improved predictions can assist in flood planning (Adams et al., 2004).

1.1.2 Modeling and Predicting Snowmelt

Because the semiarid regions of the western U.S. rely so heavily on the mountain snowpack, operational government agencies and research groups have developed a wide variety of models to predict snowpack conditions and subsequent snowmelt-driven streamflow. Operationally, these models are used to make two types of predictions: (1) short-term deterministic prediction of streamflow, including flood flows if conditions warrant, out to one to two weeks, and (2) longer-term probabilistic prediction of seasonal runoff volumes that a snowpack may yield, with lead times of several months. These agencies and groups use a variety of tools, including process-based models (which include explicit representation of the equations that describe physical processes), simpler conceptual models, traditional statistical regression, and more advanced probabilistic methods, such as ensemble prediction.

Slow, orderly snowmelt is manageable for hydrologic forecasters and modelers, water users, and emergency managers. However, when snowmelt is abnormally rapid and intense, the snowpack sheds its water volume in a short period of time. In these situations, dangerous flooding can occur, especially if the snow water equivalent (SWE) of the snowpack is large at the start of the rapid melt event. Disaster responses to and management of the flows resulting from such a snowmelt event can be challenging for emergency managers and reservoir operators. During

abnormally rapid snowmelt events, the risks of damage are highest; thus, improvements in hydrologic predictions of these events would be most beneficial to users.

Seasonal runoff volumes yielded by a snowpack may also be difficult to predict by a conceptual model if conditions deviate far from those represented by the historical period used to calibrate the model. Achieving improvements in hydrologic prediction at all lead times, irrespective of the type of forecast (deterministic vs. probabilistic, daily flows vs. seasonal runoff volumes) can be challenging.

Accurate model representation of snowmelt events in mountainous areas can be difficult to achieve for snowpack models, even those that contain detailed representation of snowpack physics. Difficulties arise because mountainous watersheds and the conditions within them are spatially diverse. Accurate representation of orographic precipitation, areal extent of snow cover, the distribution of SWE, terrain characteristics, and land cover, all of which play roles in determining the rate of snowmelt, is a challenging aspect of hydrologic modeling. Uncertainties are inherent in input data as well as in model structure.

Several methods have been proposed as ways to improve snow representation in models and, in turn, prediction of snowmelt-driven streamflow. Some examples include the incorporation of in-situ or satellite-derived snow observations into hydrologic models, the use of distributed hydrologic models at fine scales, and the use of full energy balance snow models within a hydrologic modeling framework.

1.1.3 Importance of Accurate Snow-Covered Area Estimates in Models

Successful modeling and prediction of snowmelt-driven flow in mountainous watersheds depends, in part, on accurate model representation of the portion of a watershed that is covered with snow . Hydrologic models that contain a snow module consider snow-covered area (SCA) in snowmelt calculations, particularly if only a portion of a watershed area is estimated to be snow-covered. Even if the snow model embedded within a hydrologic model is capable of accurately predicting snowmelt, application of snowpack calculations over an improper areal extent of snow cover (AESC) can lead to inaccurate estimates of the snowpack characteristics and, in turn, inaccurate predictions of subsequent meltwater runoff (Turpin et al, 1999).

Additionally, in the melt computations of many models, including SNOW17, the snow model used in this study, the snowmelt volume for a single timestep is initially computed assuming the modeled area is completely snow covered (AESC = 1.0 or 100%). If the modeled area is not fully covered by snow, the melt volume initially computed under the assumption of 100% snow cover is multiplied by an AESC value of less than 100% before being passed to subsequent processing in the model (such as routines that route the liquid meltwater through the snowpack).

1.2 MOTIVATION FOR THE STUDY AND RESEARCH NEEDS

There are two primary motivations for this study: (1) the need for a detailed analysis of the impacts, related to direct insertion (DI) of satellite-derived snow cover observations into a hydrologic model, on snowmelt-driven streamflow predictions in

an operational National Weather Service (NWS) environment, and (2) contribution to a snow modeling and data assimilation testbed being built by an operational agency in cooperation with research and development (R&D) partners. Both motivations are tightly tied to the need for operational NWS hydrologists to understand the fine details of the hydrologic modeling systems they use, particularly as they begin to explore alternative forecasting and modeling techniques.

Improvement in model estimates of snowpack properties can lead to improved flow prediction for snowmelt-driven streams and rivers in certain cases. Specifically, preliminary results of quantitative assimilation of satellite-derived fSCA observations show that assimilation of such observations has potential to improve streamflow simulations, at least during the spring and early summer, as the snowpack declines and bare ground is exposed (Clark et al., 2006).

However, quantitative ways of incorporating satellite-derived snow cover information into hydrologic models have not yet been heavily tested in-house at an operational venue such as a National Weather Service River Forecast Center (RFC). The conditions under which research and operational environments carry out their studies can be drastically different. In an operational environment, certain constraints on the modeling and prediction processes exist. For example, input data must be reliably available and, due to computing power limitations, the use of complex models and data assimilation schemes in real time is usually prohibitive. These constraints are closely tied to the need for reliability and timeliness in operational procedures (Nester et al., 2012).

Liu et al. (2012) state that the application of advanced hydrologic data assimilation as a tool for incorporating information from observations into the RFC forecasting process is currently limited in operational environments. For the operational environments of NWS RFCs, this limitation is due partially to the fact that the RFC forecast process is very subjective, relying heavily on human forecasters to make updates and adjustments to model states. The framework of the NWS RFC environment does not yet lend itself to advanced objective, quantitative methods of updating model conditions.

Despite the constraints of the operational NWS RFC environment, the NWS Colorado Basin River Forecast Center (CBRFC) is investigating ways in which satellite-derived snow cover observations may potentially improve predictions made by CBRFC, both with the current forecasting and modeling system and with systems that may be developed in the future. The simple direct insertion (DI) method is one quantitative method that *is* currently available to NWS RFCs, and it is used in this study.

This study examines one of the ways in which model snowpack estimates can be modified by inclusion of moderately high-resolution observations of snow cover extent in an operational model. Specifically, the study aims to quantitatively evaluate for a headwater basin, in terms of streamflow, the impacts of objective use of satellite-derived snow cover observations on operational streamflow predictions. The simple DI method is the focus of this study, since parsimonious methods are preferred in an operational environment (assuming their use results in improvement to the predictions). Direct insertion is a conceptually and computationally simple method to

implement, and it can be tested in-house at NWS RFCs with the current implementation of the modeling system.

The DI technique is tested *without* recalibration of model parameters and with no adjustment of the satellite-derived data for vegetation or transformation to a SNOW17-equivalent snow cover value. In 2011 and 2012, CBRFC recalibrated, for each area that it models (~1100), the SNOW17 model parameters using the 1981-2010 historical period. Currently, personnel time and resources at CBRFC are not available for an additional round of CBRFC-area-wide model parameter recalibration. If it can provide a benefit in terms of streamflow prediction, the inclusion of observed fSCA via DI without complete recalibration of all modeled points, would be the preferred option.

Some RFCs have begun to pursue more active collaboration and experimentation with each other and with the research and academic communities. The RFCs have traditionally been end users of products and methods developed by academia and the hydrologic research arm of the NWS, the Office of Hydrologic Development (OHD). However, the role of the RFC in NWS hydrology is changing as some RFCs become more actively involved in the R&D process. That both sides (operations and research) understand the unique characteristics of each other's environments and share information across traditional barriers is becoming increasingly important. The National Research Council (2012) heavily emphasizes the need for active collaboration among operational, research, and academic groups, despite barriers that have prevented such collaborations in the past. Liu et al. (2012) also emphasize collaboration among modelers, data assimilation (DA) researchers,

and operational forecasters as a cost-effective way to transition new techniques from the research community into operations.

To facilitate collaboration among the RFCs and R&D groups, the CBRFC, in Salt Lake City, Utah, is building modeling testbeds. These testbeds focus on different sub-fields of hydrology. One example is the CBRFC Snow Modeling and Data Assimilation (SMADA) Testbed (http://www.cbrfc.noaa.gov/testbeds/smada/) that focuses on snow hydrology. An additional testbed, the Seasonal to Year-2 Climate and Streamflow Forecast Testbed (http://www.cbrfc.noaa.gov/testbeds/si_y2/index.php) focuses on-long range streamflow forecasting techniques that use climate information (Wood and Werner, 2011). The testbeds are venues intended as a way to encourage and enable collaborations between the RFC and its research partners. Wood and Werner (2011) promote testbeds that partner operational RFC staff with external research groups as ways to:

- Build knowledge and skills of RFC staff, particularly operational forecasters
- Educate external partners about operational forecasting and its constraints
- Ensure that research efforts intended to improve operational forecasting are properly focused and evaluated.

Via these testbeds, CBRFC provides data sets for targeted watersheds within the Colorado River basin and the eastern Great Basin to external collaborators for experimentation. In the case of the snow hydrology SMADA testbed, the targeted

watersheds are high elevation headwater basins that are snow-dominated with few (if any) diversions or reservoirs; in the case of the climate and streamflow testbed, the targets are important as inflow sources to major reservoirs in the western United States.

The watersheds currently included in the SMADA testbed are headwater basins for which (mostly) natural flow is measured by a United States Geological Survey (USGS) stream gage. For many watersheds that the CBRFC models, the lack of flow observations for diversions and reservoirs, especially in near real time, limits CBRFC's ability to compute naturalized flow, which in turn affects the accuracy of snow and soil moisture model parameters derived in the calibration process. Impacts of diversions and reservoirs must be estimated because the availability of flow observations for the diversions and reservoirs is delayed, sometimes up to a year if the flows are available only as part of a water year report. To reduce (though certainly not eliminate) uncertainty in the streamflow observations used to evaluate experiments, and in an attempt to limit sources of uncertainty to techniques or models being tested, the initial focus of the SMADA testbed is on watersheds that (1) are minimally impacted by diversions and reservoirs and (2) have a reliable record of streamflows measured by the USGS at their outlet. Additional watersheds may be eventually included in the SMADA testbed if diversion and reservoir flow data of acceptable quality become available.

The testbeds will also serve as repositories for research results generated by studies focusing on the targeted watersheds. As the testbeds evolve, additional uses

will be identified. This study serves as one of the pilot projects in the snow modeling and data assimilation testbed (SMADA) currently being built at CBRFC.

1.3 PRINCIPAL GOALS AND OBJECTIVES

This research investigates how streamflow predictions are affected by fractional snow-covered area (fSCA) observations and a simple technique (DI) for incorporating information from such snow observations into a hydrologic model, subject to operational constraints. There are four principal goals/objectives of this study:

1. Perform an experiment with the simple DI technique and investigate benefits and drawbacks to incorporation of fSCA derived from NASA's MODerate-resolution Imaging Spectroradiometer (MODIS) into a hydrologic model, subject to realistic, operational constraints

2. Determine if DI without recalibration of the operational models can provide any benefit (since a major recalibration of model parameters was recently completed at CBRFC and personnel time for recalibration is currently limited)

3. Determine the compatibility of observed fSCA from MODIS with snow covered area as it is represented in SNOW17

4. Contribute to the snow modeling and data assimilation testbed being constructed at the CBRFC.

The objectives and goals for this study are tied closely to the concerns of an operational environment, which requires efficient and reliable data processing and modeling. This study examines ways in which remotely sensed fSCA data currently considered experimental by the NWS RFCs might be used in an operational environment. The study also investigates ways in which the operational modeling process must adapt in order to take advantage of the benefits that the remote sending data may offer.

To fulfill these objectives, the current CBRFC operational system is examined. Processing scripts and codes are set up in order to ingest MODIS-derived fSCA observations into the CBRFC data processing stream. A retrospective experiment using the fSCA observations via DI is run for a headwater basin. The study period includes water years 2000 to 2010, which are common to the MODIS period of record (2000 to present) and the historical period used in the most recent round of model calibration at CBRFC (WY1981 to WY2010). Streamflow predictions from the DI simulations are compared to simulations from the operational configuration where snow cover is completely model-driven and no satellite-derived fSCA values are used. Differences between streamflow predictions generated by the operational (control) and experimental DI systems are investigated, with a special focus on determining which system produces more accurate simulations under which conditions. Finally, recommendations for future studies are made, given the results of this study.

The results of this study will be contributed to the collaborative snow modeling and data assimilation testbed being constructed at the CBRFC. One of the

intents of this testbed is to serve as a repository for snow hydrology research that is focused on CBRFC's models and the modeling challenges that CBRFC faces.

1.4 POTENTIAL IMPLICATIONS

The results of this study will help CBRFC decide if quantitative use of MODIS-derived fSCA observations, at least in terms of the DI technique, should be pursued in the RFC's operational procedures. Depending on the outcome, pursuit of further collaborative research and experiments by the RFC and its research partners may be desirable before operational implementation is considered in any further capacity. Alternatively, if results are positive, indicating that adoption of quantitative use of satellite-derived fSCA observations in the operational environment should be actively pursued, then the results of this study could be used as a starting point to further investigation of operational implementation.

1.5 OUTLINE OF REPORT

This thesis is organized into several chapters. This chapter introduces issues related to hydrologic prediction of snowmelt-driven flows in mountain watersheds. The second chapter describes how fSCA is observed by satellite-borne instrumentation in mountainous watersheds (including the benefits and limitations of such observations). It also describes how snow is represented in the hydrologic modeling system used operationally by the NWS and introduces the DI technique used in the study. The third chapter describes the watershed used in the DI

simulations in this study. The fourth chapter describes the methods of the experimental DI simulations. The fifth chapter discusses results of the retrospective experiment. The last (sixth) chapter reports conclusions and recommends directions for further study.

CHAPTER 2: BACKGROUND/LITERATURE REVIEW

2.1 INTRODUCTION

This chapter presents overviews of several topics. Satellite-derived fractional snow-covered area observations at sub-1 km resolution are discussed. The mathematical representation of the snowpack in the NWS operational hydrologic modeling system is described. The last section describes how satellite-derived fSCA observations have been used to update model estimates of the snowpack.

2.2 SATELLITE OBSERVATIONS OF SNOW COVER

2.2.1 Benefits of Satellite-derived fSCA Observations

Over the past several decades, the CBRFC has used observations (precipitation, snow water equivalent, etc.) from point station networks such as the National Resources Conservation Service (NRCS) SNOwpack TELemetry) (SNOTEL) network and the NWS's Cooperative Observer Program (COOP) to monitor snow conditions. Despite the important contribution of these observing networks to hydrologic forecasting, the point station networks lack the extensive spatial coverage that remote sensing data can provide, especially in mountainous terrain.

Regular detailed observations of snow cover on a large scale are nearly impossible to obtain for watersheds in mountainous regions via ground field surveys.

Rough terrain, inaccessibility, and concerns for crew safety in such terrain prohibit surveys on a large scale. Ground surveys are also intensely time-consuming.

Instead, hydrologic modelers, snow hydrologists, and others who need observations of snow cover extent in mountainous watersheds often turn to remote sensing from aircraft or satellite platforms as an attractive alternative. Snow cover observations derived from satellites are particularly useful, as they can sample the spatial distribution of snow cover within basins regularly and quickly, without endangering a field crew or incurring the cost of aircraft use. Figure 1 compares the area covered by a sample gridded satellite-derived snow cover product and SNOTEL stations in southwestern Colorado. Use of data from satellites (such as MODIS-derived data sets used in this study), in combination with point observations, can provide a more complete picture of snowpack conditions.

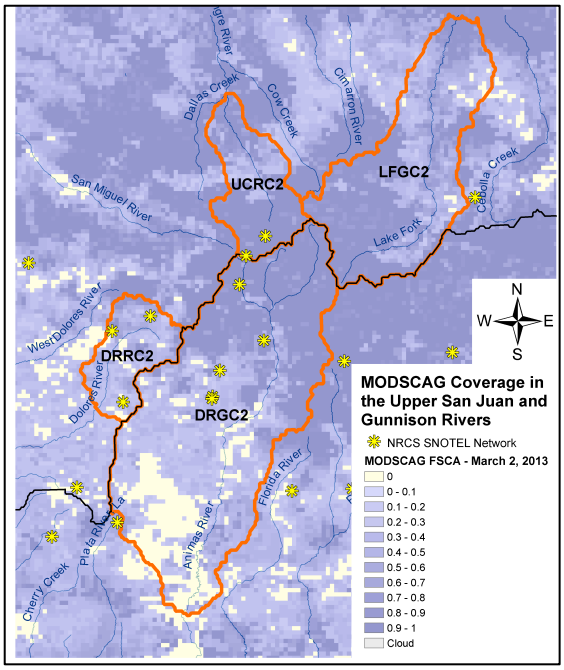

Figure 1: Spatial extent of remotely sensed snow cover data and SNOTEL station locations in southwestern Colorado, with NWS IDs of basins

Satellite-derived snow cover observations at appropriate spatiotemporal resolution can help forecasters and modelers identify and monitor abnormalities in the snow cover extent, especially when such snow cover may lead to floods if it melts rapidly. Snow cover observations of adequate resolution for mountain basins are potentially available from several satellite-borne instruments. For this study of a small mountain watershed, "adequate resolution" is defined spatially as sub-1 km resolution and temporally as daily acquisitions.

Spatial resolution of less than 1 km is desirable because mountainous terrain is very diverse; observations of higher resolution are better able to represent conditions with mountainous watersheds. The watershed that is the focus of this study is a small mountainous basin (area of ~400 square kilometers), so use of the highest number of pixels possible to represent conditions within the basins is desirable. Temporal resolution of at least daily is preferable to increase the chance of obtaining cloud-free (or mostly cloud-free) scenes during snowmelt events that span only a few days or perhaps a week. Within the study basin, the snow cover (on average) depletes over ~10 to 12 weeks (~70 to 85 days); the approximate rate of snow cover depletion is greater than 1% per day.

In conjunction with digital elevation models (DEMs), hydrologists can identify the elevation and aspect of the terrain covered by snow, along with the order in which areas of the snow cover might melt (low vs. high elevations, south vs. north faces, etc.). Lumped snow models such as SNOW17 (as it is run in NWS RFC operations) do not explicitly consider spatial heterogeneity of terrain (aspect, slope, land cover including vegetation, etc.); however, model parameters, including areal

depletion curves, can be more appropriately estimated with knowledge of terrain characteristics and their impact on snowpack depletion. Supplementary information about the spatial distribution of the snow cover is particularly helpful in years when the snowpack persists at low elevations and on south faces past the average date of snowpack depletion. An abnormally extensive late-season snowpack tends to elevate the flood potential, so additional observations of the snowpack (including those from satellites) during these years would be especially beneficial to forecasters (CBRFC Staff, pers. comm., 2011).

2.2.2 Use of the Electromagnetic Spectrum to Observe Snow Cover Extent

Various portions of the electromagnetic spectrum are useful for remote sensing of snowpack properties. The most widely used portions include the visible (VZ), near infrared (NIR), and shortwave infrared (SWIR) for monitoring snow covered area, along with gamma and microwave (MW) wavelengths for observing snow water equivalent (SWE). The short wave infrared (SWIR) wavelengths are used to differentiate between clouds and snow (Dozier, 1989). For satellite-derived fSCA observations, sensors operating in the VZ, NIR, and SWIR bands (see Table 1) generate the data of highest spatial resolution. The boundary between the NIR and SWIR bands is somewhat arbitrary in the literature, ranging from 1.0 μm to 1.4 μm. Armstrong and Brun (2008) define it as 1.1 μm.

Table 1: Wavelengths bands useful for observing snow cover extent

Band	Wavelength Range
Visible (VZ)	0.4 to 0.7 μm
Near Infrared (NIR)	0.7 to 1.1 μm
Shortwave Infrared (SWIR)	1.1 – 3 μm

Observations of sub-1 km spatial resolution that also have high temporal resolution currently come from a subset of polar orbiting satellites. Having both adequate spatial *and* adequate temporal resolution is essential for monitoring fSCA conditions in spatially diverse mountainous watersheds, especially when snow conditions change may quickly during rapid melt events. Therefore, this section and this report as a whole will focus on the use of the VZ, NIR, and SWIR portions of the electromagnetic spectrum to generate fSCA observations and instrumentation on certain polar orbiters. Instruments operating outside the VZ, NIR, and SWIR wavelengths are discussed further in only a limited manner.

Radiation received at satellite sensors within the VZ, NIR, and SWIR bands of the electromagnetic spectrum can be used to differentiate snow-covered areas from other types of land cover, when multiple bands are used in combination. In general, snow cover observation is made possible by using the spectral signature of snow and the ways in which it differs from spectral signatures of other types of land surfaces. Figure 2 (Wright, 2011) shows spectral reflectance curves for various land cover types. Clouds and fresh snow are both highly reflective of VZ light (both appear bright white to the naked eye), but their spectral signatures in the NIR and SWIR differ. Clouds are highly reflective of SWIR light, but snow and water are less

reflective of SWIR light (see Table 2, which is based on Fig. 2). The spectral reflectance of snow also varies with grain size, as shown in Fig. 3 (Wright, 2011). By exploiting the differences in the spectral signatures of snow and other land cover types, the portion of a pixel that is snow-covered can be estimated.

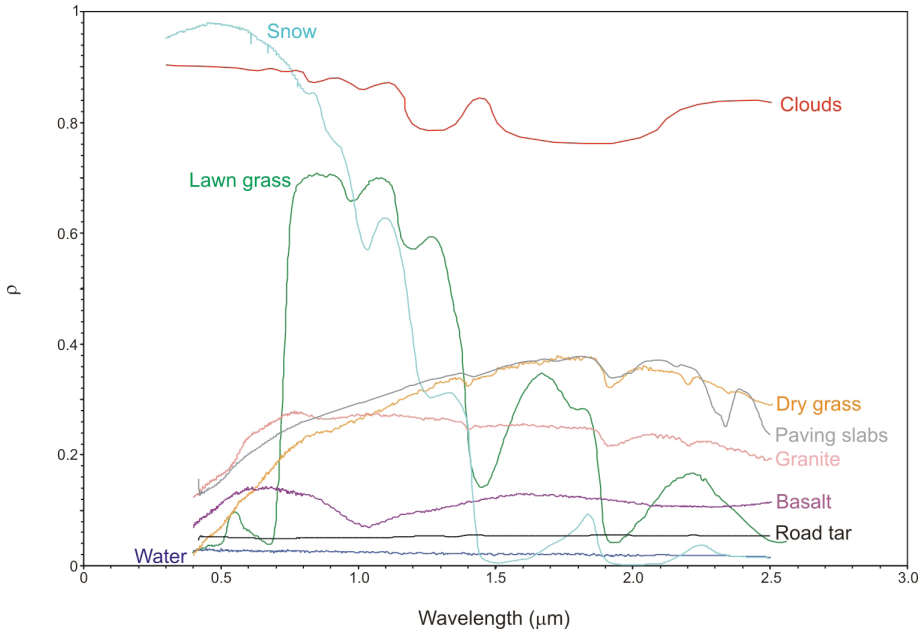

Figure 2: Spectral reflectance (ρ) curves for land cover types (Wright, 2011).

Table 2: Relative Reflectance of Land Cover Types in Different Bands

Land Cover Type	Visible (VZ): 0.4 to 0.7 μm	Near Infrared (NIR): 0.7 to 1.1 μm	Shortwave Infrared (SWIR): 1.1 – 3 μm
Clouds	High	High	High (much greater than snow)
Snow	High	Moderate to High (varies with grain size)	Low to Moderate (varies with grain size)
Water	Low	Very Low	Very Low
Snow-free Land	Low	Low	Low

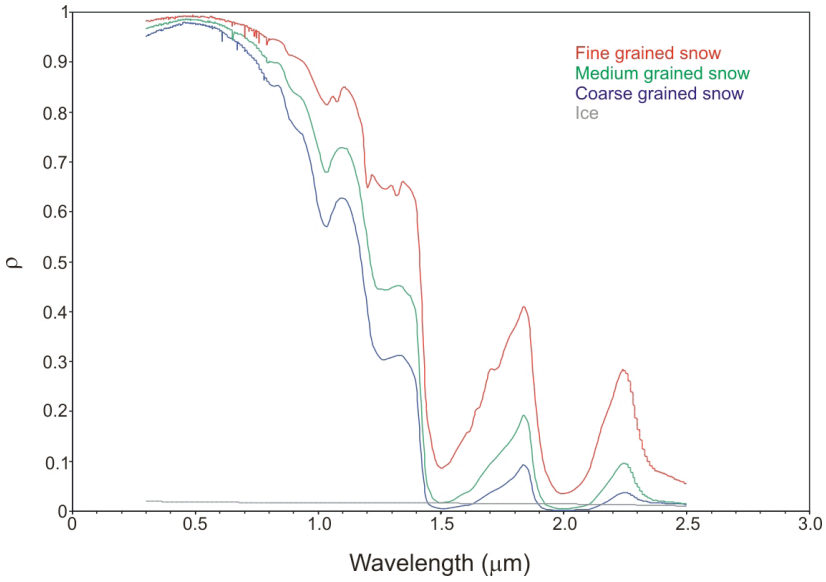

Figure 3: Spectral reflectance (ρ) curves for snow of varying grain sizes (Wright, 2011).

The observed spectrum of snow may also be altered by impurities deposited upon the snow surface, such as dust (Painter et al., 2012). Figure 4 shows an example of differences between observed "dusty" snow and modeled "clean" snow. The most notable differences occur in the VZ portion of the spectrum, and the differences decrease as wavelength increases. Albedo of dusty and clean snow may differ by as much as 50% in the visible portions of the spectrum. Since wavelengths in the VZ portion of the spectrum are essential to the detection of fSCA (see section 2.2.4.3), impurities upon the snow surface likely impact the accuracy of snow cover retrieved by satellite instrumentation.

The satellite-derived snow cover data sets used in this study are not adjusted for impacts of impurities on the snow spectrum. Investigation of fSCA derived from dusty snow cover that has an albedo much below that of clean snow is planned as part of future work.

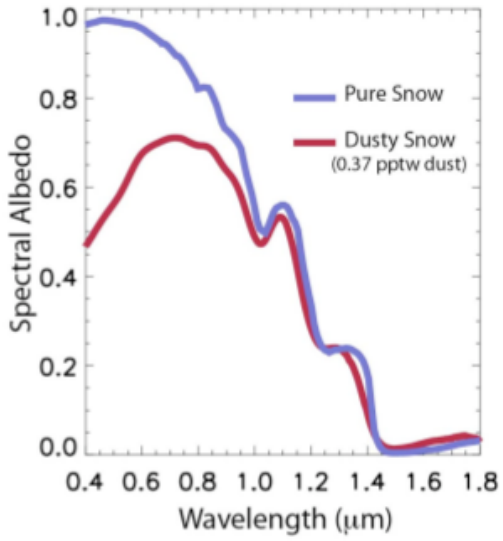

Figure 4: Spectral albedo of clean snow (modeled) and snow with dust concentration of 0.37 parts per thousand by weight of snow water or mg g^{-1} (measured) (from Painter et al., 2012)

2.2.3 Types of Satellite Snow Cover Observations: Binary and Fractional

Types of snow cover estimates from satellite-derived data sets include the traditional binary (snow or no-snow) products as well as more recently developed subpixel fSCA products. Both binary and fractional observations of snow cover extent use the differences in spectral signatures of snow, clouds, and various land covers to determine, in the binary case, whether or not a pixel should be labeled as completely snow covered or completely snow-free, and to estimate, in the fSCA case, approximately what fraction of a pixel is snow covered.

The fSCA algorithms aim to give a more complete, more detailed picture of a region's snow cover extent than the binary products do. Figure 5 shows an example of MODIS-derived snow cover in the Sierra Nevada in January 2008 (Dozier et al., 2008). Figure 5a shows an fSCA product, in which the snow cover of the pixels

spans the full range of 0 to 100%. Figure 5b shows a binary remapping of the fSCA product, in which each pixel is shown as snow-covered or snow-free using an fSCA threshold of 50%. Figure 5c shows the pixels from the fSCA product that have less than 50% snow cover. The pixels with lesser snow cover are usually at lower elevations. In the binary data, these pixels would be classified as completely snow-free if an fSCA threshold of 50% is used; the binary product would not provide information about snow cover at the lower elevations. The fSCA product implies these pixels are at least partially snow covered. Use of the fSCA product over the binary product would provide more detailed information about the extent of the snow cover to forecasters and modelers, especially at lower elevations.

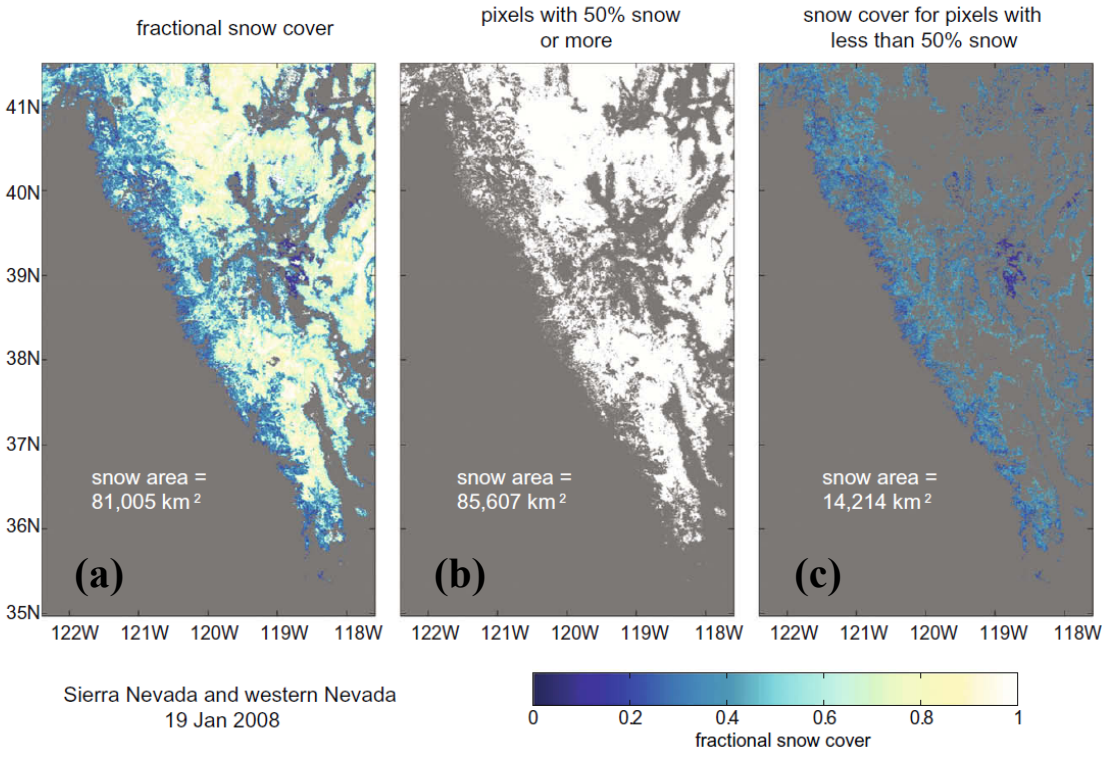

Figure 5: Fractional and binary snow cover from MODIS (Dozier et al., 2008)

In spatially diverse mountainous watersheds, the snow cover extent can easily vary at scales finer than what a satellite-borne instrument can observe in a single pixel or field of view. Because of this characteristic of high elevation, mountainous watersheds dominated by snow, subpixel analysis of fSCA is especially useful when analysts need the most complete snow cover extent information. Therefore, the binary products are not discussed further in this report. The details of specific methods of deriving fSCA observations, including those from the MODIS instrument, will be described in more detail in a later section.

2.2.4 fSCA Observations Appropriate for Mountain Watersheds

2.2.4.1 Sources and Providers

Private-sector satellite programs (QuickBird, Ikonos) can provide land cover information of very high spatial resolution (some even at sub-1 m), but these data are usually very expensive (DeWalle and Rango, 2008). In addition, they revisit the same location on a very low frequency, and this characteristic does not lend itself to snowpack monitoring, especially during rapid snowmelt events that occur on timescales of days to a week.

The most commonly used satellite-derived fSCA data sets that observe the western U.S. come from publicly funded efforts, through federal agencies such as the National Oceanic and Atmospheric Administration (NOAA), National Aeronautics and Space Administration (NASA), and the United States Geological Survey (USGS). These agencies provide satellite observations of many types at no extra charge to users. Among these publicly funded programs, the Landsat program, run by NASA

and the USGS, provides satellite observations with the highest spatial resolution, 30 m in most bands, 15 m in the panchromatic band. The Landsat satellites observe the same location on earth once every ~2.5 weeks. Additional efforts by NASA, including the MODIS instrument on its Terra and Aqua satellites, provide fSCA observations at 500 m spatial resolution. Although the MODIS spatial resolution is coarser than Landsat's (500 m vs. 30 m), the MODIS data sets are available on a daily basis (depending on cloud cover) versus only once every ~2.5 weeks for Landsat.

Table 3 summarizes characteristics of satellites and instruments used to monitor snow cover in the western United States at sub-1 km resolution as of March 2013, including planned missions (denoted by italics). These instruments, on polar-orbiting satellites, provide observations in real time or near real time as of March 2013. Table 4 lists the measurement bands applicable to monitoring snow cover for the satellite instruments listed in Table 3 (again, instrumentation on future missions is italicized). These wavelength bands and their utility for snow cover observation were discussed in more detail in section 2.2.2.

Table 3: Publicly-funded satellite instrumentation for observing fSCA. Italics indicate future missions.

Agency	NASA	NASA/USGS			NASA (primary), NOAA, DOD, private partners	*NOAA, NASA, EUMETSAT*
Satellite	Terra/ Aqua	Landsat-5	Landsat-7	LDCM	NPP	*JPSS-1*
Year of Launch	Terra: 1999 Aqua: 2002	1984	1999	Feb 2013	2011	*Jul 2017 (planned)*
Orbit Time/ Period	99 min	99 min	99 min	99 min	101 min	*101 min*
Nominal Satellite Altitude	705 km	705 km	705 km	705 km	824 km	*824 km*
fSCA Instrument	MODIS	TM	ETM+	OLI	VIIRS	*VIIRS*
Swath Width	2330 km	185 km	185 km	185 km	3000 km	*3000 km*
Temporal Resolution	~daily	16 d	16 d	16 d	~daily	*~daily*
Nominal Spatial Resolution at Nadir in the VZ/NIR/SWIR Bands	Bands 1-2: 250 m Bands 3-7: 500 m	30 m	30 m (15 m in panchromatic band)	30 m (15 m in panchromatic band)	750 m	*750 m*

Sources:
Terra/Aqua: NASA (No Date)
Landsat: NASA (2011)
NPP: CEOS (2011)
JPSS: CEOS (2012)

Table 4: Satellite instrumentation bands applicable to fSCA observation. Italics indicate future missions.

Satellite Instrument (nominal resolution)	Visible (VZ): 0.4 to 0.7 μm	Near Infrared (NIR): 0.7 to 1.1 μm	Short wave Infrared (SWIR): 1.1 – 3 μm
	Band Number, Wavelength Range, Violet/Blue/Green/Red (if VZ)		
Aqua/Terra MODIS (500 m)	3: 0.459-0.479 (B) 4: 0.545-0.565 (G) 1: 0.620-0.670 (R)	2: 0.841-0.876 5: 1.230-1.250	6: 1.628-1.652 7: 2.105-2.155
Landsat TM (30 m)	1: 0.45-0.52 (B) 2: 0.52-0.60 (G) 3: 0.63-0.69 (R)	4: 0.76-0.90	5: 1.55-1.75 7: 2.08-2.35
Landsat ETM+ (30 m)	1: 0.450-0.515 (B) 2: 0.525-0.605 (G) 3: 0.630-0.690 (R)	4: 0.75-0.90	5: 1.55-1.75 7: 2.09-2.35
LDCM OLI (30 m)	2: 0.450-0.515 (B) 3: 0.525-0.600 (G) 4: 0.630-0.680 (R)	5: 0.845-0.885	6: 1.560-1.660 7: 2.100-2.300
NPP VIIRS (launched) *JPSS-1 VIIRS (to be launched)* (Mx = 750 m)	M1: 0.402-0.422 (V) M2: 0.436-0.454 (V) M3: 0.478-0.498 (B) M4: 0.545-0.565 (G) M5: 0.662-0.682 (R)	M6: 0.739-0.754 M7: 0.846-0.885	M8: 1.230-1.250 M9: 1.371-1.386 M10: 1.580-1.640 M11: 2.225-2.275
(Ix = 375 m)	I1: 0.600-0.680 (R)	I2: 0.846-0.885	I3: 1.580-1.640

Sources:
MODIS: NASA (No Date)
Landsat TM: NASA (2011)
Landsat ETM+: NASA (2011)
LDCM: NASA and USGS (2010)
VIIRS: Zhou (2011)

2.2.4.2 Importance of Spatiotemporal Resolution in Mountain Basins

Because mountainous watersheds are spatially diverse, and because snow cover conditions within them can change rapidly, observations with both high spatial and high temporal resolution (within practical limits) are most desirable for monitoring snow cover within these watersheds. Unfortunately, no single available data set currently combines the highest spatial resolution with the highest temporal resolution. Concessions must be made with respect to one or the other.

Private satellite programs like QuickBird offer very high resolution land cover observations of less than 1 m (DigitalGlobe, 2006). However, obtaining observations from these programs can be very expensive, with costs of several thousand dollars or more. Also, their very low temporal resolution eliminates them from being used to monitor snow cover during rapid snowmelt events.

The instruments on the geostationary platforms, such as NOAA'S GOES, provide observations of the earth's surface many times a day. However, at a resolution of 1 km, the observations from GOES are thirty times coarser than the observations from polar orbiting satellites in the Landsat program. For large watersheds (e.g., the entire Colorado River Basin), a spatial resolution of 1 km for the satellite-derived snow cover observations is sufficient. However, as hydrologic modelers seek to represent processes on a regional scale and within individual small mountain watersheds, especially during rapid melt events, satellite-based snow observations at a spatial resolution finer than 1 km become more desirable.

Observations from the Landsat platforms provide data of high spatial resolution (30 m), but the frequency of observations is approximately 2.5 weeks. While they are of high spatial resolution, the low temporal resolution of the Landsat observations renders them less useful for monitoring snow conditions during snowmelt, particularly if the melt is rapid. Cloud cover further limits Landsat instrumentation from observing snow cover extent.

Starting in the early 2000s, snow cover observations became available with NASA's MODIS instrument. MODIS, which flies on NASA's Terra and Aqua satellites, represents the best compromise of spatial and temporal resolution currently available. It provides fSCA information at 500 m resolution and on a daily basis (depending on cloud cover). Its much wider swath width enables MODIS to observe the entire earth much more quickly than Landsat (185 km vs. ~2300 km, see Table 3). This higher temporal frequency of observation presents a distinct advantage of using snow cover observations from MODIS over those from Landsat when near real time observations are needed, despite the fact that the MODIS resolution is much coarser than Landsat's. Since MODIS currently provides the best spatiotemporal resolution for monitoring fSCA in mountainous watersheds, MODIS snow cover observations are used in this study.

2.2.4.3 Methods of Deriving fSCA from MODIS

Snow hydrologists seek to extract as much detailed information as possible from satellite data. The snow cover extent in mountainous basins can vary widely within the basin and even within a single grid cell or pixel. Legacy satellite-derived snow cover products are binary in nature and assume that an entire pixel is snow-covered or snow-

free. With the advent of the MODIS instrument and new fSCA algorithms in the past ten years, scientists have regular access to estimates of subpixel fSCA. Two of the techniques used to derive subpixel fSCA from MODIS data are described below.

NDSI-BASED fSCA

The standard MODIS fSCA data sets from NASA are available from February 24, 2000 to present. Collection 5 of the MODIS snow products, processed in 2006, is the latest official version of the products as of spring 2013. The data sets consist of subpixel fSCA values calculated from a linear regression relationship between the normalized difference snow index (NDSI) and snow cover observations from the Landsat ETM+, treated as "ground truth" (Salomonson and Appel, 2004). The NDSI uses reflectance values from multiple MODIS bands to distinguish snow from clouds and other types of land cover. The NDSI is a ratio, defined as:

$$\text{NDSI} = \frac{\text{VZ band} - \text{SWIR band}}{\text{VZ band} + \text{SWIR band}} \quad (1)$$

where the VZ band is band 4 for both MODIS instruments and the SWIR band is band 6 for Terra's MODIS and band 7 for Aqua's MODIS.

Most of the detectors in band 6 on Aqua's MODIS are no longer functional, so band 7 is used to derive fSCA values from Aqua's MODIS. In response to the degradation in band 6 on Aqua's MODIS, Salomonson and Appel (2006) investigated whether the second MODIS band in the SWIR portion of the spectrum, band 7, could be

used to calculate a NDSI and to identify whether or not a pixel is snow-covered. They determined that using band 7 to derive fSCA from Aqua's MODIS results in comparable values to using band 6 to derive fSCA from Terra's MODIS but that the Terra MODIS had slightly better performance when compared to snow cover from Landsat data. The fSCA values from Terra's MODIS are generally preferred by users over the Aqua MODIS values due to (a) the longer period of record for Terra's MODIS (1999 to present for Terra versus 2002 to present for Aqua) and (b) the detector problems in band 6 of Aqua's MODIS and the use of the alternate SWIR band 7 to calculate fSCA.

After the NDSI is computed, additional tests screen for water that may exhibit a snow-like NDSI value (Riggs et al., 2006). Water pixels initially identified as snow are then reclassified as non-snow. In forested areas, the NDSI value may be low and indicate a non-snow land type; yet, snow cover is nonzero. To accommodate detection of snow cover in forested areas, NASA checks for low NDSI values that coincide with certain thresholds of the normalized difference vegetation index (NDVI). If thresholds are met, pixels that may initially be labeled as non-snow because of a low NDSI value may be reclassified as snow covered.

Once a pixel passes the checks described above, its fSCA value is computed. The NDSI value is input to the linear regression equations developed by Salomonson and Appel (2006) to generate subpixel fSCA values for MODIS snow cover products. For Terra's MODIS, the relationship between the MODIS NDSI and "ground truth" observations from Landsat ETM+ was determined to be:

$$FSCA = -0.01 + 1.45NDSI \qquad (2)$$

The linear regression algorithm that generates the subpixel fSCA values is computationally frugal and reasonably accurate when compared to data from Landsat ETM+, with reported correlation coefficients of ~0.9 (Salomonson and Appel, 2006).

fSCA FROM SPECTRAL MIXTURE ANALYSIS

In recent years, spectral mixture analysis has gained traction as a way to derive subpixel fSCA estimates, especially in forested mountainous basins where the land cover types may vary widely even within a single pixel. Spectral mixture analysis assumes that the sensor observation is determined by a linear combination of contributions from individual endmembers such as rock, bare soil, vegetation, and snow. Mathematically:

$$R_{S,\lambda} = \sum_{i=1}^{N} F_i R_{\lambda,i} + \varepsilon_\lambda \qquad (3)$$

where

$R_{S,\lambda}$ = pixel-averaged surface reflectance measured by the sensor at wavelength λ
N = number of spectral endmembers
$R_{\lambda,i}$ = reflectance of the ith endmember at wavelength λ
F_i = fraction of the pixel attributable to endmember i
ε_λ = the residual error at λ for the fit of the N endmembers

F_i, the fraction of the pixel covered by the i-th endmember (which could be snow) is determined by examining different linear combinations of endmembers and minimizing the residual error via numerical methods like least squares.

Multispectral instruments like MODIS have multiple bands that allow the use of spectral mixture models. Spectral mixture analysis is more computationally intensive

than the NDSI-based algorithm for determining fSCA. However, with improvements in computing power, fSCA derived from spectral mixture analysis is becoming more widely utilized. As one example of this method, Painter et al. (2009) developed a model called MODSCAG (MODIS Snow-Covered Area and Grain size) that uses spectral unmixing to derive subpixel fSCA information. MODSCAG uses the 16-bit MODIS surface reflectance product (MOD09GA), examines the reflectance values in each of seven bands, and searches a library of endmembers for combinations of endmembers that minimize the error in equation (3) above.

The library contains endmembers representing spectral signatures of various land covers such as soil, rock, vegetation, etc. The spectral signatures are generally derived from field or lab measurements. The library also contains model-derived snow endmembers with different grain sizes. The snow endmembers are spectrally similar, but with subtle differences. Because the snow endmembers are too similar to allow resolution of multiple unique snow grain size endmembers within the same pixel, the MODSCAG algorithm allows only one snow endmember per pixel. However, the snow endmember *is* allowed to vary from pixel to pixel. MODSCAG solves for each different combination of endmembers and generates thousands of candidate combinations for each pixel (Dozier and Frew, 2009). The chosen combination is the one with the lowest root mean square error (RMSE), defined as:

$$RMSE = \left(\frac{1}{N} \sum_{\lambda=1}^{N} \varepsilon_{\lambda}^{2} \right)^{1/2} \qquad (4)$$

2.2.5 Limitations of Satellite-derived fSCA Observations

Despite their growing use and popularity, the snow cover products from satellites have limitations and drawbacks. Methods of correcting for these drawbacks exist for some of the limitations. Some of these limitations are described below.

2.2.5.1 Lack of SWE Information

By themselves, fSCA observations do not provide any volumetric estimates of the water content of the snowpack, which could be used to infer the potential snowmelt runoff volume. In mountain basins, much SWE may be lost and appear as streamflow before the fSCA drops below 1.0 (100%). Satellite instruments operating in the microwave wavelengths can provide SWE information, but the horizontal resolution of these data sets is too coarse (e.g., 25 km for the AMSR-E instrument on the Aqua satellite) to be used in spatially diverse mountain watersheds. While SWE information is not available directly from satellite-derived fSCA observations, SWE is often inferred through the use of snow cover depletion curves (SDCs). Liston (1999) describes relationships among melt rate, SWE distribution, and snow cover extent that could be used to model snowpack characteristics if two of the three pieces of information listed are available.

2.2.5.2 Limited Seasons of Usefulness

Satellite-derived fSCA information is most useful during the accumulation and ablation seasons. There are finite bounds on fSCA values; these bounds are 0% and 100%. Algorithms used to derive fSCA, such as the NDSI method and algorithms based

on spectral mixture models, also have practical limits in the lower bound. They are less accurate when only a small fraction of the pixel is covered by snow. The signal from the small amount of snow may be overwhelmed by spectral signatures from other surface types (soil, rock, vegetation, etc.). The practical lower detection capacity of subpixel fSCA for the MODSCAG algorithm, for example, is 10-15% (Painter et al., 2009). As fSCA approaches zero, the uncertainty in the fSCA is large enough that confidence in the derived fSCA below a 10-15% threshold diminishes greatly. In fact, fSCA values below this threshold are zeroed out in the MODSCAG data sets (T. Painter, pers. comm., 2013).

The water content of the snowpack can change drastically while the fSCA observation for a grid cell or basin-wide areal fSCA average remains at 100%. A significant amount of snow may melt before the fSCA drops below the upper bound of 100% (Clark et al., 2006). Until the fSCA values drop below 100%, satellite-derived fSCA observations do not provide additional information to a hydrologic model or a hydrologic forecaster, even if snowmelt is indeed ongoing and driving streamflow. Any improvements in streamflow prediction due to the inclusion of fSCA are limited to the period when fSCA values are less than 100%. However, even though the time during which the fSCA values are able to inform a hydrologic model or forecaster may be short, the rapid melt events are when the additional information is most needed.

2.2.5.3 Inaccurate Observations at Large Scan Angles

Observations derived from satellite-borne instrumentation are most accurate at nadir (directly below the spacecraft). At off-nadir viewing angles, the sensor observes a much larger area at the edge of a scan than the nominal spatial resolution of the

observations (500 m for MODIS data sets used to derive fSCA). Figure 6 (Dozier et al., 2008, amended with qualitative indication of pixel size) illustrates the viewing geometry for off-nadir pixels and the larger area that the sensor observes at a large scan angle (θ) compared to the instantaneous field of view (IFOV) seen at nadir. MODIS's maximum scan angle of 55°, along with effects of the earth's curvature, causes pixels far from nadir to be stretched to about ten times larger than nadir pixels (Dozier et al., 2008).

In MODIS-derived snow cover data sets that have their roots in the MODIS spectral reflectance data, the stretched pixels from large scan angles are resampled to 500 m, and the reflectance value from the stretched pixel is assigned to the resampled 500 m pixels. In this case, all of the 500 m pixels derived from the stretched pixel are assigned the same reflectance value, that of the stretched pixel. Subsequently, snow cover derived for these resampled reflectance pixels will be the same since their assigned reflectance values are the same. When these stretched pixels (caused by large scan angles) are included in satellite data sets, even if they are resampled to 500 m, the satellite observations of snow cover are less accurate than those at nadir.

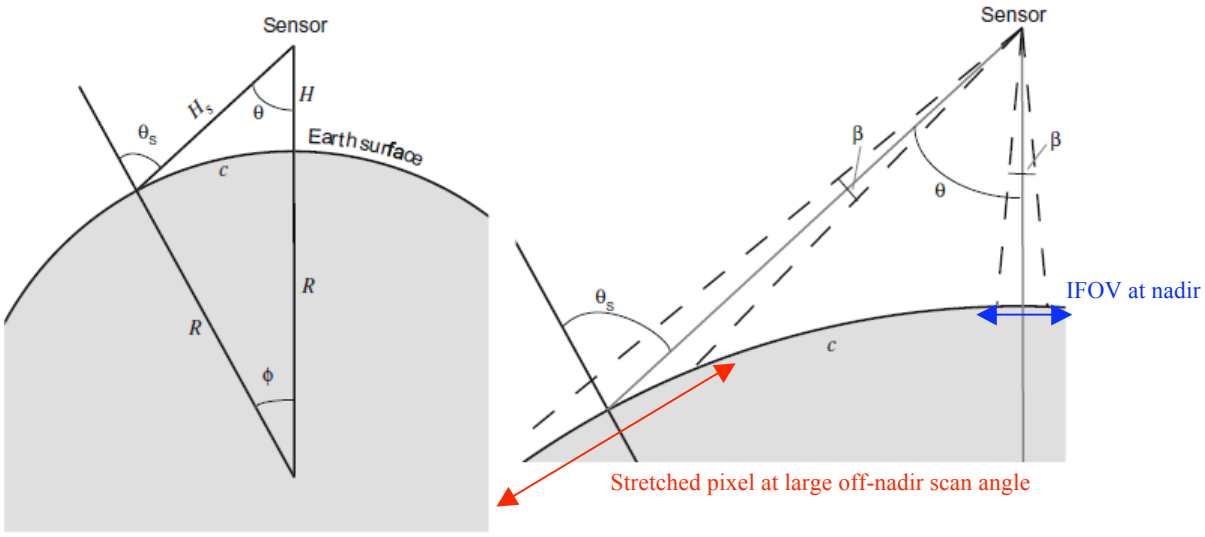

Figure 6: Viewing geometry for off-nadir pixels (after Dozier et al., 2008). The variables in the figure are defined as follows: θ = instrument scan angle, $θ_s$ = sensor zenith angle, H = sensor altitude above the earth's surface, H_s = path length from the sensor to the surface (H = H_s at nadir), c = the arc length along the surface, from nadir to the image point, β = the angle that subtends the instantaneous field of view (IFOV).

2.2.5.4 Forest Cover

Because MODIS is an optical sensor, it does not detect emitted radiation from objects beneath tree canopies. Instead, it sees the land surface only in open areas and through canopy gaps. Hence, the snow conditions observed by the sensor are often different from the actual snow cover, especially in heavily forested regions where the breaks in the forest canopy are small. The problem is exacerbated at large off-nadir scan angles.

Forest cover poses a challenge in snow cover monitoring, because extensive forest cover in mountainous areas often coincides with snow-covered areas. For example, Klein et al. (1998) estimate that, for the month of February, approximately 36% of the snow covered areas in North America are also covered by forests, and that detection of snow

under the canopy, where it remains in the spring when open areas have melted out, is challenging.

Attempts have been made to correct for vegetation in snow cover mapping. Raleigh et al. (2011) describe one vegetation correction to fSCA values. The correction uses the "viewable gap fraction," which is defined as 1 – F, where F is the fractional forest canopy density from the 2001 National Land Cover Data Set. Mathematically, their corrected fSCA value is:

$$FSCA_{CORR} = \frac{FSCA_{OBSERVED}}{1 - F} \qquad (5)$$

They acknowledge that this type of correction may not be robust, as it assumes that snow conditions in the forest are proportional to snow conditions in clearings and forest gaps.

The Raleigh et al. (2011) study compared snow cover from a ground network of snow sensors with individual MODSCAG fSCA pixels. At one (moderately forested) of their three test sites, there was reasonable agreement between the MODSCAG fSCA and the fSCA computed from the ground sensor network. At the other two sites (one heavily forested, one lightly forested), the MODIS-derived fSCA declined much more rapidly and much earlier than the ground sensors indicated. Though, in the lightly forested area, the fSCA data were impacted by off-nadir angles and cloud cover. The assumption that snow conditions in a forested area are proportional to those in open areas is often violated because snow cover patterns depend on types of trees, among other factors. Their study suggests that the vegetation correction method should not assume that the snow conditions in clearings and under forest canopies are similar. Further studies of sub-

canopy conditions would be necessary to develop a robust vegetation correction. However, validation of vegetation correction methods on a basin scale may be difficult due to the need for high resolution, ground-based validation data sets. NASA's Jet Propulsion Laboratory (JPL) recently received funding to begin a study related to adjustment of remote sensing data for vegetation (T. Painter, pers. comm., 2012).

2.2.5.5 Cloud Cover

While other characteristics of satellite-derived fSCA observations limit their usefulness, cloud cover is the dominant drawback of snow cover observations derived from optical satellite instrumentation like MODIS. Optical instruments like MODIS cannot penetrate cloud cover in order to determine snow cover conditions on the land surface. Snow-covered area products from MODIS, including the NDSI-based fSCA observations and alternatives like the MODSCAG algorithm, are both hindered by cloud cover. In a study focusing on Austria, Parajka and Blöschl (2006) found that the utility of the MODIS snow cover data varies with cloud coverage, and, because the cloud cover varies seasonally, so does the utility of the MODIS observations.

Prolonged periods of extensive cloud cover, which tend to occur in the winter months in the western United States, can obscure the land surface conditions (including snow cover) for days. For example, in January 2008 over the Sierra Nevada, clouds covered 70% or more of the area on eight days out of the month (Dozier et al., 2008). As the cloud cover persists for longer periods of time, the uncertainty in satellite-derived fSCA estimates over a basin increases dramatically.

The uncertainty due to cloud cover in satellite-derived fSCA estimates should be considered when these observations are used in hydrologic prediction, especially during snowmelt events on short time scales. Models generate continuous snow-covered area estimates without consideration of cloud cover. So, if the satellite-derived estimates of fSCA are used to update snowpack conditions in a hydrologic model, the effect of cloud cover on the fSCA estimate should be considered in some manner.

There are two parts to the cloud cover problem when considering snow cover estimation for cloudy pixels. First, clouds must be correctly identified from snow in the satellite observations. Secondly, one must decide whether or not to interpolate or approximate fSCA for cloudy pixels, in hopes of making a basin fSCA estimate more informative.

Cloud detection algorithms of many varieties have been developed in the past two decades, aiming to correctly and efficiently differentiate cloud from snow. These cloud detection algorithms are generally successful for thick clouds. However, thin clouds may still sometimes be mistaken for snow.

The standard MODIS snow cover product at 500m resolution, produced by NASA (Terra: MOD10A1, Aqua: MYD10A1), labels pixels as cloud-covered, but the standard 500 m product does not currently provide an estimate of fSCA for cloudy pixels. In the MODSCAG fSCA product, fSCA is not currently estimated for cloudy pixels. NASA's JPL has plans to incorporate fSCA estimates for cloudy pixels into their product in the future (T. Painter, pers. comm., 2012).

In attempts to make fSCA estimates derived from MODIS usable even on cloudy days, efforts have been made by users of MODIS fSCA data to estimate the snow cover

for cloud-obscured pixels. These methods are successful to varying degrees. Examples of snow cover estimation methods for cloudy pixels are described below.

COMBINATION PRODUCTS

Combination products are a popular way of reducing data loss due to cloud cover in MODIS grids. Gao et al. (2010) describe a method that combines Terra and Aqua MODIS data with snow cover information implied by the AMSR-E SWE product. Their method first combines Terra and Aqua MODIS snow cover grids, reclassifying the cloudy pixel as snow if the grid cell from either the Aqua or Terra MODIS is snow. If the grid cell is cloudy in both the Aqua *and* Terra MODIS, then the pixel is left as cloudy. For the cloudy pixels that remain after the Terra and Aqua MODIS combination is performed, information from the microwave AMSR-E instrument is used to infer snow conditions.

SPATIAL AND TEMPORAL FILTERS

Filters use neighboring pixels in space and time to estimate snow cover conditions for cloudy or otherwise indeterminate pixels. The techniques aim to reduce the amount of cloud coverage in a scene, in hopes of generating more useful snow cover estimates over basins.

Parajka and Blöschl (2008) replaced cloudy pixels with estimates of snow conditions derived from a combination of Terra and Aqua snow cover data, as well as spatial and temporal filters. Before applying the spatial and temporal filters, they

combined the MODIS snow information from Terra and Aqua into a combination product. In this combination product, any cloudy pixels from the Aqua MODIS grids took the class of the corresponding Terra pixel if the Terra pixel was non-cloudy. If both were cloudy, then the pixel was left as cloud and was subjected to the spatial and temporal filters. The spatial filter replaced the cloudy pixel with the class (land or snow) of the majority of non-cloud pixels in the eight pixel neighborhood. If there was a tie, the cloudy pixel was assumed to be snow covered. The temporal filter replaced cloudy pixels by the most recent preceding non-cloud observation at the same pixel within various time windows of 1, 3, 5, and 7 days. The authors found that use of the combined and filtered MODIS snow cover data improved their estimates of snow conditions in their snow model when compared to snow depth measurements from independent ground stations.

Hall et al. (2010) applied a similar methodology of replacing cloudy pixels with snow cover values from previous days, to fill in gaps due to cloud cover in the 0.05 degree snow cover data set (MOD10C1). Accompanying the "cloud gap filled" (CGF) snow cover data set is a data set of cloud-persistence-count (CPC) values that indicates, if the grid cell in the original data set was cloudy, the age (in days) of the snow cover value that replaces the cloud value. This quality indicator allows users to choose their own tolerance with respect to age of the snow cover observation that replaced cloudy grid cells. Their results indicate that 80 to 100% more snow cover values are included in the CGF product when the CPC threshold is relaxed from 0 to 3 days.

USING THE LOCATION OF THE SNOWLINE

Parajka et al. (2010) proposed that cloudy pixels be reclassified as snow or land according to their elevation with respect to the regional snow line. Their evaluation was conducted over Austria using MODIS data from the Terra satellite. In their pixel reclassification method, they compared the elevation of each cloudy pixel to the mean elevation of all the snow pixels and the mean elevation of the snow-free land pixels. Cloudy pixels were assigned as snow if their elevation was above the mean snow line, and they were assigned as snow-free land if their elevation was below the mean elevation of land pixels (the "land line"). Cloudy pixels between the snow line and the land line were reclassified as "partially snow covered." They realized that extensive cloud cover would limit the use of this method of estimating snow conditions for cloudy pixels, so they applied cloud cover thresholds. If cloud cover was above a certain percentage on a day, the snow cover estimation was not performed, and pixels were left classified as they were in the original Terra data set.

2.3 OPERATIONAL MODELING OF SNOW AT NWS RFCS

2.3.1 Overview of the Operational NWS Hydrologic Modeling System

The NWS RFCs are responsible for providing operational hydrologic guidance, including streamflow predictions, to their partner NWS weather forecast offices (WFOs). The WFOs are tasked with the responsibility of issuing official flood watches and warnings when necessary.

Included in the hydrologic guidance from the RFCs is output from the NWS hydrologic forecasting, prediction, and modeling system called the Community Hydrologic Prediction System (CHPS). CHPS is a forecasting and modeling framework that manages input data, execution of the models, and output data, including real-time streamflow forecasts. Within CHPS, forecasters are able to run the hydrologic model in near real time, including its embedded snow and soil moisture modules, on demand. Typically, updated hydrologic guidance is available from the RFCs once a day, but updates can be issued more frequently in flood situations. Figure 7 shows an overview of the processes and modules involved in the operational NWS hydrologic forecasting system. This study focuses on the snow model, SNOW17 (Fig. 8), which is included in "Snow accumulation and ablation" in the "Hydrologic and Hydraulic Models" portion of the overall modeling system (Fig. 7).

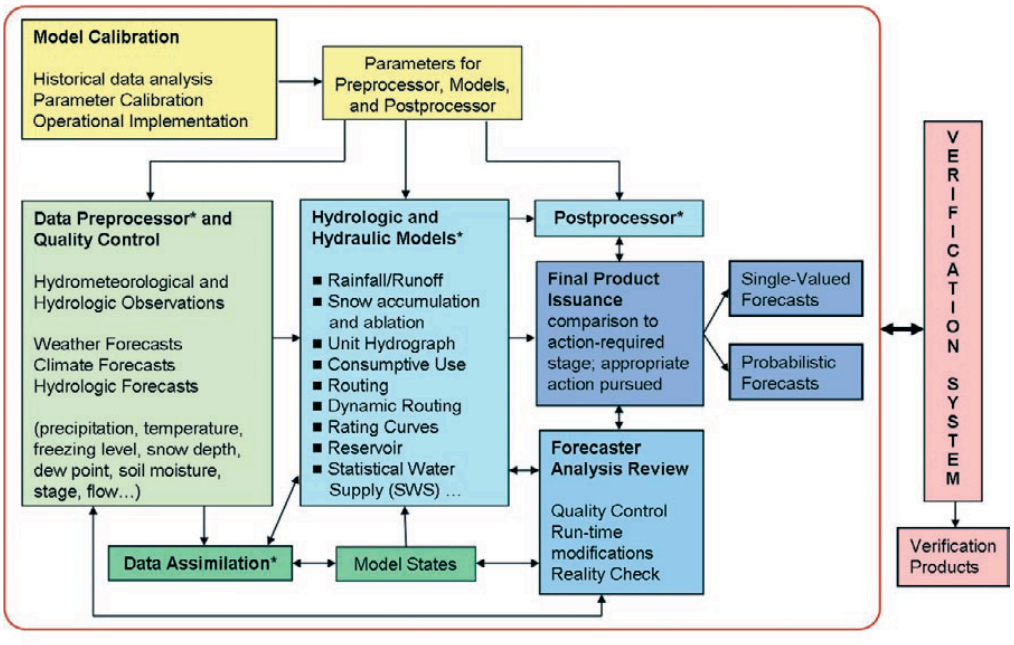

Figure 7: RFC hydrologic forecast system (Demargne et al., 2009)

2.3.2 Overview of SNOW17

The NWS RFCs currently use the SNOW17 snow accumulation and ablation model in a lumped fashion as the snow model in their operational hydrologic modeling systems. SNOW17 is a relatively simple conceptual model that requires only temperature and precipitation as the minimum input observations (Anderson, 2006). SNOW17 is primarily a temperature-index snow model that computes snowmelt under non-rain conditions by multiplying the difference between the air temperature and a base temperature by a melt factor [mm C^{-1} day^{-1}]. It also includes simplified energy balance calculations to handle rain-on-snow events. Air temperature has been shown to be highly correlated with snowmelt and several energy balance components (Hock, 2003).

Snowpack processes represented within SNOW17 include the accumulation of the snowpack, energy exchange at the snow-air and snow-soil interfaces, snowpack heat deficit accounting, and transmission (including lag and attenuation) of liquid meltwater within the snowpack. Vertically, SNOW17 represents the snowpack as a single layer, in contrast to alternative snow models that model the snow in multiple layers, such as SNTHERM (Frankenstein et al., 2008). SNOW17 can be applied at a point or to an area. The primary SNOW17 state variables are listed in Table 5. Figure 8 shows the major physical processes considered by SNOW17.

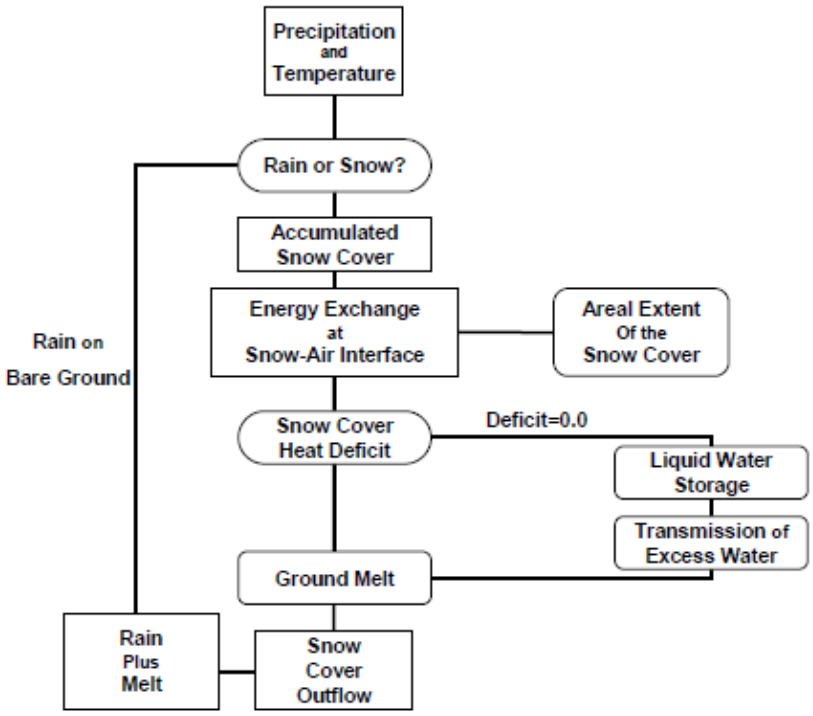

Figure 8: Flowchart of SNOW17 (Anderson, 2006)

Table 5: Primary SNOW17 state variables (Anderson, 2006)

State Variable	Description	Units
W_i	Water equivalent of the ice portion of the snow cover	mm
D	Heat deficit	mm
ATI	Antecedent temperature index	C
W_q	Liquid water held by the snow	mm
W_{max}	Max water equivalent during an accumulation period	mm
W_{ns}	Water equivalent when new snowfall first occurs on a partly bare area (i.e., the water equivalent at the point where the areal cover leaves the depletion curve)	mm
A_{ns}	Areal cover when new snowfall occurs on a partly bare area (i.e., the depletion curve value at the point where the areal cover leaves the curve)	decimal fraction
W_{100}	Amount of water equivalent where the areal cover drops below 100% when melt occurs after new snowfall takes place on a partially bare area	mm
S	Amount of lagged excess liquid water in storage	mm
A_{adj}	A_i value computed for use in depletion curve computations after an adjustment to the areal extent of snow cover – allows the water equivalent to remain the same as before the adjustment	mm
E_l	Average hourly lagged excess water for each precipitation Δt	m
H	Depth of snow cover	cm
T_s	Average snow cover temperature	C
$T_{a,t-\Delta t}$	Air temperature for the previous computational time interval	C

SNOW17 is designed to run for one specific point (where snow cover extent is not considered) or an area (where snow cover extent *is* considered). For both points and areas, a set of model parameters is derived in the calibration process. When applied to an area, SNOW17 uses an areal depletion curve (ADC) and the SI parameter (the SWE index value below which the ADC is in effect) to model the snow cover extent (AESC).

When SNOW17 is used in mountainous areas, watersheds are typically divided into two or three subareas by elevation, and SNOW17 is applied over each subarea, which the NWS terms an "elevation zone." Figure 9 shows the elevation zones for the Weber River headwater basin, the basin used in this study. The intention of dividing a modeled watershed into subareas and running SNOW17 over each subarea is to better capture spatial variability of the modeled watershed's physiographic characteristics, at least as far as the constraints of the NWS operational environment allow. The potential implementation of a fully distributed hydrologic model is currently limited in operations at NWS RFCs, particularly with respect to computing power.

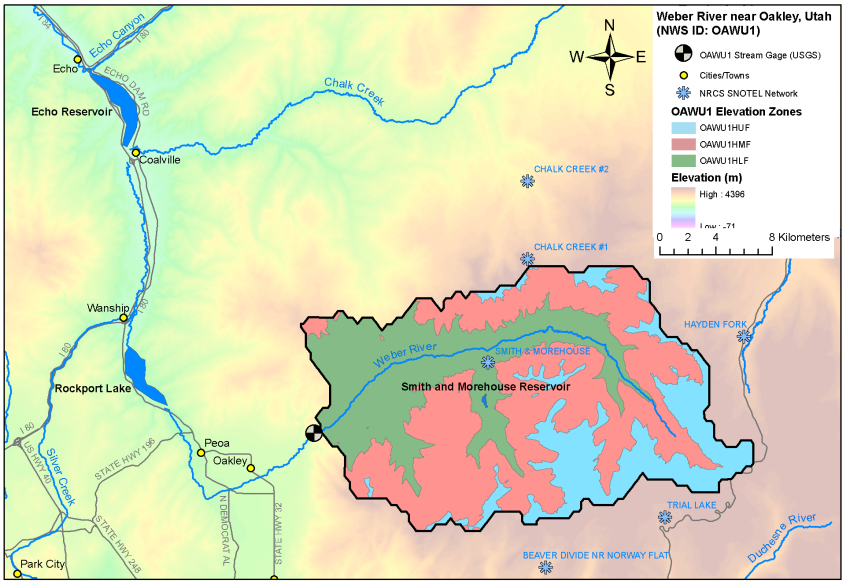

Figure 9: OAWU1 basin, with elevation zone divisions used in the NWS hydrologic model

The limited number of inputs makes SNOW17 attractive for use in an operational environment, as precipitation and temperature observations are more likely than other types of observations (radiation, wind, etc.) to be available in real time for operational forecasting (Hock, 2003). Estimates of mean areal temperature (MAT) and mean areal precipitation (MAP) are computed from point station data (usually stations from the NRCS's SNOTEL network and from the NWS's COOP network) for each elevation zone. The point stations are assigned weights that are determined in the calibration process, and those weights are used in conjunction with the point data to generate MATs and MAPs for each elevation zone. The MATs and MAPs are used to build the snowpack and drive snowmelt within SNOW17. SNOW17 is applied to each elevation zone to generate meltwater outflow that can then be passed to subsequent modules (including a soil moisture accounting model) in the forecasting system.

SNOW17 is a calibrated model; model parameters are necessary because every detail of snowpack physics is not explicitly represented in SNOW17. The parameters are intended to represent the physical characteristics of the elevation zone to which SNOW17 is applied, as well as the prevailing weather patterns (storm types, etc.). With knowledge of the characteristics of the basin to be calibrated (and parameters for surrounding basins if nearby basins are already modeled with SNOW17), users can make initial educated estimates of the SNOW17 parameters for the basin to be calibrated. The initial estimates of the model parameters can be fine-tuned within the calibration process itself. Table 6 lists the model parameters, both major and minor.

Table 6: SNOW17 Parameters (Anderson 2006, NWS 2004, and Franz and Karsten, 2013)

Model Parameter (units)	Description	Major (large effect on modeled snowpack) or minor parameter	Purpose	Typical Values	Effects on simulated snowpack
SCF [dim'less]	Snow Correction Factor	Major	Accounts for: changes to snowpack volume precipitation gage catch deficiencies caused by wind sublimation	<1.0 – high sublimation 1.0 – sheltered, non-windy sites 1.2 – reasonable default >1.2 – windy, exposed sites	Affects : water balance amount of snow that needs to melt before bare ground appears max accum SWE volume of runoff
MFMAX (mm/C/6hr)	Maximum Melt Factor – June 21	Major	Accounts for climatic and physiographic characteristics of an area, including forest cover, which is not explicitly input to SNOW17	0.5 – 0.8 – dense forest 0.8 – 1.0 – mixed forest 1.0 – 1.3 – coniferous forest 1.3 – 2.0 – open areas MF in windy areas > MF in calm areas MF in areas w/ south facing areas > those w/ north facing areas	Affects melt rate in late winter and spring (after March 21) Affects timing of snowmelt and rate of snowmelt Since MFMAX affects melt rates, it affects SWE, and also fSCA, since fSCA = f(SWE)
MFMIN (mm/C/6h)	Minimum Melt Factor – December 21	Major	Account for climatic and physiographic characteristics of an area, including forest cover, which is not explicitly input to SNOW17	0.2 – 0.3 – dense forest 0.25 – 0.4 – mixed forest 0.35 – 0.5 – coniferous forest 0.5 – 0.9 – open areas	Affects melt rate during the winter (if melt does occur during the winter). Important for areas that melt out early (southern latitudes, lower elevation, maritime climates)

Model Parameter (units)	Description	Major (large effect on modeled snowpack) or minor parameter	Purpose	Typical Values	Effects on simulated snowpack
UADJ (mm/mb/6h)	Average wind function during rain-on-snow events	Major	Account for acceleration of melt during windy rain-on-snow events	0.03 – 0.19 Lower in sheltered, less windy areas Higher in open, windy areas	Increases or decreases melt rate
ADC (no units)	Areal depletion curve	Major	Relates the snow cover extent to the amount of water equivalent left in the snowpack	Represents modeled snow cover extent (AESC) as a function of simulated SWE Consists of ten pairs of values that relate a mean areal SWE index to the areal extent of snow cover Shape depends empirically on characteristics of modeled area (land cover, heterogeneity in melt rates, etc.)	Affects rate of snowpack depletion once AESC drops below 100%
SI (mm)	Amount of water equivalent above which 100% snow cover exists	Major	Threshold below which the areal depletion curve goes into effect	During initial calibration, at least equal to or greater than the max water equivalent that occurs during the calibration period, but usually less.	If SI is increased, then ADC goes into effect earlier during the melt season. If ADC is in effect earlier, the snowpack melts more slowly. If SI is decreased, the ADC goes into effect later. If ADC is in effect later, then the snowpack melts more quickly.

Model Parameter (units)	Description	Major (large effect on modeled snowpack) or minor parameter	Purpose	Typical Values	Effects on simulated snowpack
NMF (mm/C/6hr)	Maximum negative melt factor	Minor	Determines amount of energy exchange that occurs when melt is not taking place at the snow surface. Accounts for the thermal conductivity changes within the snowpack. Function of snow density and depth	~0.05- ~0.4, depending on snow density	Affects heat conduction through the snowpack Varies with the MF. Heat conduction is scaled by NMF.
TIPM (dim'less)	Antecedent Temperature Index Parameter	Minor	Used in computation of the ATI (antecedent temperature index), which is an approximation of the temp within the snowpack at some depth	0.01 – 1.0 > 0.5 – gives weight to air temps w/in the past few 6h periods when computing ATI (appropriate for shallow snow cover) < 0.2 – gives weight to air temp over the past 3-7 days (appropriate for deep snow covers due to increased depth and heat storage capacity)	Impacts the rate at which the snowpack ripens

Model Parameter (units)	Description	Major (large effect on modeled snowpack) or minor parameter	Purpose	Typical Values	Effects on simulated snowpack
MBASE (C)	Base temperature for non-rain melt	Minor	Allows user to vary the temp. above which melt typically occurs (used when the point stations for estimating the mean areal temp. have different characteristics than the modeled area itself)	Typically 0 C in vast majority of watersheds. May be set to 0.5 to 1 C in areas w/ dense forest where stations used to estimate temperature in the area are in open areas	Impacts timing of melt
PXTEMP (C)	Threshold that defines precipitation type (rain or snow)	Minor	Provide a threshold by which to type precipitation	0.5 – 2 C. May be 3 -5 C if area characteristics allow snow to fall at higher temperatures.	Affects the volume of SWE, and fSCA, since fSCA = f(SWE) PXTEMP uncertainty is greater at lower, warmer elevs. (He et al., 2011)
PLWHC (decimal fraction)	Percent liquid water holding capacity for ripe snow	Minor	Defines the how much liquid water might be stored in a snowpack	0.02 – 0.05 Larger (0.2 – 0.3) in areas with slush layers and shallow slopes that slows the drainage rate of melt water	Impacts attenuation of meltwater through the snowpack
DAYGM (mm/day)	Average daily ground melt during a typical winter	Minor	Allows for melt at the snow-soil interface in areas where the soil is not completely frozen	0.0 - areas w/ frozen ground 0.3 – areas with mild climates and deep snow cover (e.g., Sierra Nevada) > 0.3 – areas with infrequent snow	Impacts amount of melt that may occur during the winter, at the snow-soil interface

Two important SNOW17 parameters that impact snowmelt (especially its timing) are the "maximum melt factor" (MFMAX) and the "minimum melt factor" (MFMIN), used to define a sine curve that represents the seasonally varying melt factor, which relates the amount of snowmelt to a unit change in air temperature. In the northern hemisphere, the maximum value of the SNOW17 melt factor occurs on June 21 and the minimum on December 21, indicating the relative amount of radiation incident on the snowpack at different times of the year. Incoming solar radiation peaks on the summer solstice, though the actual amount of radiation that reaches the snowpack may be altered by cloud cover or a forest canopy. As the snowpack melts through the spring and into the summer and snow grain size increases, the albedo of the snowpack is also reduced, which also affects the amount of energy absorbed by the snowpack.

The melt factor representation of the relative contributions of various energy balance components is certainly not perfect. However, implementation of a snow model into NWS operations, that includes more details of the energy balance, is still years away.

SNOW17 works well under most conditions, especially within the constraints of an operational environment. For example, Franz et al. (2008) found that SNOW17 and an energy balance model performed comparably, and in some cases, SNOW17 bested the energy balance model. However, conditions that deviate from those observed within the historical period used in the model calibration challenge SNOW17 as a temperature index model. Anderson (2006) cites one such example of warm temperatures combined with high humidity and strong winds permitting a larger than normal contribution of the sensible and latent heat terms to the energy balance. In this case, SNOW17 tends to underestimate meltwater volume (Anderson, 2006). Also, large deviations of albedo

from the assumed average conditions (perhaps from dust deposited onto the snowpack's surface) affect the energy input to the snowpack, as well as melt timing and melt rates. Since SNOW17 does not explicitly account for albedo, situations where the snowpack albedo differs greatly from assumed normal conditions render the temperature index model less representative. Updates of model conditions via inclusion of snow observations may alleviate this shortcoming of SNOW17.

2.3.2.1 Importance of Snow Cover Extent in SNOW17

SNOW17 tracks the areal extent of snow cover (AESC) for each elevation zone of a basin as the model marches forward in time. Many of SNOW17's calculations, including those related to snowpack melt, are made assuming mean areal values and are based on 100% snow cover. For example, the equations representing melt under rainy and non-rain conditions, the change in heat storage in the snowpack, and ground melt are all based on 100% snow cover (Anderson, 2006).

SNOW17 adjusts the computed melt volumes at the surface of the snowpack and at the soil-snow interface by the snow covered area fraction before passing any melt volume to other routines or modules in the NWS hydrologic modeling system. If the modeled area or elevation zone is less than 100% snow covered, then any melt volume computed by the equations that assume 100% snow cover is multiplied by the AESC value. That volume of snowmelt (initially computed assuming 100% snow cover and then reduced by the AESC value if AESC is less than 1.0 or 100%) ultimately becomes part of the outflow from SNOW17.

Tracking snow covered area is necessary so that water volumes output from SNOW17 (initially computed assuming 100% snow cover) are adjusted before they are passed to subsequent routines and/or modules within SNOW17, such as the subroutine that routes liquid water through the snowpack, or, downstream and outside of SNOW17, the SAC-SMA soil moisture accounting model. Mathematically, the total outflow from SNOW17 that is available to other modules is defined as

$$O = \left(O_s \cdot A_s\right) + \left[\left(1.0 - A_s\right) \cdot \left(P \cdot f_r\right)\right] \qquad (6)$$

where:
O = total outflow from SNOW17 (snow cover outflow + rain-on-bare-ground) in mm
O_s = total outflow from snow cover in mm
A_s = areal extent of snow cover (fraction)
P = total precipitation amount input to the model in mm
f_r = fraction of precipitation falling as rain

2.3.2.2 Modeling Snow Cover Extent in SNOW17

SNOW17 uses an areal depletion curve (ADC), in which snow covered area is a function of snow water equivalent. Specifically, the SNOW17 ADC relates the areal extent of snow cover to a ratio of the mean areal snow water equivalent (including the ice content and water held within the snowpack against gravity) to an index, A_i (the ratio is SWE/A_i). The index A_i is the smaller of (a) the model parameter that defines the water equivalent above which 100% snow cover always exists (SI) and (b) the maximum amount of water equivalent that existed during the accumulation period (state variable

W_{max}). If W_{max} does not exceed SI in a given water year, then W_{max} is used as the A_i value. As the snowpack accumulates during the winter, W_{max} increases and may exceed the SI parameter value; in this case, A_i is set to SI.

ADCs are empirically derived for each elevation zone of a basin in the calibration process (Anderson, 2006). No single continuous function defines the ADC in SNOW17. Discrete SWE/A_i values between 0.0 and 1.0, in increments of 0.1, for a modeled area are associated with snow cover extent values (as fractions) via a look-up table. For SWE/A_i values of 0.1 to 0.9, the AESC values in SNOW17 can vary from basin to basin and elevation zone to elevation zone.

For all areas, the endpoints of the ADC are the same. At the upper end, when the modeled areal extent of snow cover in SNOW17 is equal to 1.0 (100%), SWE/A_i is also 1.0. At the lower end, as SWE/A_i approaches and goes to 0.0, AESC is held at 0.05 (AESC never reaches zero on the ADC). The lower end of the ADC is configured this way in the operational SNOW17 source code so that the remains of the snowpack, when the snowpack persists into the summer, are quickly melted. Since the AESC value acts as a multiplier on the snowpack melt volume that is computed under 100% snow cover conditions, an AESC value very near zero (for example 0.00001) would greatly reduce the melt volume in each time step as the last remaining bit of snowpack is melted. In this case, the remaining snowpack would melt very slowly and could easily persist unrealistically into the summer and early fall, every year. Holding the AESC value at 0.05 while the snowpack dwindles in terms of SWE is intended to prevent this unrealistic situation when SNOW17 is used in NWS hydro operations.

The SNOW17 ADC is empirically derived in the model calibration process at CBRFC and is not currently based on observations of SWE or snow cover. Extremely detailed observations of SWE and snow cover are usually available only as part of sharply focused research studies. The NWS RFCs model thousands of watersheds throughout the United States, and the observations needed to derive ADCs for each watershed and area modeled by the NWS (particularly SWE) simply do not exist at the current time. Hence, the NWS empirically derives the ADC to be used by SNOW17 during the model calibration process.

Users of SNOW17 (including the NWS) can estimate the shape of the ADC since the general shape is empirically associated with the basin's physiographic characteristics (elevation, forest cover, etc.) and its weather patterns. Generally, these patterns do not vary much (if at all) from year to year. Possible exceptions would be vegetation changes due to severe wildfires or outbreaks of forest pests such as mountain pine beetle. Events such as these that affect the vegetation patterns may require recalibration of SNOW17 and derivation of a new ADC for the impacted area. Figure 10 and Table 7 show and explain examples of ADCs used in SNOW17. ADCs in the CBRFC-modeled watersheds typically take the shapes of the B and C curves.

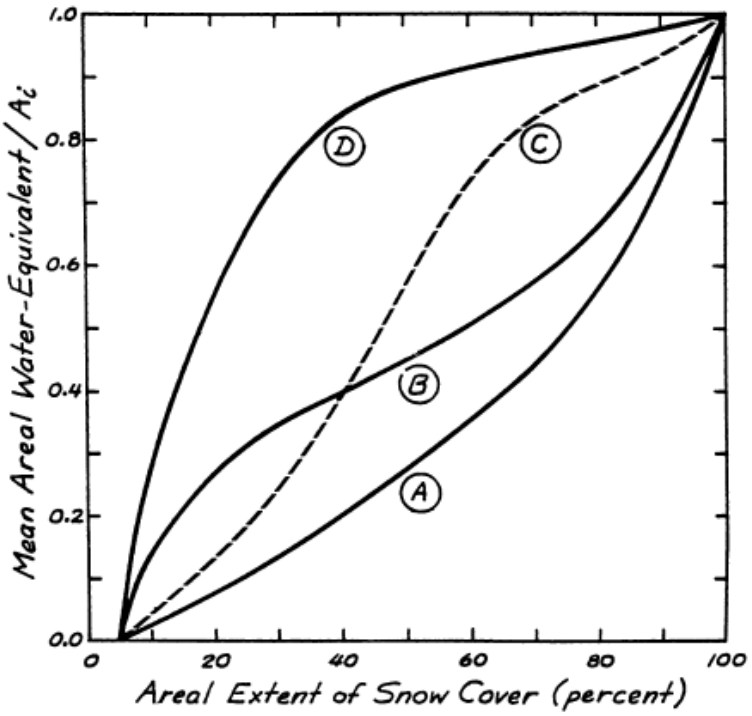

Figure 10: Examples of conceptual ADCs used in SNOW17 (NWS, 2004)

Table 7: NWS Descriptions of ADCs (NWS, 2004)

Curve	Brief Summary of Area Characteristics (NWS, 2004)
A	• As snow cover extent decreases, snow-free areas appear at an increasing rate • Common in areas where the accumulation and melt are spatially heterogeneous but where the variability is scattered across the area
B	• Similar to curve A when exposure of soil begins. Much SWE may be lost at first without much change in AESC • Common in areas where parts of the area accumulate deeper snow and/or have a significantly lower melt rate than the rest of the area. • Examples: areas in which portions are densely forested, north-facing, ravines
C	• Snow cover drops off quickly without much loss of water volume to start • Common in areas where parts of the area accumulate much less snow and/or have a much higher melt rate than the remainder. • Examples: open areas, south aspects, open areas with some forest where the forest is usually blown free of snow
D	• Area with subareas of two drastically different regimes (large accumulation/low melt rates vs. small accumulation/high melt rates) • In areas where the best ADC fits a pattern such as Curve D, the area should be divided and each portion modeled separately.

2.3.2.3 Snow Cover Extent from SNOW17 vs. Observed fSCA

An additional caveat of SNOW17 is that the snow cover extent value calculated by the model, AESC, is not 100% directly comparable to fSCA observations from satellite instruments like MODIS. SNOW17, like all models, does not perfectly represent all physical processes. The SNOW17 AESC value is calculated from a depletion curve that is determined in the model calibration process; the depletion curve is not directly derived from observations during the calibration process at CBRFC.

The calibration-derived depletion curve does not *explicitly* include certain aspects of the physical areal depletion of snow cover such as the decrease in melt rate that occurs over time as the snow cover extent decreases. For example, as the snow melts, shallow snow or snow on south faces melts more quickly than deep stashes of snow in shaded areas. Areas of deep snow endure the longest into the melt season, as they melt slowly.

The empirically-derived ADC represents an attempt to address the decrease in melt rates with time for a modeled area, as a function of SWE. As the snowpack depletes and the SWE decreases, the AESC value diagnosed from the ADC as a function of SWE changes. Before the snowpack SWE accounting occurs within a model timestep, the AESC value is used as a multiplier on the melt volume that is initially computed assuming 100% snow cover. Therefore, as the SWE changes, the amount of meltwater that is ultimately deducted from the snowpack and, subsequently, the snowpack melt rate are impacted by the AESC value diagnosed from the ADC curve.

Dividing a basin into additional, smaller elevation zones (i.e., moving towards a distributed model), for which model parameters could be estimated from an analysis of

the basin's physical characteristics, may allow for better representation of the variation in melt rates across a mountainous area. Yet, even with higher spatial resolution, no model can perfectly represent real world hydrologic systems, so calibration of model parameters by a user will still be needed, at least to some extent.

Verification of melt rates and the values of model parameters related to melt rates would still be difficult even if a watershed was subdivided into smaller areas. NRCS's SNOTEL network provides the most extensive network of point SWE measurements in the western U.S., but the network of point stations is not dense enough to comprehensively represent the variation in melt rates across mountainous terrain on a fine scale. Satellite-derived SWE retrievals from microwave sensors such as NASA's AMSR-E instrument are spatially more extensive than the SNOTEL network. Yet, they are of coarse horizontal resolution (25 km), and their use is limited by accuracy problems, especially in areas with deep snowpacks and dense vegetation (Derksen et al. 2003). For a melt rate verification study, obtaining a data set of SWE observations sufficient for verification (either from point networks such as SNOTEL, from satellite microwave retrievals, or a combination of the two) would be difficult. Due to limitations in observations available to verify melt rates in SNOW17, users still need to rely on the calibration process and empirical derivation of model parameters related to the simulated melt rate and snow cover depletion.

The fact that snow covered area values expected by SNOW17 do not exactly correspond to what observed fSCA from MODIS represents manifests itself in streamflow simulations when DI of observed fSCA takes place. These impacts will be explained in detail in Chapter 5.

2.3.3 Updating Hydrologic Models with Observed fSCA

Many objective, quantitative data assimilation methods for updating model states (including those related to snow cover) are available for use in hydrologic modeling systems. Data assimilation methods blend information from observations and information from models into more accurate estimates of a system's true state. Hydrologic applications of sophisticated data assimilation techniques, such as the Kalman filter (KF) and its variations such as the Ensemble Kalman Filter (EnKF), as well as particle filters, are currently limited to the research community. None are used in NWS hydro operations as of June 2013. However, sophisticated data assimilation is attractive as a potential way to improve the NWS's operational streamflow predictions (Liu et al., 2012). Sophisticated DA techniques could help the NWS advance its hydrologic science and potentially reduce errors in its streamflow predictions. Yet, the infrastructure of the NWS operational environment does not currently support such methods and their requirements, especially with respect to computing power required by advanced methods. Techniques to update hydrologic models with snow covered area observations in the current (June 2013) NWS hydrologic operational implementation are limited to subjective manual updates and/or DI.

Direct insertion is a simple substitution of an observed value in place of a model estimate of that value, without attempting to correct the model step or steps that led to the difference. Information from a remotely sensed fSCA observation would replace a model's AESC estimate. The observed fSCA value can be substituted as-is, or rule-based DI schemes may be applied, in which the information from the observation is

transformed in some way before being inserted into the model. These transformations usually involve a small amount of SWE being added to a modeled area if the model has no snow and the observed data indicate snow is still present, and zeroing out the model snow if the observed data indicate that the area is snow-free. The amount of SWE added to the snow model varies among research studies that use this technique. For example, Fletcher et al. (2012) added 0.01 m of SWE to a model cell when their snow model had melted out and the MODIS snow cover data indicated that the snowpack was still present. Rodell and Houser (2004) added 5 mm of SWE to the modeled areas, at the timestep coincident with the Terra satellite overpass, if the MODIS snow cover was greater than 40% and the model was snow free. They found that the addition of SWE, as inferred by MODIS snow cover data, improved their model's SWE simulations over the Great Plains of the central United States and over the Midwestern United States when compared to observations from ground-based point stations. Tang and Lettenmaier (2010) added the same amount of water equivalent (5 mm) when MODIS indicated that snow was present yet the model indicated it was absent. The amount of added SWE in these studies is usually only a small amount, in order to minimize impacts on the model water balance.

The current operational version of SNOW17 allows updating of snow cover extent via DI. To activate the DI option, a flag is set in the SNOW17 configuration file, indicating which elevation zones of a modeled basin should use the DI. A tolerance value is also set in the SNOW17 configuration file, specifying when the observed fSCA should be inserted into the model. If the difference between the observed and modeled snow cover extent values exceeds the set threshold, then the fSCA observation is used in place of SNOW17's AESC estimate. Otherwise, the observation is ignored.

Configuration of SNOW17 to include DI is discussed further in Section 4.6 with respect to the set up specific to the case study experiment.

While DI is a simple technique that does not require many computer resources, even with rules applied beyond the most basic implementation of DI, it assumes that the information contributed by the observations is perfect. When the model estimate of AESC is completely replaced by the observation's fSCA value, DI implies that the model does not contribute any information. Direct insertion does not make use of any kind of error estimates for either the model or the observations. Caution must be exercised because of inaccuracies that do in fact exist in the observed data sets due to a variety of causes (e.g., cloud cover, vegetation, properly identifying snow from clouds, etc.). Also, DI of one type of observation does not propagate information from the inserted observation to other model states.

Despite the drawbacks of the DI technique, DI is the easiest way for operational NWS RFCs to quantitatively use observed fSCA values in their modeling efforts as NWS hydrologic operations are currently organized. Given the constraints of the operational NWS hydrologic forecasting environment, and because the current operational environment of NWS RFCs requires generation of hydrologic predictions in a timely and reliable manner, simpler techniques that are computationally frugal are desirable. Hence, this study focuses on the simple DI technique and the impacts of using remotely sensed snow cover via the DI method.

CHAPTER 3: OVERVIEW OF STUDY BASIN

3.1 GENERAL BASIN CHARACTERISTICS

This study focuses on the headwaters of a snow-dominated, mountainous basin: the Weber River. Figure 11 shows the location of the Weber River headwaters within the region. The Weber River is a tributary of the Great Salt Lake; its headwaters are located in the western Uinta mountains of northeastern Utah. The basin snowpack has distinct accumulation and ablation seasons, and the basin's flow is dominated by snowmelt.

The drainage spans 418 km^2 (161 mi^2). Elevations within the basin range from 2024 m (6640 ft) at the outlet near the town of Oakley to 3570 m (11,714 ft) in the southeastern part of the basin. Flow at the outlet is measured by United States Geological Survey (USGS) stream gage #10128500. The higher elevations of the basin are popular for recreational activities in the Uinta-Wasatch-Cache National Forest (Fig. 12). The basin is heavily forested, with some development in the form of farms and residential areas in the lower elevations.

There is one reservoir within the basin, Smith and Morehouse Reservoir, operated by the Weber Basin Water Conservancy District (WBWCD). The reservoir is small (1.7 MCM/1,360 AF) and typically fills and spills each spring (UT DWQ, 2006). The Weber River is a major source of inflow to Rockport Reservoir, which provides water to WBWCD customers. Table 8 summarizes the characteristics of the headwaters of the Weber River, and Fig. 12 shows the watershed and the surrounding area.

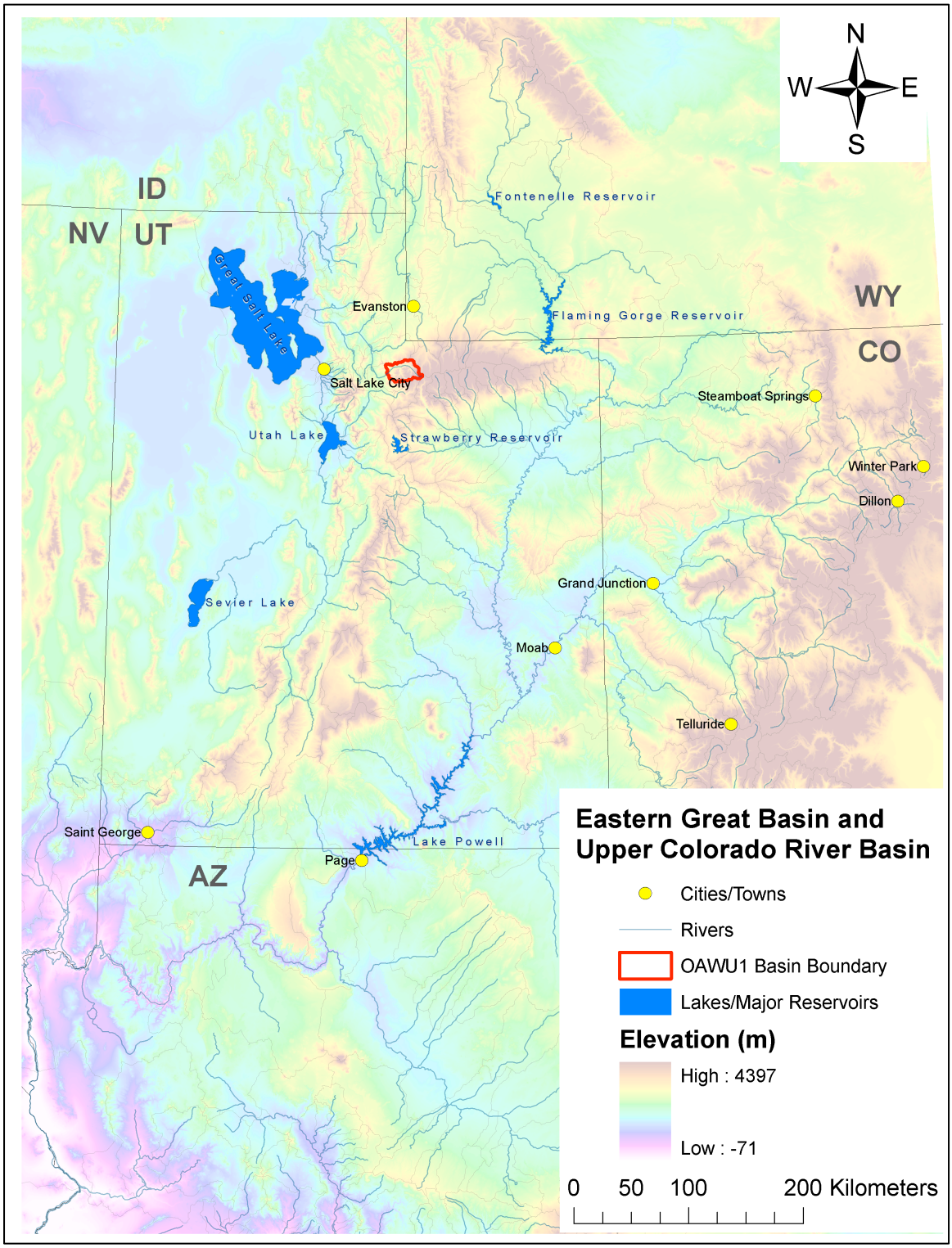

Figure 11: Overview map of the Upper Colorado River Basin and the Eastern Great Basin, including case study basin

Table 8: Characteristics of the Weber River Headwaters

Weber River Headwaters Characteristics	
NWS ID:	OAWU1
Tributary of:	Great Salt Lake
Mountain Range:	Uinta
Drainage area:	418 km^2 (161 mi^2)
Elevation: Maximum: Minimum:	 3570 m (11,714 ft) 2024 m (6640 ft)
Land Use/Cover:	Primarily forested, open rocky areas at highest elevations
Population Centers:	Headwater area above Oakley: mostly farms, some homes Downstream: Oakley, UT
Reservoirs/Diversions:	Smith and Morehouse Reservoir is located within the OAWU1 basin but is not explicitly modeled by CBRFC. The reservoir has a small capacity of 1.7 MCM or 1,340 AF (UT DWQ, 2006). It fills and spills with spring snowmelt, so it generally has minimal effect on streamflow predictions.

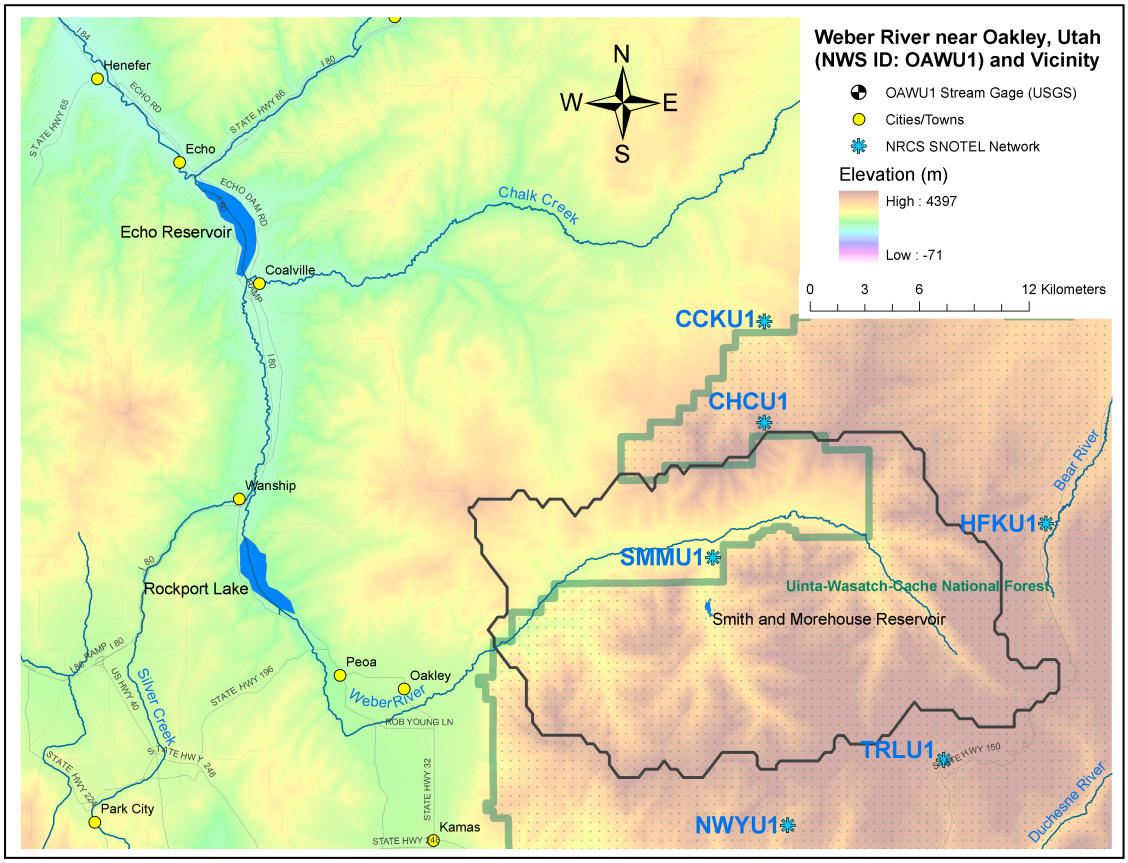

Figure 12: Weber River headwater basin and surrounding area, including nearby SNOTEL sties

3.2 LAND COVER AND VEGETATION PATTERNS

The OAWU1 watershed is divided into three subareas (upper, middle, and lower subarea), which are modeled as separate units by the NWS. (Model configuration for the OAWU1 basin is discussed in detail in Section 4.4.) Because the operational NWS hydrology program currently uses lumped models, the spatial variation of vegetation patterns and land use patterns within each elevation zone is not explicitly accounted for within the operational NWS hydrologic modeling system. However, the patterns are discussed in this chapter that summarizes characteristics of the Weber River headwaters because they do play an important role in the derivation of MODIS-derived snow cover, especially the MODSCAG product, and in the variability of actual snow melt rates.

Patterns in vegetation and land use were analyzed with the 30 m 2006 National Land Cover Database (NLCD) (Fry et al., 2011). The gridded data were downloaded from the Multi-Resolution Land Characteristics Consortium (MRLC). The percentage of the OAWU1 areas identified with various land cover types was computed; the land cover types are summarized in Table 9. As shown in Fig. 13, the OAWU1 basin and its subareas are heavily forested. Forest cover overwhelmingly dominates the basin as a land cover type, with 70% of the upper subarea, 87% of the middle subarea, and 86% of the lower subarea covered in some type of forest. The forest type for the upper and middle subareas is mostly evergreen, and the lower subarea is mostly deciduous forest. The large extent of deciduous forest impacts the MODSCAG retrievals during the winter, when the deciduous canopy is absent (discussed later in section 3.4.2).

A large portion (18%) of the upper subarea is identified as “barren land” or rock. The middle and lower subareas have less than 5% of the “barren land” class. Figures 13 and 14 show typical land cover of the upper and middle portions of the Weber River headwaters, including several clear examples of “barren land”. Peaks are rocky and mostly above the treeline, and the terrain leading up to the peaks is steep with little vegetation. Expansive vegetation (mostly coniferous, evergreen forest with accompanying understory) spans the flat and more gently sloped areas of upper and middle portions of the basin. The vegetated areas also include alpine meadows and bogs.

The lower subarea of the OAWU1 basin is also heavily forested, but instead of evergreen forest, deciduous trees dominate the lower elevations. Shrub, grassland, and pastures also appear in the lower subarea, where several ranches and farms are located. As elevation decreases, the amount of developed land (large residential lots with grass as well as parks) increases.

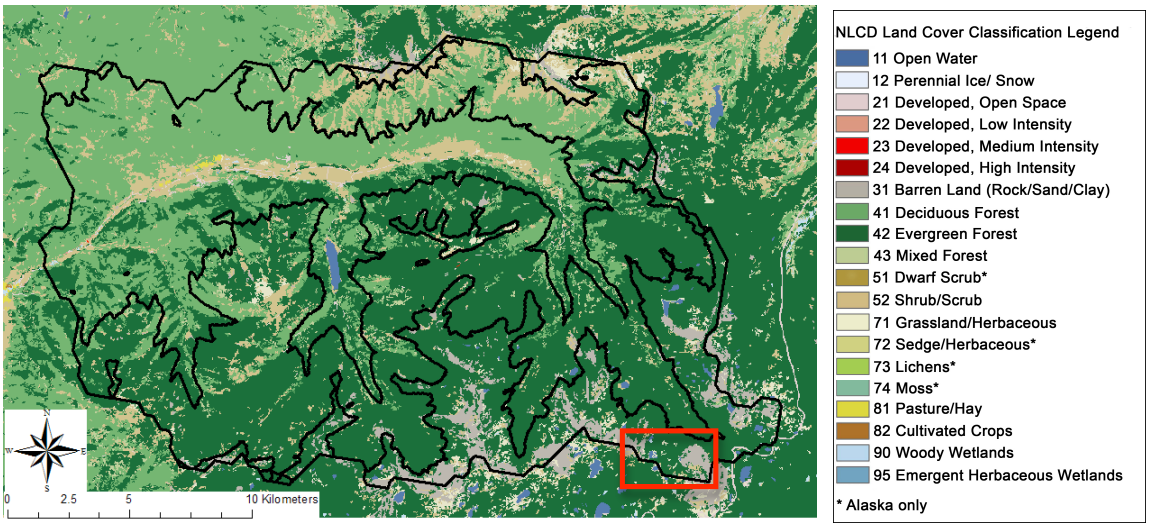

Figure 13: NLCD 2006 land cover for OAWU1 basin and subareas. The red box indicates area shown in Figure 14.

Figure 14: Typical landscape of the far upper Weber R. headwaters basin, as viewed from just outside OAWU1 basin boundary atop Bald Mountain at 3640 m. (Credit: T. Love, United States Forest Service)

Table 9: OAWU1 land cover types according to NLCD 2006, with dominant land cover types in bold

NLCD Class	Upper Elev Zone Pixel Count	% of elevation zone area	Middle Elev Zone Pixel Count	% of elevation zone area	Lower Elev Zone Pixel Count	% of elevation zone area	Total Basin Pizel Count	% of total basin area
11 – open water	1,002	1.1%	246	0.1%	790	0.5%	2,038	0.4%
21 - Developed - Open Space	162	0.2%	110	0.0%	1,337	0.9%	1,609	0.3%
22 - Developed - Low Intensity	0	0.0%	20	0.0%	61	0.0%	81	0.0%
23 - Developed - Medium Intensity	0	0.0%	7	0.0%	6	0.0%	13	0.0%
31 – Barren Land (Rock/Sand/ Clay)	15,825	17.6%	2,356	1.0%	103	0.1%	18,284	3.9%
41 - Deciduous Forest	209	0.2%	43,403	19.0%	**84,630**	**58.4%**	128,242	27.6%
42 - Evergreen Forest	**62,101**	**69.0%**	**155,853**	**68.1%**	39,709	27.4%	**257,663**	**55.5%**
43 - Mixed Forest	110	0.1%	5,061	2.2%	2,054	1.4%	7,225	1.6%
52 - Shrub/Scrub	6,351	7.1%	20,222	8.8%	15,557	10.7%	42,130	9.1%
71 - Grassland/ Herbaceous	4,249	4.7%	1,642	0.7%	247	0.2%	6,138	1.3%
81 - Pasture/Hay	0	0.0%	0	0.0%	272	0.2%	272	0.1%
90 – Woody Wetlands	49	0.1%	51	0.0%	170	0.1%	270	0.1%
95 - Emergent Herbaceous Wetlands	0	0.0%	0	0.0%	15	0.0%	15	0.0%
Total num 30 m pixels	90,058	100.0%	228,971	100.0%	144,951	100.0%	463,980	100.0%
Area (km^2)	81	100.0%	206	100.0%	130	100.0%	418	100.0%

3.3 WY2000 TO WY2010 STREAMFLOW

During the study period of water years 2000 to 2010, the annual streamflow at the outlet gage for the OAWU1 basin consists of a distinct snowmelt-driven peak in the spring and baseflow for the remainder of the year (Fig. 15). The snowmelt peak flow slightly exceeded the flood threshold established by the Salt Lake City NWS Weather Forecast Office (WFO) in the spring of 2010. For all other years in the study period, the peak flows remain below the flood flow threshold (71.1 $m^3 s^{-1}$).

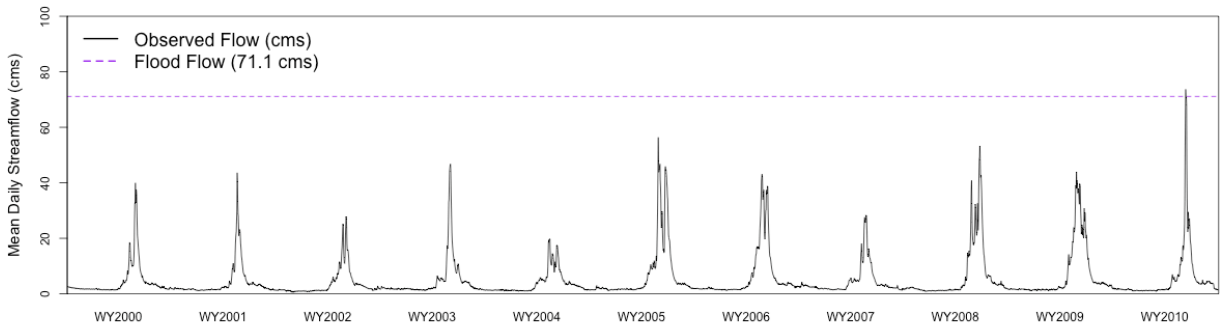

Figure 15: Observed mean daily streamflow for WY2000-WY2010 for the Weber R. near Oakley, UT

Seasonal runoff volumes for April – July range from 80.85 million cubic meters (MCM) in WY2004 to 174.32 MCM in WY2005 (Table 10). Water years 2002 and 2004 had the lowest runoff volumes while 2005 and 2009 had the highest. The mean streamflow volume for the April – July period for WY2000 to WY2010 is 118.99 MCM, and the median is 105.30 MCM.

Table 10: Observed seasonal runoff volumes for OAWU1 for WY2000 to WY2010

Year	Observed April – July Runoff Volume (MCM/KAF)	Rank (1 = smallest runoff volume of study period,11 = largest runoff volume of study period)
2000	94.48 MCM (76.60 KAF)	5
2001	87.56 MCM (70.99 KAF)	3
2002	82.96 MCM (67.26 KAF)	2
2003	105.30 MCM (85.37 KAF)	6
2004	80.85 MCM (65.55 KAF)	1
2005	174.32 MCM (141.32 KAF)	11
2006	150.68 MCM (122.16 KAF)	8
2007	88.36 MCM (71.63 KAF)	4
2008	158.38 MCM (128.40 KAF)	9
2009	168.54 MCM (136.64 KAF)	10
2010	129.64 MCM (105.10 KAF)	7

3.4 TYPICAL SNOWPACK PATTERNS

The snowpack within the Weber River headwaters exhibits distinct seasonal accumulation and ablation patterns. Under normal conditions, the snowpack begins to accumulate in October and November. Peak snowpack generally occurs near April 1, and the snowpack normally melts out between late May and early July. Typical snowpack evolution patterns evident in SWE data from SNOTEL stations, as well as patterns in MODIS snow cover data, are discussed below.

3.4.1 SNOTEL SWE

The NRCS SNOTEL network is a crucial source of snowpack information, especially SWE information, throughout the western United States. These automated

monitoring stations report precipitation, snow water equivalent, temperature, soil moisture, and other variables at hundreds of locations in the western U.S.

The OAWU1 basin has one SNOTEL site located within the basin (SMMU1) and five others nearby, just outside the basin boundary (CCKU1, NWYU1, CHCU1, HFKU1, TRLU1 – see Table 11 and Fig. 12). The elevations of the SNOTEL sites range from a moderate elevation of 2317 m (7,600 ft) to high elevations of nearly 3040 m (10,000 ft).

Table 11: Characteristics of SNOTEL sites within and near OAWU1 (shown in Fig. 12)

Long Name	NWS ID	NRCS ID	Elevation	Installation Date
Smith & Morehouse	SMMU1	763	2317 m (7600 ft)	1978-10-01
Chalk Creek #2	CCKU1	393	2487 m (8158 ft)	1978-10-01
Beaver Divide Near Norway Flat	NWYU1	330	2524 m (8280 ft)	1978-10-01
Chalk Creek #1	CHCU1	392	2742 m (8993 ft)	1978-10-01
Hayden Fork	HFKU1	517	2808 m (9212 ft)	1978-10-01
Trial Lake	TRLU1	828	3036 m (9992 ft)	1978-10-01

The WY2000 to WY2010 mean peak SWE among SNOTEL sites within and surrounding the OAWU1 basin ranges from 240 to 580 mm, and the range of the median peak SWE is similar, from 250 to 540 mm (Fig. 16). The mean meltout dates range from mid May to late June, and the median meltout dates occur earlier than the mean meltout dates, ranging from approximately May 1 to June 1. The higher elevation and north slope sites (TRLU1, CHCU1) melt out last, which is expected.

NWYU1, a lower elevation SNOTEL site to the south of the OAWU1 basin, tends to accumulate the smallest snowpack, in terms of SWE, and it also melts out the earliest. CHCU1, with an elevation of approximately 2800 m (9000 ft), tends to accumulate the largest snowpack. Along with TRLU1, CHCU1 is typically the last of the

six SNOTEL stations in the group to melt out. TRLU1, the SNOTEL site with the highest elevation accumulates a slightly smaller snowpack, in terms of mean SWE, than CHCU1, which is ~230 m (750 ft) lower in elevation. Local site characteristics and/or a limited time period of analysis (only 11 years) may be the cause of the lower elevation site (CHCU1) apparently accumulating a larger snowpack than the upper elevation site (TRLU1). TRLU1 is more open and susceptible to wind, and CHCU1 is located in a more heavily forested area on a north slope.

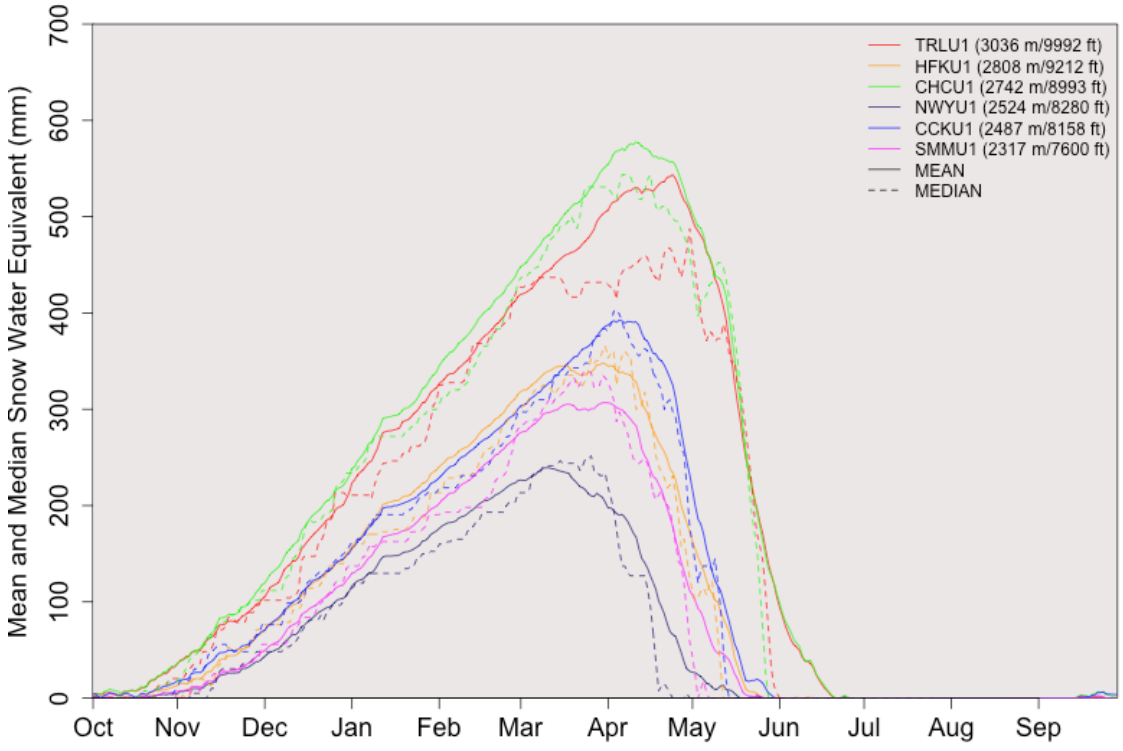

Figure 16: Mean and median SWE for WY2000 to WY2010 (n=11) for SNOTEL sites within and near the OAWU1 study basin

3.4.2 MODIS-derived fSCA

The mean and median of the spatial averages of fSCA were computed over the OAWU1 elevation zones for WY2000 to WY2010 for data sets of two MODIS-derived snow cover (MOD10A and MODSCAG). Mean areal fSCA from days when cloud cover was 50% or less was used to compute the mean and median fSCA time series for the elevation zones, shown in Fig. 17.

The most obvious difference between the two data sets is that mean areal fSCA from MODSCAG is much less than the mean areal fSCA from MOD10A, particularly during the winter. This pattern is consistent with Rittger et al. (2013), who found that, when compared to fSCA from Landsat ETM+ in the western United States, MOD10A tends to overestimate viewable fSCA (no correction for vegetation) during the winter and underestimate fSCA in the late spring, as the snowmelt runoff season progresses. Also, in mid December through late March, the lower elevation zone (in green) is estimated to have more extensive snow cover than the middle zone (red) by the MODSCAG mean areal fSCA time series. This difference between snow cover patterns in the middle and lower elevation zones is most likely due to deciduous trees (canopy-free in the winter) dominating the lower subarea/elevation zone while the middle and upper elevation zones are dominated by coniferous, evergreen forest (Fig. 13, Table 9). During the winter, when the deciduous trees are free of leaves, MODIS would be better able to detect the snowpack on the ground. A higher fSCA value would be observed in a deciduous forest in the winter, simply because MODIS can detect the snowpack on the ground more easily in the deciduous forest than the evergreen forest that has a denser winter canopy. This effect is exacerbated when the coniferous forest is *not* covered in fresh snow. The

MODSCAG fSCA data used in this study are *viewable* fSCA, with no correction or adjustment for vegetation.

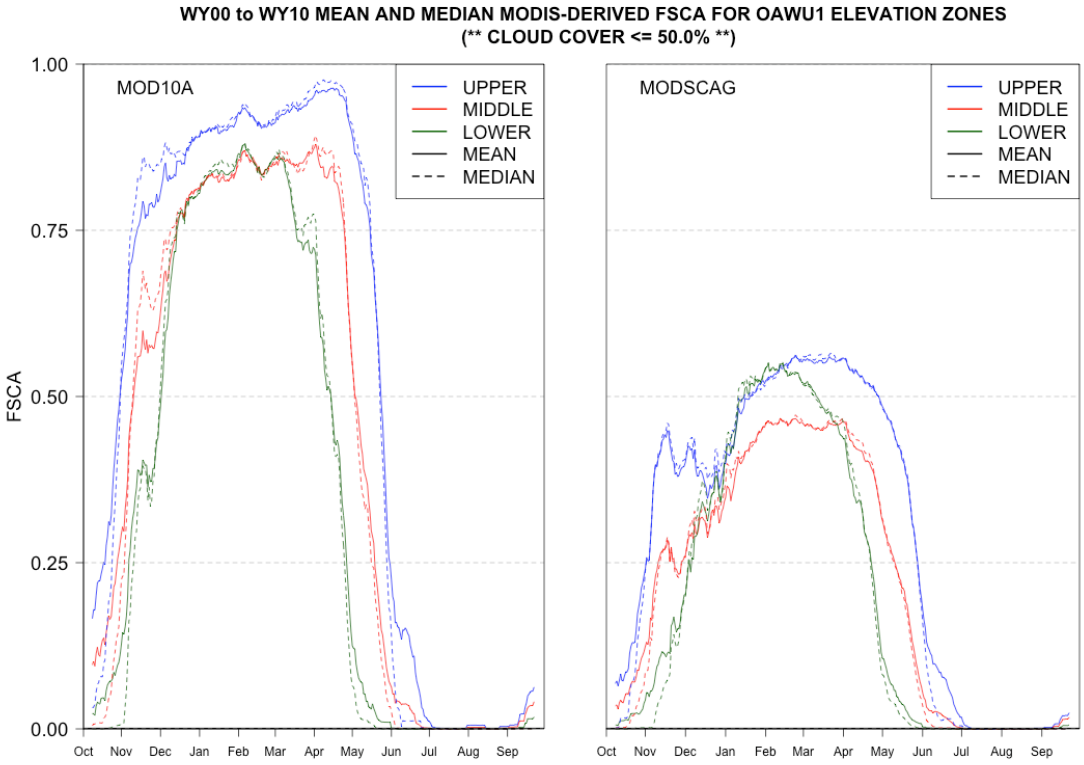

Figure 17: Mean and median MODIS FCA for WY2000 to WY2010 for OAWU1 elevation zones

When the snowpack begins to melt, Fig. 17 shows a logical order with respect to elevation. The snowpack in the lower elevation zone (green) begins to melt first, then the middle, and finally the upper elevation snowpack. Once the snow cover begins to deplete in earnest, it depletes more quickly at the lowest elevations (green curve), especially when patterns in the MODSCAG product are examined. The more rapid rate of snow cover depletion in the lower elevations is related at least in part to the fact that (1) higher temperatures exist at lower elevations and (2) the lower areas of the OAWU1 basin are

covered in deciduous trees, which allow more incoming solar radiation to reach the snowpack before the deciduous canopy is fully realized later in the spring and early summer. Longwave radiation from a coniferous forest could be argued as a major contributor to snowmelt in the middle and upper elevations and it does, in fact, contribute to snowmelt. However, the incoming solar radiation usually dominates the energy balance in the spring, especially the late spring as the summer solstice approaches. A detailed examination of energy balance components is reserved for future work (see Section 6.3).

CHAPTER 4: CASE STUDY DATA SETS AND METHODS

4.1 INTRODUCTION

The methods of this case study are used to evaluate how DI of satellite-derived fSCA observations might impact model estimates of the snowpack and subsequent streamflow simulations in an operational environment. This research focuses specifically on the impacts of moderately high-resolution (defined as sub 1 km spatial resolution and daily temporal resolution) satellite-derived snow cover observations in conjunction with a simple snow updating method on streamflow predictions, during the water years of 2000 to 2010.

4.2 TYPES OF PREDICTION: SIMULATIONS VS. FORECASTS

In the operational environment at CBRFC, hydrologic models (including SNOW17) are used to make two types of predictions: simulations and forecasts. Simulated streamflow is the best estimate of streamflow that a model, with forcing data derived from quality-controlled observations and with parameters tuned by a user with comprehensive knowledge of a basin, can provide. Simulations are usually run retrospectively, that is, for events that have occurred in the past and for which verified observational data are available. Streamflow forecasts use the model parameters derived during the calibration process, as well as forecasts of forcing variables (e.g., temperature and precipitation).

The calibration process uses thoroughly quality-controlled input data (temperature and precipitation) to force the model and, ultimately, simulate streamflow. Typically, the point observations used in the model calibration process (which are subsequently transformed into mean areal forcing data for the calibration period) require a dedicated effort and a large amount of time to collect and quality-control, either by CBRFC or by other agencies, such as the NRCS, the agency responsible for the SNOTEL network. Use of quality-controlled observations to produce model forcings reduces the amount of system uncertainty that results directly from the input observations. With this reduced uncertainty, model users can be more confident that the model parameters they derive are more representative of the physical processes that the modeling system aims to represent. Calibration of the snow and soil moisture models may require multiple iterations as the model user finely tunes the parameters. Ultimately, a model that uses more appropriate parameters and coefficients has a better chance of predicting the streamflow that is eventually observed, whether in simulation mode or forecast mode.

The model parameters derived in the calibration process are then used in real-time operational model runs. Forecasts are the prediction of streamflow in real-time, using input data that are available in real time. Temperature and precipitation observations that are available in real time typically have more uncertainty in them than observations that have been thoroughly reviewed in a retrospective manner. Streamflow forecasts also rely on temperature and precipitation forecasts. Forecasts of the forcing variables can be highly uncertain, especially forecasts of precipitation. Due to these important differences between the input data sets for the simulations and forecasts, the simulations usually provide better predictions than forecasts.

All simulations (control and DI) use the same temperature and precipitation observations as input and the same model parameter set that was derived as part of the most recent CBRFC calibration effort. As mentioned above, the forcing data used in the study simulations has been quality-controlled retrospectively by both the data provider and CBRFC.

Using the mean areal temperature and precipitation, the model simulates accumulation and melt (which then drives the majority of simulated streamflow during the melt season, barring a large rain event). Observed fSCA is not included in the control simulation in any manner. As in current RFC operations, snow water equivalent and areal snow cover extent are completely model-driven in the control simulation.

4.3 INPUT DATA SETS

4.3.1 Meteorological Input Data Sets

Since SNOW17 is run operationally at CBRFC in lumped mode over elevation zones, mean areal temperature (MAT) and mean areal precipitation (MAP) estimates are input to and used as forcing data in the operational CBRFC modeling system. These estimates are derived by CBRFC from point station observations (primarily from the NRCS SNOTEL and NWS COOP networks) over the WY1981-2010 historical period used in the most recent round of calibration. In the calibration process, weights that depend on distance and elevation relative to the elevation zones are determined for each point station. Then, these weights are used to compute the mean areal temperature and precipitation values from point observations at each time step in the WY1981-WY2010

historical period. This study uses MAT and MAP estimates for WY2000 to W2010 (water years common to both the MODIS period of record and the historical period used in the most recent calibration). The forcing data are used as-is from CBRFC; no modifications are made to them.

No explicit quantitative estimates of uncertainty in the mean areal forcing data for areas that CBRFC models in its operations are currently available. Qualitatively, the snowmelt simulations will result in streamflow predictions that deviate noticeably from observations if mean areal temperature is altered by an increment of more than approximately 2 F (1.1 C) (RFC Staff, pers. comm., 2013), and Smith et al. (2003) note that a bias of just a few degrees can shift the timing of snowmelt. Anderson (2002) states that a bias of 10% in the MAP values may lead to a change in runoff of 10-25%. Uncertainty in the forcing data should be explicitly estimated but is left as task for future work (see Section 6.3).

4.3.2 MODIS-derived fSCA Observations Used in the Study

The MODIS fSCA data sets used in this study are the MOD10A and MODSCAG data sets described in Chapter 2. Both MODIS fSCA data sets are daily gridded products, available at 500 m resolution. Though MODIS data sets span the globe, they are made available as a collection of smaller pieces in order to facilitate management and transmission of the data. Each individual subset of the global data set, or tile, is made available from NASA in a sinusoidal projection. Four individual MODIS tiles are needed for complete coverage over CBRFC's area of responsibility (AOR). Figure 18 shows the necessary tiles (reprojected to the Universal Transverse Mercator Projection).

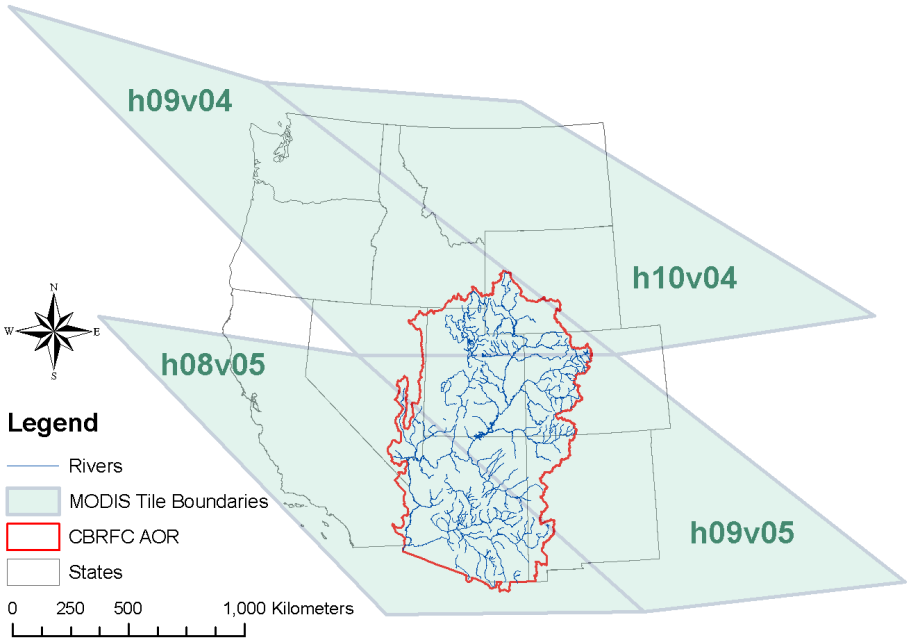

Figure 18: MODIS tiles that cover the CBRFC area of responsibility (AOR)

MODIS provides global coverage, so, spatially, data are potentially available across the entire CBRFC area of responsibility, depending on cloud cover. Over the case study basin, hundreds of pixels are available across each elevation zone on clear days. On cloudy days, the number of non-cloudy pixels that provide fSCA information may be as low as zero.

Overall, RMSE of the MOD10A fSCA data set is 0.10 when validated against 30 m Landsat ETM+ data processed with the binary SNOWMAP algorithm, aggregated to 500 m pixels (Salomonson and Appel, 2004 and 2006). Salomonson and Appel (2004, 2006) included several areas of North America, as well as Scandinavia, Russia, Chile, and Argentina in their study of MODIS-derived fSCA. Rittger et al. (2013) validated the MOD10A and MODSCAG fSCA products against Landsat ETM+ fSCA derived with spectral mixture modeling over several areas of North America and the Himalaya. Their

results indicated that the overall RMSE for MOD10A is 0.23 while overall RMSE of the MODSCAG data set is 0.10 when the validation data set, Landsat ETM+ fSCA, is derived with spectral mixture models. In their study, the mean and median differences between Landsat ETM+ fSCA and MODIS-derived fSCA for each study area were similar, so they focus on median differences in their report. For the areas in their study, the median differences in fSCA between the Landsat and MODIS fSCA data ranged from -0.34 to 0.35 for the MOD10A product and -0.16 to 0.04 for the MODSCAG product.

In this study, each gridded MODIS fSCA data set was averaged over the OAWU1 elevation zones to create a time series of mean areal fSCA for each elevation zone. Only non-cloudy pixels were considered when generating mean areal fSCA. The OAWU1 basin and its elevation zones lie within MODIS tile h09v04. No corrections for vegetation are included in the versions of the data sets used as part of this study. Use of MODIS fSCA adjusted for vegetation is left for future work (see Section 6.3).

The MOD10A mean areal fSCA values were derived from the gridded data sets for the time period of February 24, 2000 to June 30, 2011 by RTi (2011), using MODIS tiles downloaded from the National Snow and Ice Data Center, a polygon shapefile of elevation zones provided by CBRFC, and ESRI's ArcGIS Zonal Statistics tool. The percentage of the polygons that had indeterminate snow cover (including cloudy pixels) was also computed and included in the data set as a data quality indicator.

CBRFC generated MODSCAG mean areal fSCA values for the study basin's elevation zones for the MODIS period of record (February 24, 2000 to present). Data for February 2000 through December 2012 were processed as a batch in late 2012. For 2013 data, CBRFC downloaded MODSCAG tiles and processed the gridded data sets into

scalar mean areal fSCA values in near real time, on a daily basis. The MODSCAG tiles are available in near real time; they are typically posted to the NASA/JPL server 18 to 36 hours after MODIS first acquires the scene. The mean areal fSCA values are computed by CBRFC using open source tools, including R and utilities from the Geospatial Data Abstraction Library (GDAL). Specifically, the rgdal and raster packages are used in addition to the default R and GDAL utilities. The percent of the elevation zone that is cloud covered is also computed and saved for the MODSCAG data sets.

This study uses mean areal fSCA from days when cloud cover over each elevation zone is 50% or less, for WY2000 to WY2010. For days when cloud cover is greater than 50%, the mean areal fSCA value is set to missing in the fSCA files that are input to SNOW17. The 50% cloud cover threshold is arbitrary. Investigation of the sensitivity of the streamflow simulations to a variety of cloud cover thresholds is planned as future work (see Section 6.3).

Figure 19 shows a time series of MODIS-derived observed mean areal fSCA for the entire study period, for both MODIS-based data sets (MOD10A and MODSCAG). MODIS-derived mean areal fSCA for all three elevation zones within the OAWU1 basin (Fig. 9) are shown in Fig. 19 (upper zone in blue, middle in red, lower in green). These data are used in the DI simulations. Gaps appear in the time series where the cloud cover exceeded the 50% threshold on a particular day, or because data were missing or flagged for another reason (e.g., the source files were not available from the data server, or another problem occurred, such as MODIS fSCA erroneously being set to zero in all scenes in mid winter).

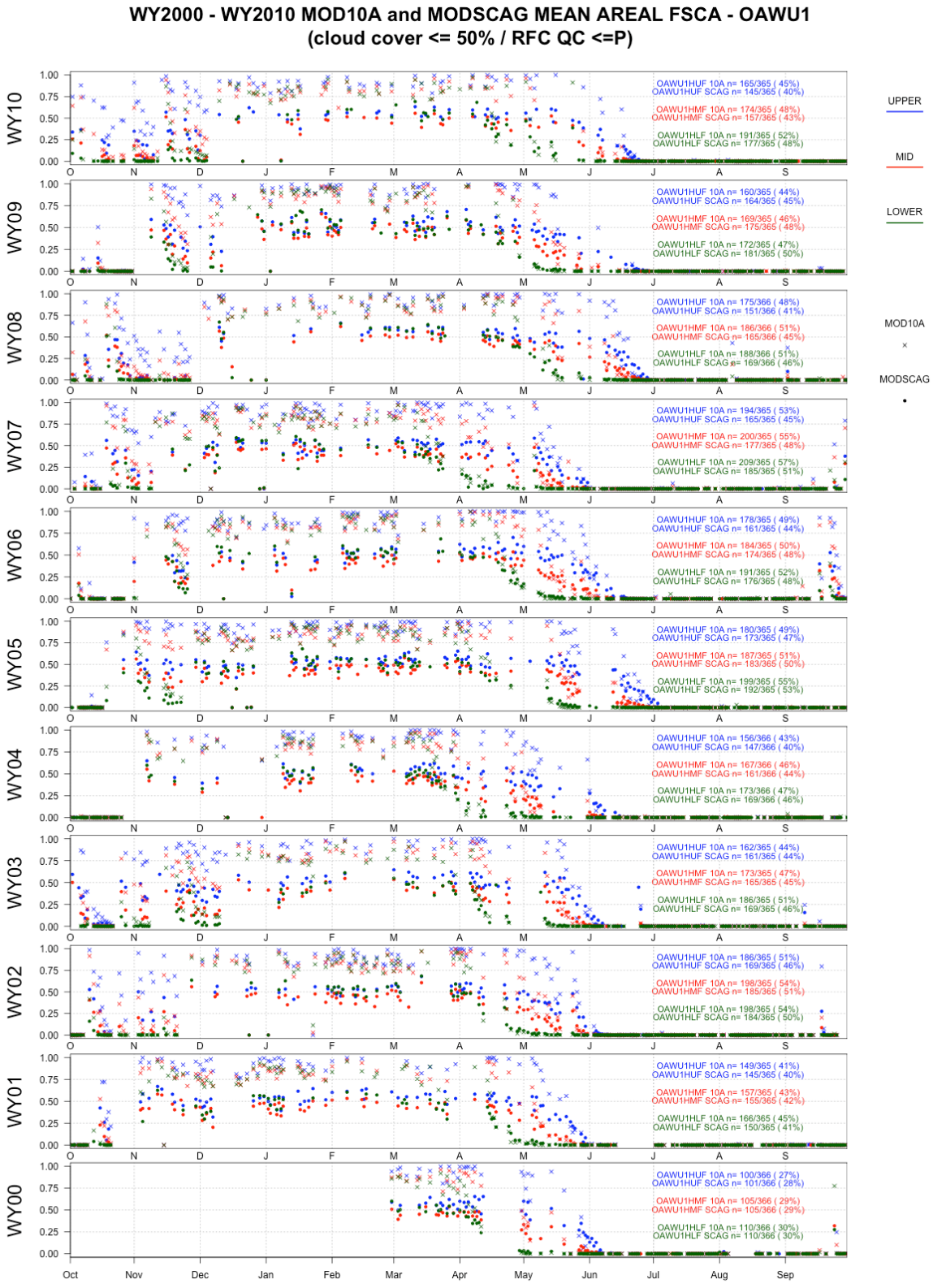

Figure 19: MOD10A and MODSCAG mean areal fSCA for OAWU1 elevation zones, with data counts and availability as a percent of days in the year shown on the right for each water year.

4.3.3 Comparison of MOD10A vs. MODSCAG Mean Areal fSCA

Overall, MODSCAG mean areal fSCA values tend to be less than those derived from the MOD10A grids for the OAWU1 elevation zones (Figs. 17, 19, and 20). This pattern is evident in years across a range of snowpack conditions. Figure 20 compares MODSCAG and MOD10A-derived fSCA in years with low (WY2002), large (WY2005), and moderate (WY2010) snowpack. Figure 20 also shows that mean areal fSCA from MODSCAG is always less than 0.75 in the sample water years selected from the study period (which range from dry to wet). The mean areal fSCA from MOD10A spans the allowable fSCA range of 0.0 to 1.0. In most years, as the fSCA values approach zero, mean areal fSCA values from MOD10A and MODSCAG are in better agreement (Fig. 20).

These differences between the two MODIS-derived fSCA data sets are expected due to differences in the algorithms that derive fSCA for each MODIS pixel (Rittger et al., 2013). The differences in the MODIS-derived fSCA data sets lead to different impacts on streamflow predictions when the fSCA values are used via DI (see Chapter 5).

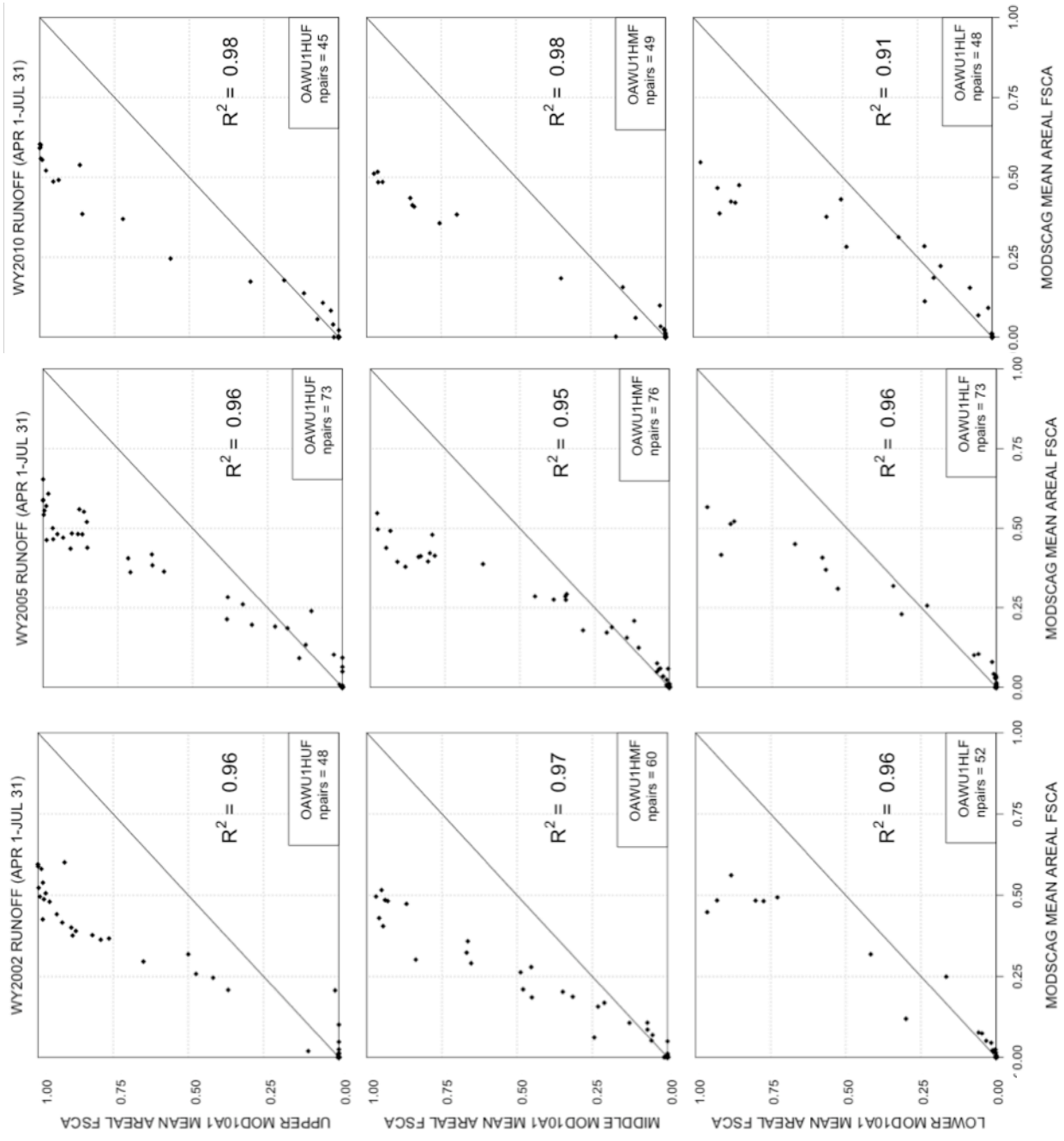

Figure 20: WY2002, WY2005, and WY2010 runoff season (April – July) MOD10A vs. MODSCAG mean areal fSCA for OAWU1 elevation zones (mean areal fSCA derived from days when cloud cover less than or equal to 50%).

4.4 NWS HYDROLOGIC MODEL CONFIGURATION FOR OAWU1

4.4.1 Modeled Areas

The hydrologic modeling system at CBRFC is used operationally in both a forecasting and a simulation mode. In this study, the models are run in simulation mode for the historical period of WY2000 to WY2010. The predictions are deterministic single values, and no uncertainty information accompanies the predictions.

The OAWU1 watershed is divided into three zones (upper, middle, lower). The elevation breaks are determined subjectively by CBRFC during the calibration process. Interannual patterns of SNOTEL SWE and snow cover extent have been used in past calibration efforts to determine which areas of a basin have a persistent winter snowpack and which areas fluctuate between snow covered, partially snow covered, and snow-free during the winter. Spatial variability in snowpack patterns is sometimes used to subdivide the modeled watershed into elevation zones. CBRFC also subjectively considers overall land cover and vegetation type when determining elevation zone boundaries during the calibration process.

For each elevation zone, the snowpack is modeled by SNOW17, and snowpack output from each zone is routed through the SAC-SMA soil moisture submodel. Runoff is transformed into streamflow via a unit hydrograph. At the OAWU1 basin outlet, flow contributions from each zone are aggregated into streamflow for basin as a whole. Area and elevation characteristics for each elevation zone are listed in Table 12, and the elevation zones themselves are shown in Fig. 9.

Operationally, SNOW17 is not calibrated with satellite-derived snow cover observations, and streamflow is the only performance variable used in the calibration process. The experiment conducted as part of this research runs SNOW17 *without* recalibration of the model's parameters using fSCA as a performance variable, either in place of or in conjunction with streamflow. Experiments using a SNOW17 parameter set from recalibration that *does* use MODIS-derived fSCA as a performance variable are planned for the future (see section 6.3).

Table 12: Areas and elevation characteristics of OAWU1 elevation zones

UPPER	Area (km^2/mi^2)	81.07	31.30
	Max elevation (m/ft)	3570	11714
	Min elevation (m/ft)	3048	10000
	Relief (m/ft)	522	1714
	Mean elevation (m/ft)	3148	10327
MIDDLE	Area (km^2/mi^2)	206.06	79.56
	Max elevation (m/ft)	3048	10000
	Min elevation (m/ft)	2591	8500
	Relief (m/ft)	457	1500
	Mean elevation (m/ft)	2840	9319
LOWER	Area (km^2/mi^2)	130.46	50.37
	Max elevation (m/ft)	2591	8500
	Min elevation (m/ft)	2024	6640
	Relief (m/ft)	555	1822
	Mean elevation (m/ft)	2388	7835

4.4.2 SNOW17 Parameters for Elevation Zones

Most of the SNOW17 parameters derived during most recent calibration (historical period of WY1981 to WY2010, calibration completed in 2011) for the Weber River headwaters are typical of parameters derived for mountainous basins. Streamflow is the performance variable used in the CBRFC calibration process, and model parameters are tuned with the goal of closely matching the simulated to the observed streamflow. The parameters derived by CBRFC during the most recent calibration are shown in Table 13. The parameters are indicative of forested areas that are not particularly affected by wind and that build deep snowpacks annually.

Table 13: SNOW17 parameters for OAWU1 elevation zones

Model Parameter	Conditions Indicated by OAWU1 parameter	Upper Zone	Middle Zone	Lower Zone
SCF (dim'less)	1.0 – sheltered sites not susceptible to wind	1.05	1.05	1.05
MFMAX (mm/C/6hr)	1.0 – 1.3 – coniferous forest	1.1	1.0	1.0
MFMIN (mm/C/6h)	0.2 – 0.3 – dense forest	0.2	0.2	0.2
UADJ (mm/mb/6h)	0.03 – 0.19: lower in sheltered, less windy areas	0.02	0.02	0.02
SI (mm)	During initial calibration, at least equal to or greater than the max water equivalent that occurs during the calibration period, but usually less.	350	350	275
NMF (mm/C/6hr)	~0.05- ~0.4, depending on snow density	0.2	0.2	0.2
TIPM (dim'less)	0.01 – 1.0 < 0.2 – gives weight to air temp over the past 3-7 days (appropriate for deep snow covers due to increased depth and heat storage capacity)	0.1	0.2	0.2
MBASE (C)	Typically ~0 C in vast majority of watersheds.	0.25	0.25	0
PXTEMP (C)	0.5 – 2 C.	1.5	1.5	1.5
PLWHC (decimal fraction)	0.02 – 0.05	0.05	0.05	0.05
DAYGM (mm/day)	0.0 - areas w/ frozen ground 0.3 – areas with mild climates and deep snow cover (e.g., Sierra Nevada)	0.1	0.2	0.3

Note: Parameters are defined in Table 6

The ADCs for the OAWU1 elevation zones are shown in Fig. 21, and the individual values for the ADC are listed in Table 14. The ADCs for all OAWU1 elevation zones exhibit a shape similar to the ADC curve type C (Fig. 10, Table 7). ADC Type C occurs in areas consisting of a mix of open and forested portions. Type C ADCs indicate that portions of the modeled area accumulate less snow than others (perhaps due to changes in land cover type) and/or have a much higher melt rate than the remainder of the area (NWS, 2004).

In the case of ADC Type C (Fig. 10) and the OAWU1 ADCs from the most recent CBRFC calibration (Fig. 21), the ADC attempts to represent the variation in melt rates as the snowpack depletes. When snowmelt has progressed to the point where the snow cover extent first drops below 100%, the snow cover extent decreases quickly per unit change of a SWE index (the WE/A_i ratio), as the portions of the modeled area with more shallow snow melt rapidly and bare ground is exposed. The middle portion of the ADC represents snowmelt in areas where the snowpack is deeper. As these areas melt, much SWE may be lost with only a smaller change in snow cover extent than when shallow areas of snow are melting. Finally, when enough SWE has melted such that the snow cover extent drops below about 50% for the OAWU1 elevation zones, the remaining snow cover extent depletes rapidly per unit change in the WE/A_i SWE index.

At the lower end of the ADCs, as WE/A_i approaches 0.0, AESC is held at 0.05 (AESC never gets to zero on the ADC). The lower end of the ADC is configured this way so that the remains of the snowpack are melted and do not persist into the summer under normal conditions, as discussed in section 2.3.2.2. In SNOW17, the SWE (and, in turn, the WE/A_i ratio) must reach zero before AESC is allowed to be zero.

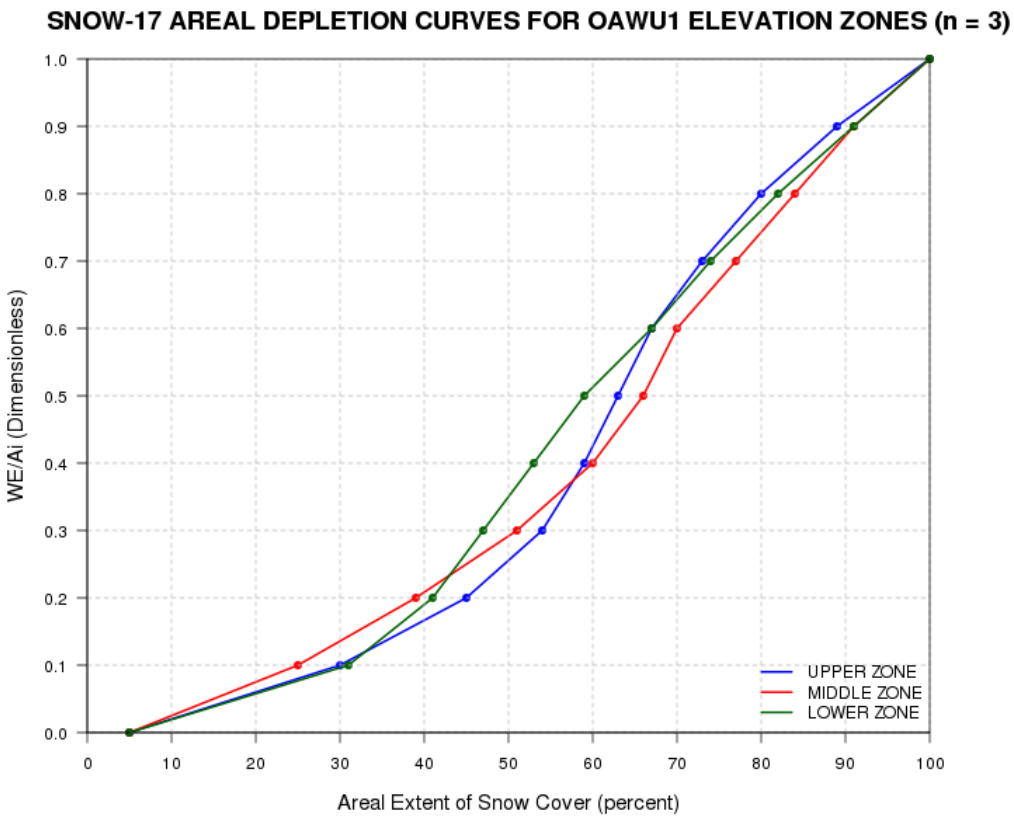

Figure 21: Areal depletion curves for OAWU1 elevation zones that relate AESC (model snow cover extent) to a SWE index (a ratio of SWE to an Ai). The index Ai is the smaller of (a) the model parameter that defines the water equivalent above which 100% snow cover always exists (SI) and (b) the maximum amount of water equivalent of the accumulation period (see section 2.3.2.2).

Table 14: ADC values for OAWU1 elevation zones

	Areal Extent of Snow Cover (fraction)		
WE/A_i	UPPER	MIDDLE	LOWER
0.0	0.05 (fixed)	0.05 (fixed)	0.05 (fixed)
0.1	0.30	0.25	0.31
0.2	0.45	0.39	0.41
0.3	0.54	0.51	0.47
0.4	0.59	0.60	0.53
0.5	0.63	0.66	0.59
0.6	0.67	0.70	0.67
0.7	0.73	0.77	0.74
0.8	0.80	0.84	0.82
0.9	0.89	0.91	0.91
1.0	1.0 (fixed)	1.0 (fixed)	1.0 (fixed)

4.5 MEAN AREAL FSCA FROM MODIS VS. SNOW17 AESC

Mean areal fSCA values derived from both MOD10A and MODSCAG are almost always less than the SNOW17-estimated AESC values from the control simulation. Example scatterplots of MODIS-derived mean areal fSCA vs. SNOW17 AESC for the three OAWU1 elevation zones for three water years (WY2002 – dry, WY2005 – wet, and WY2010 – average) are shown in Fig. 22.

During the runoff season of April – July for the sample water years shown in Fig. 22, an exponential relationship appears to exist between the MODIS-derived fSCA (both MOD10A and MODSCAG) and SNOW17's estimate of AESC. The SNOW17 model structure (specifically the use of AESC as a multiplier on the melt volume computed assuming 100% snow cover) and the fact that MODIS-derived fSCA values are almost always less than 100% (due to vegetation, soil, rock, and other mixed pixel issues) impacts the DI streamflow simulations. The extent of the impacts due to differences between MODIS-derived fSCA and SNOW17 AESC is discussed in Chapter 5.

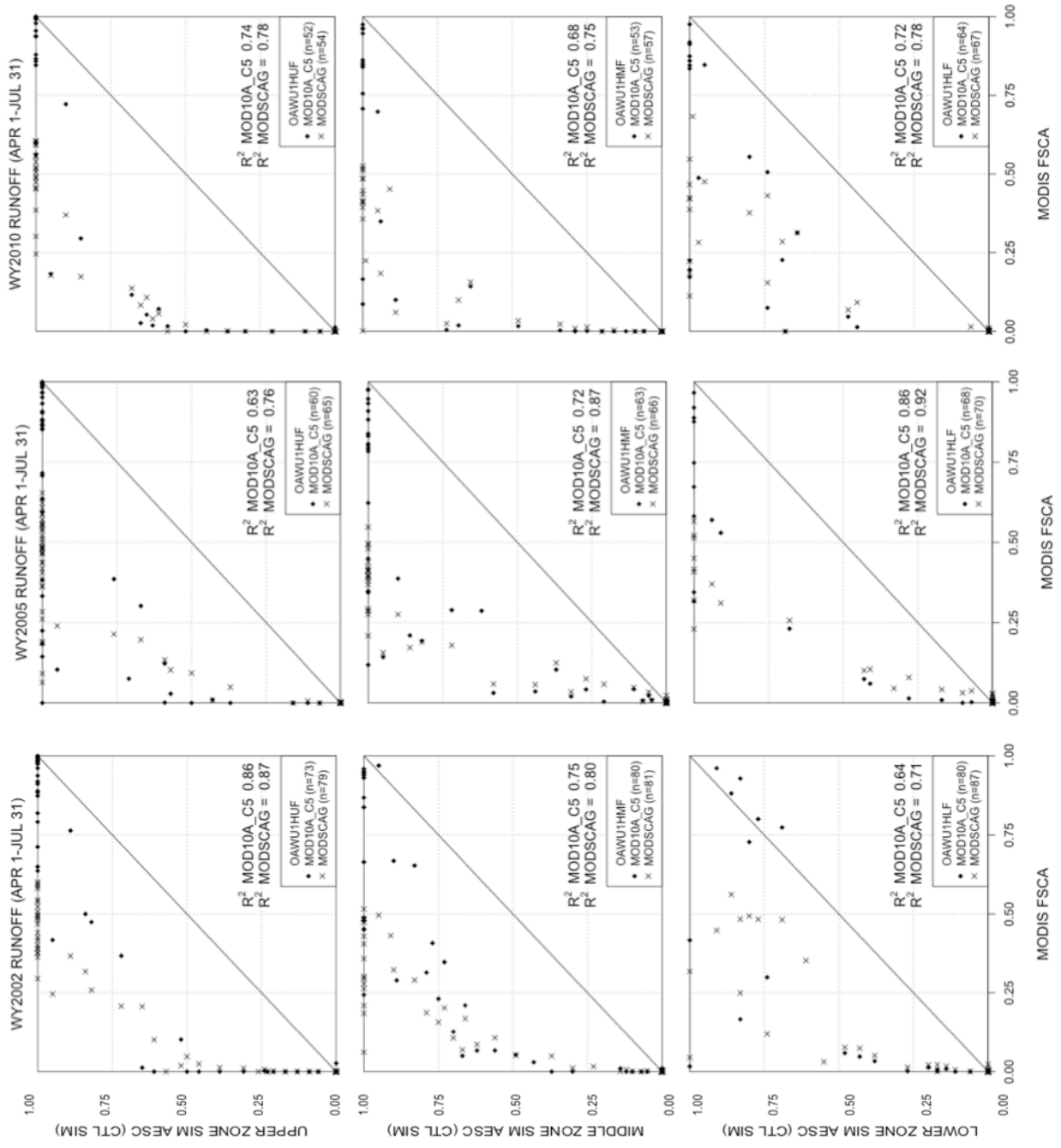

Figure 22: WY2002, WY2005, and WY2010 runoff season (April – July) MOD10A and MODSCAG mean areal fSCA values vs. control simulation of AESC (CTL) for OAWU1 elevation zones.

4.6 DIRECT INSERTION OF PREPARED FSCA ESTIMATES

The experiment in this study tests the impact of the simple DI scheme, where satellite-derived fSCA observations are directly substituted for modeled snow cover extent in SNOW17. SNOW17 is capable of ingesting external sources of snow data (snow water equivalent and snow cover) provided the data are in the correct format (NWS, 2005). In the SNOW17 input configuration files, a user can set a flag to notify SNOW17 that an external source of snow cover values should be used in place of the model driven snow covered area value. The external source of snow cover values can come from any source; usually, the external snow cover values are estimates of fSCA derived from some type of observations.

A user can also specify a "snow covered area tolerance" value, which is used to determine which observations presented to the model are actually used to update model snow cover conditions within the model. If the absolute value of the difference between the simulated and observed snow cover values is greater than the specified tolerance, then the observed fSCA estimate will be substituted for the model's estimate of snow covered area.

For the DI simulations in this study, these features of SNOW17 were used. MODIS-derived fSCA values from days when cloud cover was 50% or less were presented to SNOW17 as an additional input file. The indicator flag that specifies whether or not to update SNOW17 AESC values with the external fSCA values (in this study, MODIS-derived fSCA) was set to "UPDATE". The "snow covered area tolerance" value was set to 0.0, indicating that any MODIS-derived fSCA value that

differed from the SNOW17 simulated snow cover value would replace the SNOW17 estimate of snow cover. Thus, any time a MODIS-derived fSCA value is available, it is used in the model, in the experimental simulations. An example of the SNOW17 configuration for the upper elevation zone of OAWU1 is shown in Fig. 23. The flag indicating that DI should be used is highlighted in red, and the "snow cover toleranace value" is highlighted in blue.

```
SNOW-17     UPPER
WEBER NEAR OAKLEY   3146.40.73       YES  YES SUMS    UPDATE      AVSE
    6  UPPER    MAP        1.00       UPPER    RAIM
  UPPER    MAT     6     3146.
   11    10000.    10974. ENGL  UPPER    RSEL
    10033  0.08    10075  0.16    10121  0.25    10177  0.33
    10213  0.42    10279  0.50    10338  0.59    10403  0.67
    10495  0.76    10600  0.84    10663  0.91
                                  OAWU1SUH AESC   24
  UPPER    SWE     6              UPPER    SASC    6
 1.05  1.1  0.2 0.02 350.
  0.2  0.1 0.25  1.5 0.05  0.0      0.0
  0.3 0.45 0.54 0.59 0.63 0.67 0.73  0.8 0.89
```

Figure 23: SNOW17 settings for the upper elevation zone of OAWU1.

For this study, the focus is on determining whether or not DI is a viable option for updating snow pack conditions without recalibration of SNOW17. Recalibration would involve using MODIS-derived snow cover observations as a performance variable in addition to streamflow. At least some of the SNOW17 parameters would likely change in a recalibration if observed fSCA is used as a performance variable in place of or in addition to streamflow.

During 2011 and 2012, CBRFC completed a major recalibration of SNOW17 and SAC-SMA for all of the hundreds basins included in the CBRFC forecasting system. Recalibration for the entire hydrologic modeling system at CBRFC occurs typically once every ten years, when the historical period used in calibration is moved forward by a decade. The most recent recalibration used the historical period of WY1981 to WY2010. Hundreds of basins are modeled by CBRFC, and those basins are divided into one, two, or three elevation zones (usually two or three). Since the modeled basins are usually divided into multiple elevation zones, and SNOW17 is run over each elevation zone, CBRFC runs SNOW17 for approximately 1100 elevation zones. A complete recalibration would involve checking approximately 1100 sets of SNOW17 parameters. Dedicated staff time for an additional complete recalibration of elevation zones for all modeled basins is not currently available at CBRFC, so the immediate question to be answered is related to whether or not MODIS-derived fSCA values can be used via DI without recalibration.

4.7 STREAMFLOW PREDICTION EVALUATION METRICS

To be considered useful, a modeling system must be able to predict (i.e., reproduce in simulation mode and also to forecast) the observed hydrograph. In the model calibration and daily forecasting processes at CBRFC, streamflow is the variable used to judge the performance of the operational system.

Tolerance of error varies with the intended end use of the model. Various metrics can be used to judge the utility of a model and how well the model predicts the observed

hydrograph. No single metric can describe a model's performance by itself. Two types of metrics are used in this study to evaluate the streamflow predictions produced by the control experimental simulations that use the DI technique: subjective and objective.

4.7.1 Subjective Evaluation of Streamflow Forecasts

The subjective, or qualitative, checks involve visual inspection of the hydrograph generated by the model, to determine how well the predicted hydrograph fits the streamflow observations. The peaks and their sharpness are examined to see, qualitatively, how closely the highest predicted flow values match the observations. The timings of the modeled and observed peak flow values are compared. The timing of the peak flow in snow-dominated watersheds is strongly influenced by the condition of the snowpack, the diurnal cycle, time of year (especially incoming solar radiation), and temperatures. The flow volume (area under the hydrograph) is examined for each snowmelt simulation, to roughly estimate if the right amount of water is being contributed to the streamflow from the snowpack. These features of the hydrograph are summarized in Table 15. All of these characteristics (peak flow, timing, water volume) are important to emergency responders, other flood management groups, and water managers in general.

Table 15: Qualitative Evaluation Measures of Hydrographs

Hydrograph Aspect	Questions Answered
Highest peak flows	Are the peak flow magnitudes predicted?
Peak Timing	Is the timing of the peak flows predicted?
Flow Volume/Area under hydrograph	Is the annual volume of water predicted?

4.7.2 Objective Evaluation of Deterministic Streamflow Predictions

In addition to qualitative visual inspection of the predicted hydrographs, many objective, quantitative metrics are applied in hydrologic practice to evaluate simulation and forecast performance. This section discusses the quantitative metrics used to judge the DI simulations conducted for this research. The streamflow simulations from model runs with DI are compared to (1) streamflow observations and (2) the simulation derived during the CBRFC calibration process, which uses model-calculated snow cover only (AESC) and no MODIS-derived fSCA (which is treated as an experimental control).

This study focuses on deterministic prediction; therefore, deterministic metrics are used to evaluate the predictions. Multiple metrics are necessary to evaluate model performance. No single metric can provide a complete picture of the model's performance. The objective verification measures used in these comparisons are listed in Table 16 and described in further detail below.

Table 16: Deterministic Verification Metrics

Type of Verification Metric	Deterministic
Association	Scatterplots Pearson Correlation Coefficient (R)
Accuracy/Error Measures	Mean Error (ME) Root Mean Squared Error (RMSE) Percent Bias (PB)
Measures of Forecast Skill	Root Mean Squared Error Skill Score (RMSE-SS)

Despite the importance of categories and thresholds to streamflow prediction, the ability of the modeling system to predict when and how frequently flows meet or exceed a flood threshold is not evaluated in this study. During the time period of the study

(WY2000 – WY2010), the observed streamflow for the study basin slightly exceeded the flood threshold only once, in early June 2010. The observed peak mean daily flow in early June 2010 was 71.3 $m^3 s^{-1}$, while the flood threshold is 71.1 $m^3 s^{-1}$ (see Fig. 15 in Chapter 3). Given the time period of the study and the basin that is the focus of this study, the flood sample size (n = 1) does not allow an appropriate evaluation of the simulations with respect to the flood threshold.

All performance metrics are computed with R scripts. The R, ME, RMSE, and PB values (Table 16) are computed with the hydroGOF R package (Zambrano-Bigiarin, 2013). The coefficient of determination (R^2 for linear regression), and the skill score (RMSE-SS) is computed within a custom R script.

4.7.2.1 Predicted Streamflow vs. Observations

MEASURE OF ASSOCIATION

A measure of association indicates the strength of the linear relationship between the streamflow observations and predictions and, to some extent, how well the model predicts the observed hydrograph. The measure of association used in this study is the Pearson correlation coefficient (R). Scatter plots communicate the association visually.

ACCURACY AND ERROR METRICS

Accuracy can be described quantitatively with error metrics. This study uses error metrics that are commonly used in hydrology, including the mean error (ME), root mean squared error (RMSE), and the percent bias (PB). All of these statistics are defined and summarized in Table 18.

Table 17: Relationship Indicator for (Predicted, Observed) Pairs for Deterministic Prediction

Objective Streamflow Performance Metric	Description	Equation(s)	Range, Best and Desirable Values, Additional Explanation (if necessary)
Pearson Correlation Coefficient (R)	Measure of how well the model reproduces the observed streamflow; measure of the LINEAR association between P and O Insensitive to differences in hydrograph size	$R = \frac{1}{n-1}\sum\left(\frac{Q_{pi} - \overline{Q_{pi}}}{S_p}\right)\left(\frac{Q_{oi} - \overline{Q_{oi}}}{S_o}\right)$ where: Q_{pi} = predicted Q Q_{oi} = observed Q n = number of Q prediction-observed pairs	**Range:** -1 to +1 **Best:** +/-1 **Desirable Values**: Far from zero; close to -1 or close to +1

Table 18: Accuracy and Error Metrics (after COMET, 2008 and CBRFC, 2004)

Objective Streamflow Performance Metric	Description	Equation(s)	Range, Best and Desirable Values, Additional Explanation (if necessary)
Mean Error (ME) (also referred to as "bias")	Indicates over/under prediction Disadvantage – can be misleading, as large errors of opposite sign will cancel each other out.	$ME = \frac{1}{n}\sum_{i=1}^{n} e_i$ where: $e_i = Q_{pi} - Q_{oi}$ Q_{pi} = predicted Q Q_{oi} = observed Q n = number of Q prediction-observed pairs	**Range:** -∞ to ∞ **Best**: 0 **Desirable Values**: As close to zero as possible
Root Mean Square Error (RMSE)	Indicates error magnitude More sensitive to large errors than other metrics. Large errors (more common in high flows) will dominate RMSE. Does not indicate over/under prediction	$RMSE = \sqrt{\frac{1}{n}\sum_{i=i}^{n}(e_i)^2}$ where: $e_i = Q_{pi} - Q_{oi}$ Q_{pi} = predicted Q Q_{oi} = observed Q n = number of Q obs	**Range:** 0 to ∞ **Best**: 0 **Desirable Values**: As close to zero as possible
Percent Bias (PB)	Measure of **total volume difference** between two time series ***Does not*** measure differences in timing.	$PB = \frac{\sum_{i=i}^{n} e_i}{\sum_{i=i}^{n} Q_{oi}} \times 100\%$ where: $e_i = Q_{pi} - Q_{oi}$ Q_{pi} = predicted Q Q_{oi} = observed Q n = number of Q obs	**Range:** -∞ to ∞ (usually -100 to 100%) **Best**: 0 **Desirable Values**: As close to zero as possible

4.7.2.2 Predicted Streamflow vs. Reference or Control

In addition to comparisons with observations, this study compares experiment results with a control, using a skill score. A skill score (SS) represents a percent difference between verification metrics for two different model predictions (NWS, 2006). Even if error statistics indicate less than desirable results for a model, skill scores may indicate that the experimental predictions improve over control or reference predictions. The control or reference prediction could be streamflow values from climatology, persistence, or predictions from other models. The skill score for this study is the RMSE skill score (RMSE-SS). Mathematically, a skill score is defined:

$$\mathrm{SS} = \frac{X_{predicted} - X_{control}}{X_{perfect} - X_{control}} \qquad (7)$$

where:

$X_{predicted}$ = value of a verification metric, computed for the experimental predictions
$X_{control}$ = value of a verification metric, computed for the control
$X_{perfect}$ = value of a verification metric, if the predictions are perfect

If the SS is less than zero, then the experimental simulations are worse than the control, in terms of the specified verification metric X. If SS is equal to zero, then the prediction skill is the same as that of the control (no better, no worse than the control). If SS is greater than zero, then the model's predictions are better than those of the control, in terms of the specified verification metric.. This study applies RMSE. For RMSE, $X_{perfect}$ is zero; therefore, RMSE-SS is defined specifically as:

$$\mathrm{RMSE-SS} = \frac{RMSE_{prediction} - RMSE_{control}}{0 \ - RMSE_{control}} = 1 - \frac{RMSE_{prediction}}{RMSE_{control}} \qquad (8)$$

CHAPTER 5: CASE STUDY RESULTS AND DISCUSSION

This chapter presents and discusses the results of the experimental simulations, in which MODIS-derived fractional snow covered area values were directly inserted into the SNOW17 model for the headwater basin of the Weber River in Utah, without model recalibration. Because streamflow is ultimately the most important quantity in the CBRFC operational forecasting and modeling systems, this study evaluates model performance on the basis of this variable. In this chapter, the simulations are identified as listed in Table 19:

Table 19: Identifiers and characteristics of streamflow simulations

Simulation ID	Active DI	MODIS fSCA data set	DI Time Period
CTL	No	n/a	n/a
MO1.WY	Yes	MOD10A	Full Water Year
MO1.AJ	Yes	MOD10A	April - July
MO2.WY	Yes	MODSCAG	Full Water Year
MO2.AJ	Yes	MODSCAG	April - July

5.1 OVERALL PERFORMANCE OF SIMULATIONS

In general, the CTL simulation predicts the observed streamflow reasonably well. The DI simulations mostly under predict the streamflow and exhibit a negative average error (or negative bias); severe under prediction is common. There are a few cases in which the DI simulations over predict the observed streamflow with a positive bias. Overall, over prediction is uncommon in the DI simulations. Examples of under

prediction (negative bias) and over prediction (positive bias) are given throughout this chapter. The overall performance of the various simulations with respect to peak flows and annual streamflow volume, judged by the evaluation measures listed in Table 15, is summarized in Table 20.

Table 20: Qualitative performance measures for study simulations

	Highest Peak Flows	Peak Timing	Flow Volume/Area under hygrograph
Simulation	Are the peak flow magnitudes predicted?	Is the timing of the peak flows predicted?	Is the annual volume of water being predicted?
CTL	Peak magnitudes are predicted to within +/-10% overall, though sharp peaks tend to be under predicted (by as much as -25% when averaged over the study period)	Peak flow timing is predicted; the timing of the predicted peaks matches the timing of the observed peaks.	Annual flow volumes are predicted to within a bias of +/- 5% of the observed annual flow volume in the majority of years. Under prediction occurs of ~ - 17% in two of the study years.
MO1.WY	Peak magnitudes are predicted only in a few cases. Almost always, the peaks are under predicted, sometimes severely so.	The peak timing is predicted in about half of the years. Otherwise, peaks are nonexistent, or the timing is not predicted.	Under prediction occurs in all years, most of the time severe. Under prediction occurs to a lesser degree in WY2008, WY2009, and WY2010.
MO1.AJ	Peak magnitudes are predicted only in a few cases. Almost always, the peaks are under predicted, sometimes severely so.	The peak timing is predicted in about half of the years. Otherwise, peaks are nonexistent, or the timing is not predicted.	Under prediction occurs in all years, most of the time severe.
MO2.WY	Peak flow magnitudes are not predicted well. In many years, there is no discernable snowmelt-driven peak flow. Only WY2010 comes close.	For the most part, timing of peak flows are not predicted well. Simulated peaks often occur later than observed peaks, or not at all.	The annual volume of water is severely under predicted in almost all years. WY2010 is close but still under predicted.
MO2.AJ	For most years, there is no obvious snowmelt-driven peak flow.	Peaks are either predicted too late when compared to observed flow, or no peak is predicted at all.	The annual volume of water is severely under predicted in almost all years. WY2010 is close but still under predicted.

5.1.1 Scatterplots

The scatterplots in Figs. 24-28 compare simulated to observed streamflow on a daily basis for the five simulations, for the study period of WY2000 to WY2010. The coefficient of determination () is shown on each scatterplot to indicate the degree to which the model predicts the observed streamflow values.

The CTL simulation performs the best overall during the study period, with an R^2 value of 0.92. The performance of the DI simulations is overall poorer than that of the CTL simulation during the study period. The under prediction (negative bias) of the observed streamflow by the DI simulations is particularly evident in Figs. 25-28. The R^2 values for the DI simulations range from 0.22 (MO2.AJ DI simulation to 0.70 (MO1.WY DI simulation). Despite an R^2 of 0.70, which would generally indicate acceptable model performance by itself, the performance of the MO1.WY simulation exhibits a negative bias (Fig. 25). The scatterplots for the CTL and DI simulations are discussed in detail below.

5.1.1.1 Control Simulation

The CTL simulation reasonably simulates the streamflow during the study period of WY2000 to WY2010, across all seasons of the water years included in the study period (Fig. 24). For the overall study period, the R^2 value for observed streamflow and streamflow simulated by the control is 0.92. A few cases of under prediction (negative bias) of approximately 50% occur when the mean daily streamflow is greater than 40 m^3

s^{-1} (Fig. 24). These cases of under prediction occur when the observed hydrograph exhibits a sharp single peak, as will be discussed in section 5.1.2.

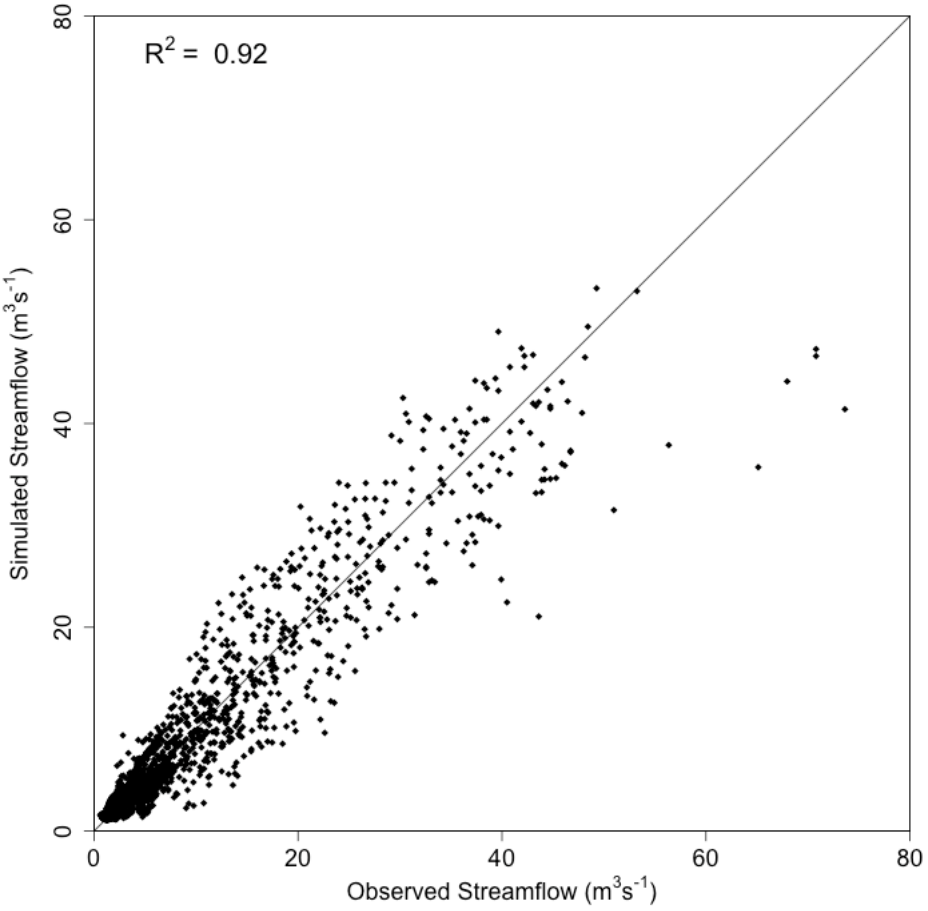

Figure 24: WY2000 to WY2010 simulated vs. observed mean daily streamflow for CTL simulation

5.1.1.2 Direct Insertion Simulations

All of the scatterplots that compare simulated to observed streamflow for the DI simulations show that the DI simulations usually under predict the observed streamflow (Figs. 25-28). The under prediction of the observed streamflow is especially evident for observed mean daily streamflow greater than ~ 5 $m^3 s^{-1}$. The under prediction is partially a result of reduced snowmelt rates in the simulations with active DI; reasons for the under prediction are discussed in section 5.3. A mix of under and over prediction occurs at low flows (<5 $m^3 s^{-1}$).

Overall, the DI simulations that use the MOD10A version of MODIS fSCA under predict the observed streamflow to a lesser degree than the DI simulations that use the MODSCAG fSCA product. Figures 27 and 28 show that the greatest extent of under prediction occurs in the MO2 simulations (DI of MODSCAG fSCA). There is also generally a wider range of differences between the simulated and observed streamflow in the DI simulations that use the MODSCAG fSCA product (Figs. 27 and 28).

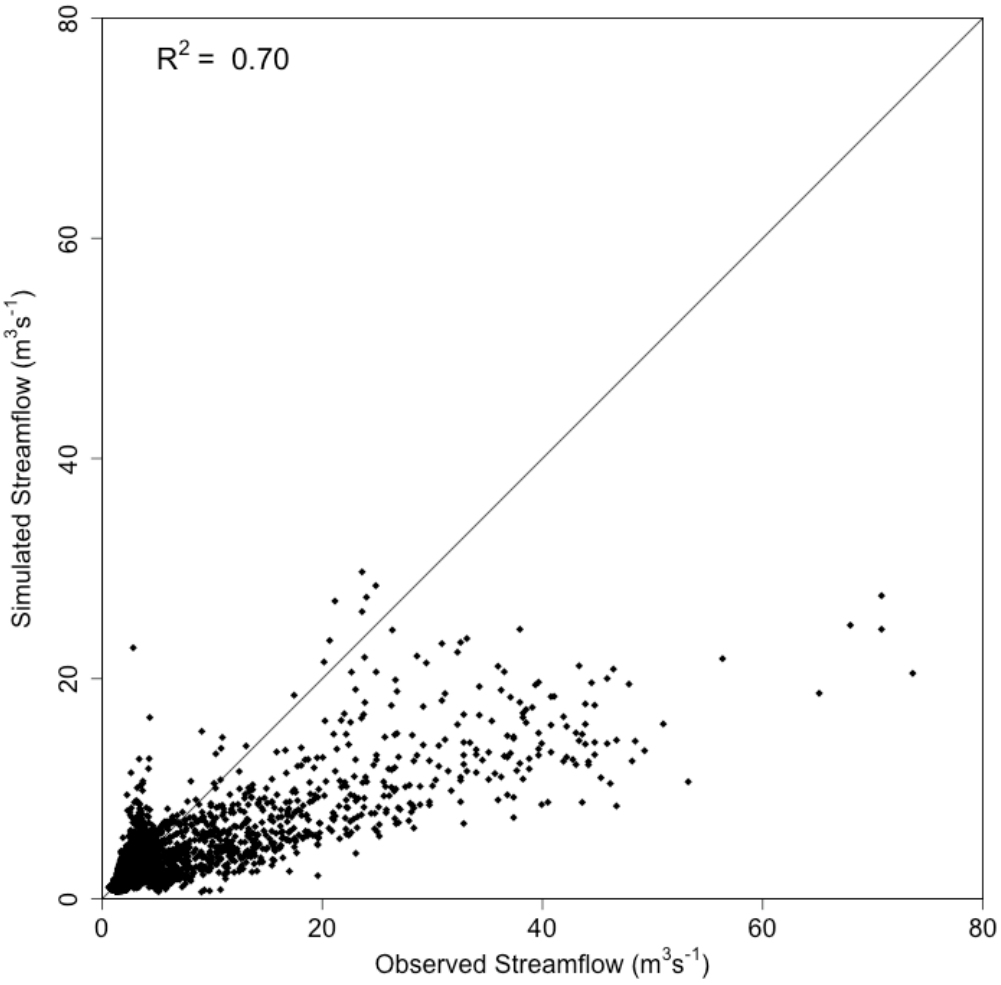

Figure 25: WY2000 to WY2010 simulated vs. observed mean daily streamflow for MO1.WY DI simulation

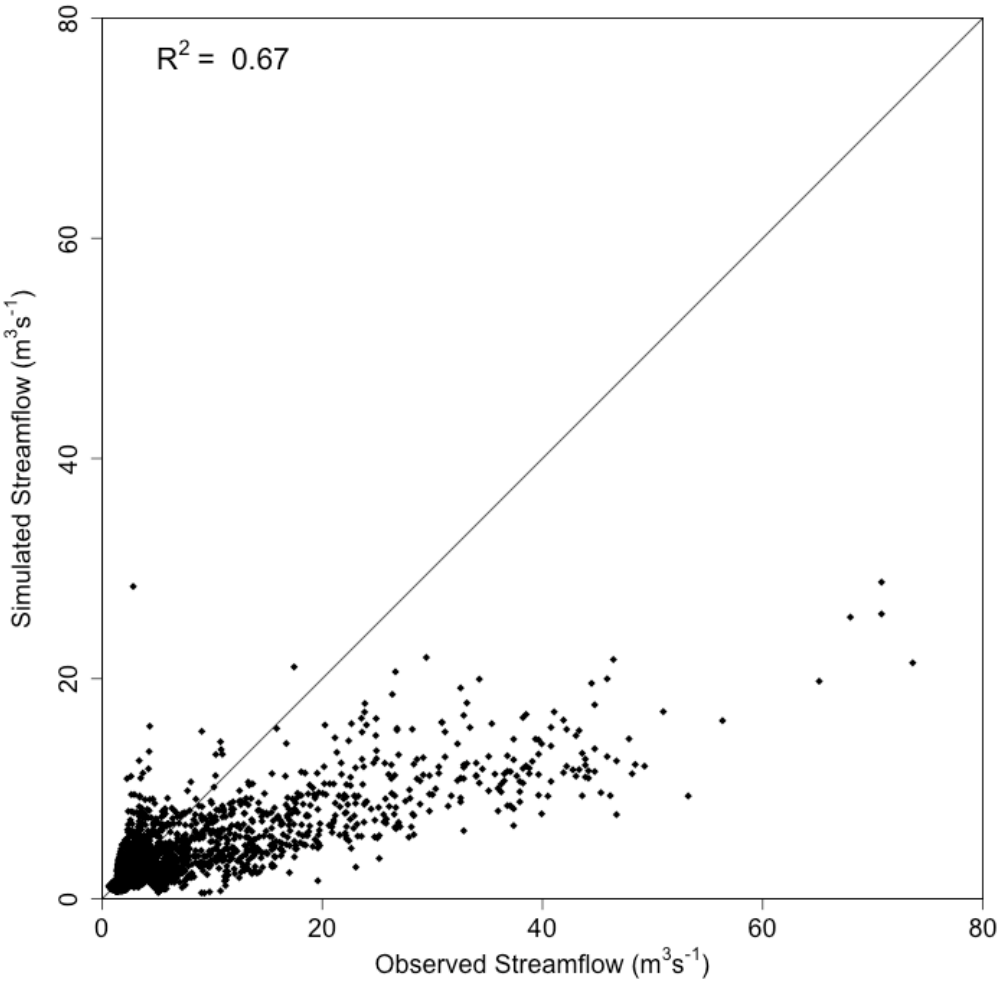

Figure 26: WY2000 to WY2010 simulated vs. observed mean daily streamflow for MO1.AJ DI simulation

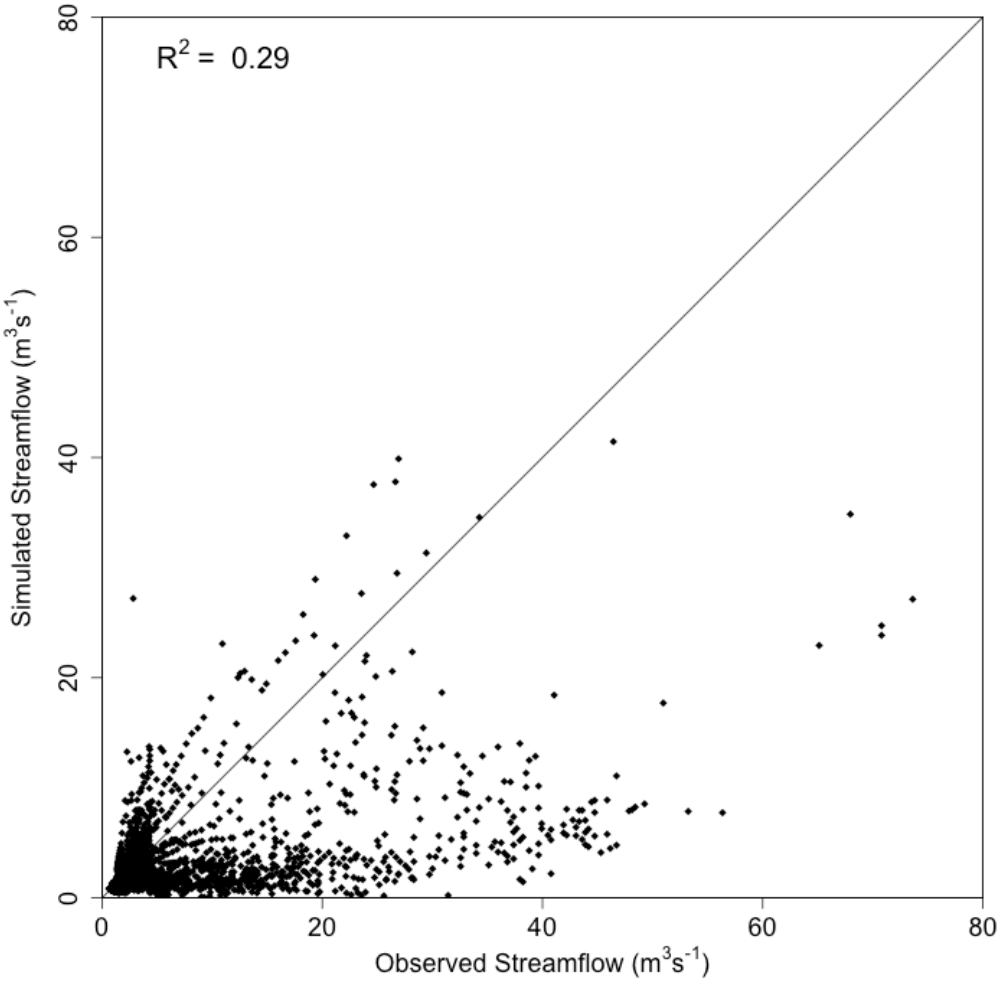

Figure 27: WY2000 to WY2010 simulated vs. observed mean daily streamflow for MO2.WY DI simulation

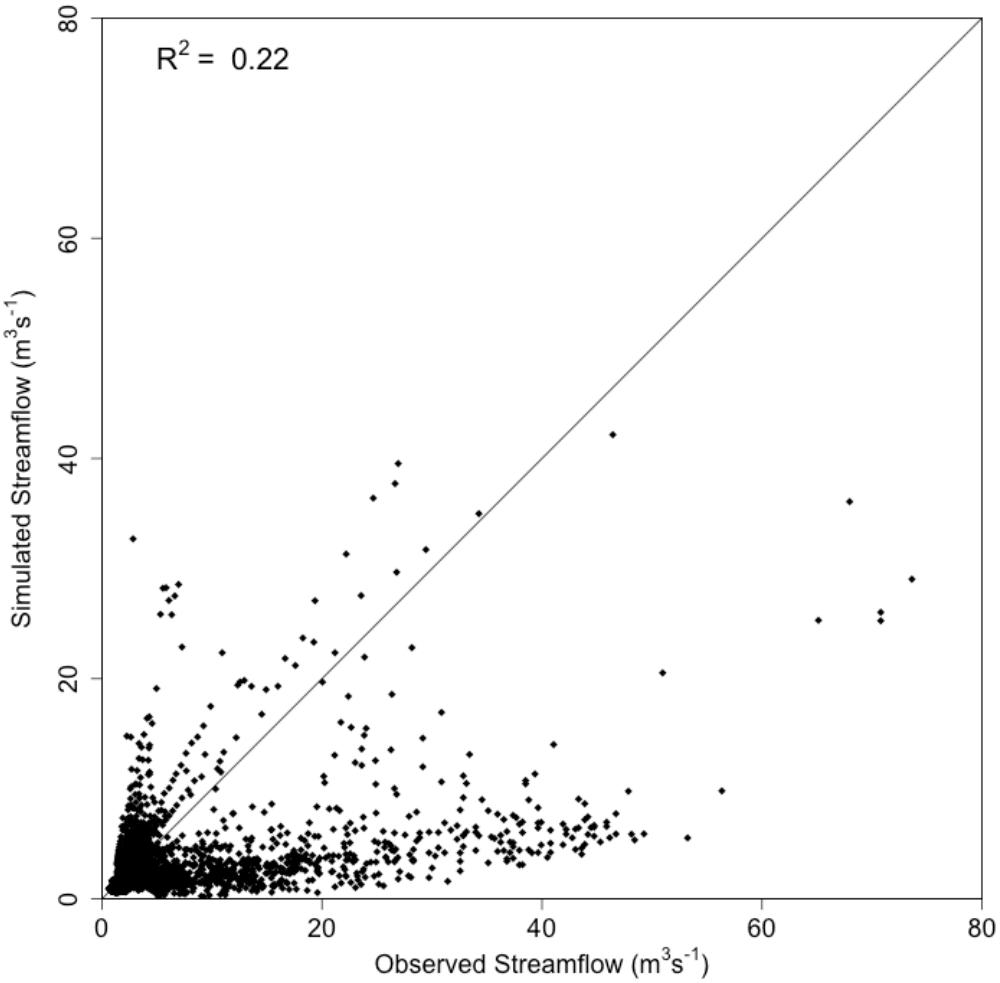

Figure 28: WY2000 to WY2010 simulated vs. observed mean daily streamflow for MO2.AJ DI simulation

5.1.2 Example Hydrographs

In this section, several examples of hydrographs from both the CTL and DI simulations are shown. Aspects of the hydrographs examined include peak magnitudes, peak timing, and volume of water indicated by the area under the hydrograph. While the monthly statistics are shown in the hydrograph figures, they are discussed in a limited manner in this section (5.1). Detailed discussion of the performance of the simulations (as judged by the statistical metrics) is included in section 5.2.

5.1.2.1 Hydrographs from Control Simulation

The CTL simulation adequately predicts the observed hydrograph in most cases (Fig. 24, 29). One example of high-quality simulation is WY2008, in which multiple peaks of various magnitudes were observed during the snowmelt runoff season (Fig. 29). While the control simulation under predicts in early May (mean error of -4.1 $m^3 s^{-1}$), the magnitude of the largest peaks is generally met, and the timing of the simulated peaks matches the timing of the observed peaks.

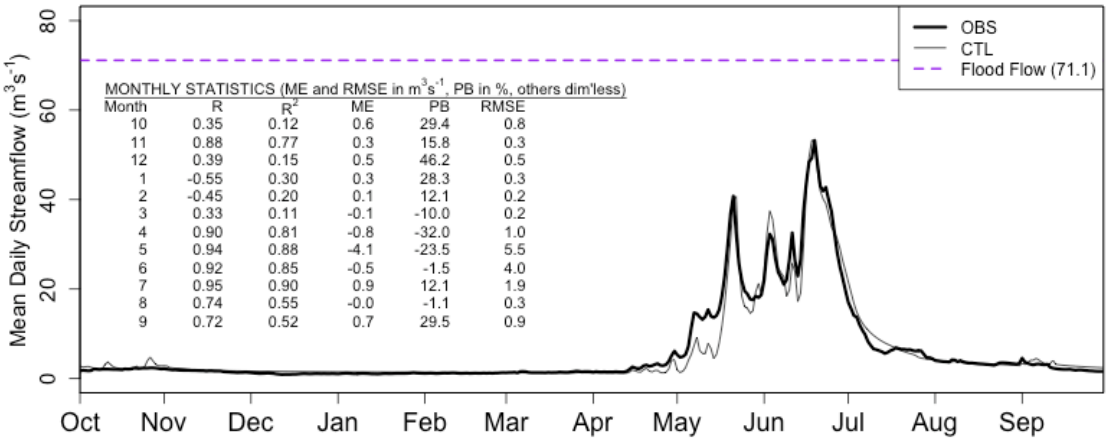

Figure 29: WY2008 observed (bold) and CTL simulated (thin) streamflow for OAWU1

The CTL simulation consistently under predicts the magnitude of sharp single peaks in the snowmelt-driven hydrograph in other years of the study period. Examples are shown of under predicted snowmelt runoff peaks for water years 2001, 2003, and 2010 (Figs. 30-32). The sharpest observed peak of the study period occurs in June 2010 (Fig. 32), when the streamflow slightly exceeds the flood threshold set by the NWS. In these cases of sharp peaks in the observed hydrograph, the simulated peaks sometimes have a negative bias of ~40% on a daily basis. Calibrated temperature index models such

as SNOW17 generally have difficulty capturing sharp streamflow peaks in the observed hydrograph, especially when the sharp peaks are due to abnormal conditions that are not representative of the historical period used to calibrate the model. For example, the sharp streamflow peak that occurred in June 2010 (Fig. 32) was preceded by cooler than average May temperatures (Fig. 33). The cool May temperatures delayed snowmelt and allowed the snowpack to persist longer than it normally would have. By mid to late May, the snowpack was above average in terms of SWE, according to SNOTEL sites within and near the OAWU1 watershed. When temperatures increased in early June, the snowpack melted, driving streamflow to reach and exceed the NWS flood threshold.

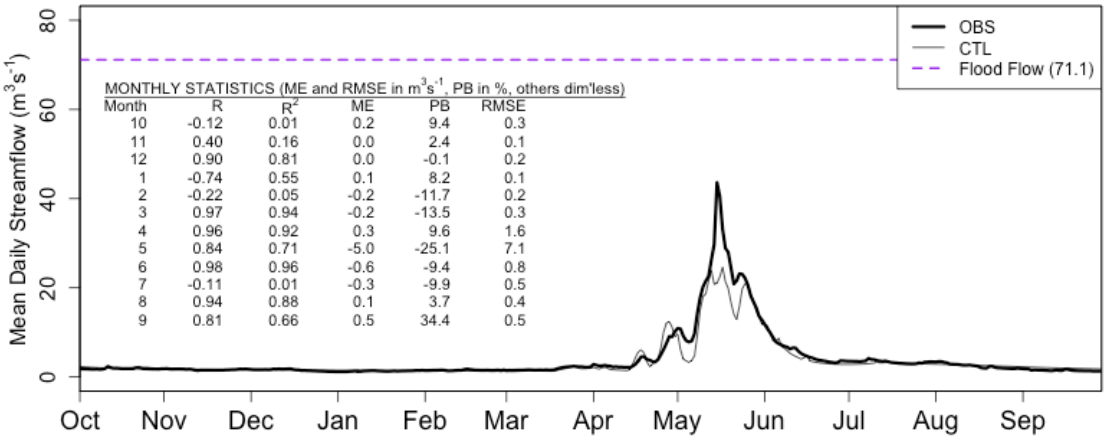

Figure 30: WY2001 observed (bold) and CTL simulated (thin) streamflow for OAWU1

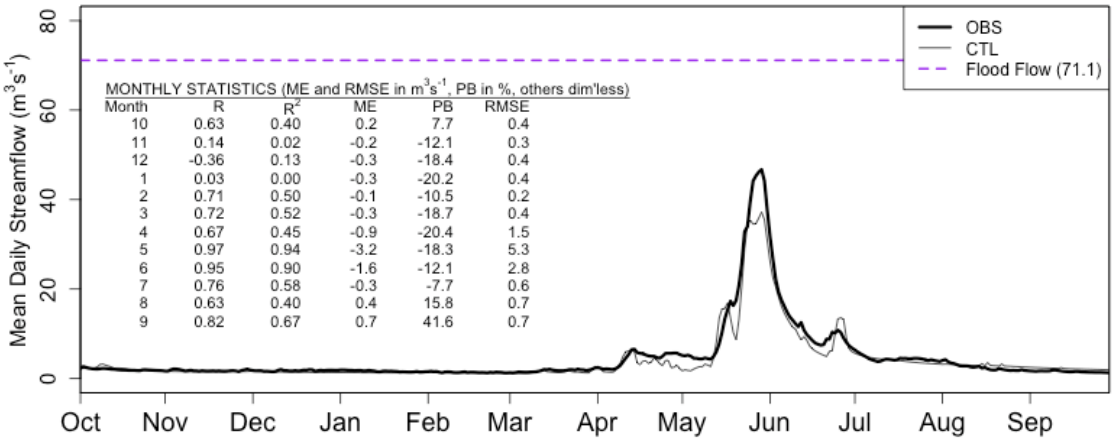

Figure 31: WY2003 observed (bold) and CTL simulated (thin) streamflow for OAWU1

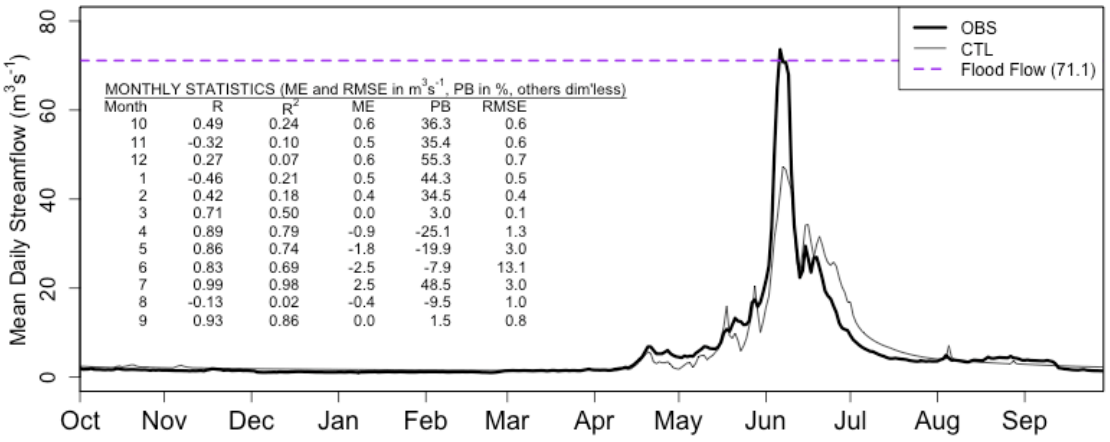

Figure 32: WY2010 observed (bold) and CTL simulated (thin) streamflow for OAWU1

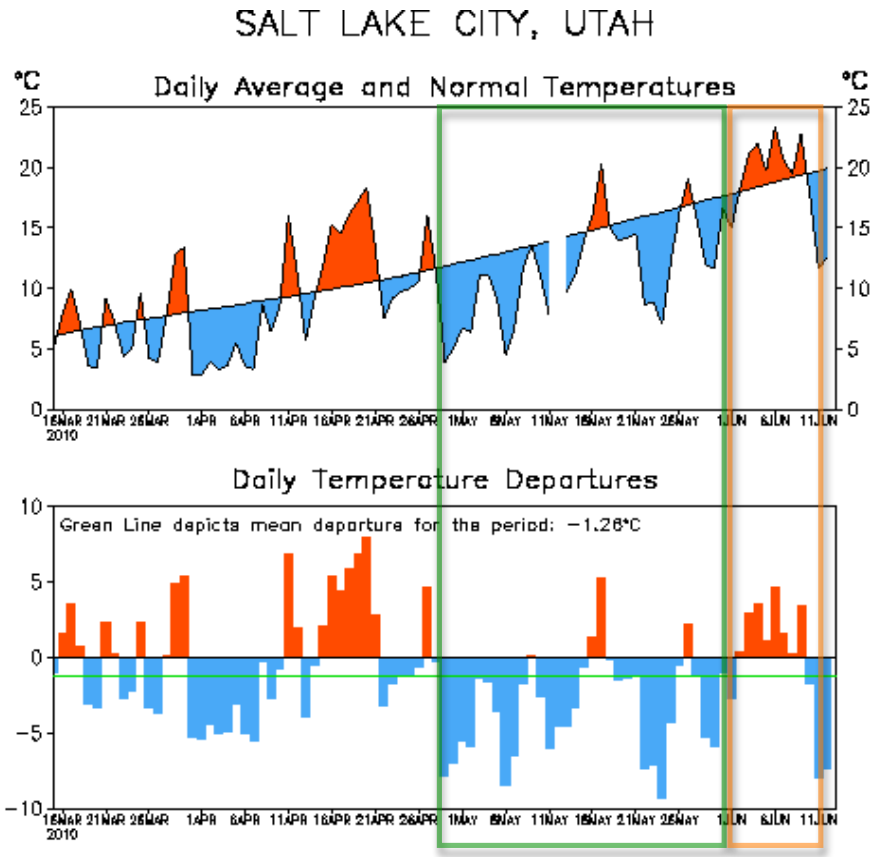

Figure 33: Temperature and temperature departures from normal for Salt Lake City, UT for spring (late March through early June) 2010 (CBRFC, 2010). May 2010 was overall cooler than normal (highlighted in green) while the first week of June was warmer than normal (highlighted in orange).

5.1.2.2 Hydrographs from Direct Insertion Simulations

As mentioned previously, the DI simulations under predict the observed streamflow most of the time. The negative bias is sometimes severe; for example, the monthly mean error for June 2008, for the MO2.AJ DI simulation is nearly -30 $m^3 s^{-1}$ (-84% bias) when compared to the observed streamflow. The observed hydrograph is particularly under predicted during the snowmelt runoff season in most of the years of the WY2000 to WY2010 period. A few cases of over prediction occur during the study period; most over prediction (simulations with positive bias) occurs outside of the snowmelt runoff period of April - July. Several examples of simulated hydrographs that illustrate under and over prediction during the study period are discussed in this section.

Figure 34 shows an example of severely under predicted flow from the MO2.AJ DI simulation for WY2008. In this case, two minor peaks are barely simulated in late May and early June. The simulated peaks of late May and early June of WY2008 for the MO1.WY simulation (Fig, 35) are not as severely under predicted as in the MO2.AJ simulation (Fig. 34), but they still fall short of the magnitude of the observed peak.

Prediction of peak timing by the DI simulations varies. In many cases, the simulated flow is very low compared to the observations, and the simulation lacks an obvious snowmelt-driven peak (Fig. 34). The timing of the snowmelt-driven peak is predicted correctly in some years (e.g., WY2010 for the MO1.AJ simulation shown in Fig. 36) but the predicted peak timing predicted by the DI simulations does not match the observed time of peak in other cases (e.g., WY2006 and WY2007 from the MO2.WY DI simulation, as shown in Figs. 38-39).

Cases of over prediction occasionally occur, usually in the late summer or fall but occasionally as early as June. Figures 34-39 show cases of over prediction (positive bias), primarily in the months of August and September. The degree of over prediction is generally not as dramatic as the under prediction (negative bias) in the DI simulations. Figure 39 shows over prediction by the MO2.WY DI simulation during June 2007. During June 2007, on a monthly basis, the mean error (ME) of the MO2.WY DI simulation is low (0.4 $m^3 s^{-1}$), suggesting that the model performance may be good for the month of June 2007. However, the monthly RMSE for June 2007 is 6.8 $m^3 s^{-1}$, indicating that the overall magnitude of the errors is nonzero; that is, the small monthly bias is due to large positive and negative errors that cancel.

The observed volumes for the water year as a whole are mostly under predicted as well, though there is one instance of over prediction (MO2.AJ simulation, WY2007 – see section 5.2.1.2). The water year streamflow volumes predicted by the DI simulations, in terms of under and over prediction of the observed water year volumes, range from -65% to 5% of the observed water year volume.

For the DI simulations, *all* April – July streamflow volumes are under predicted when compared to observations, regardless of the type of MODIS fSCA data used and regardless of the period during which the DI is active. The DI simulations under predict the observed April – July streamflow volumes and are less than the observed volumes by 22 to 81%. The under and over prediction of streamflow volume for the April – July period and the water years as a whole is discussed in detail in sections 5.2.1.2, 5.2.2.1, and 5.3.3.

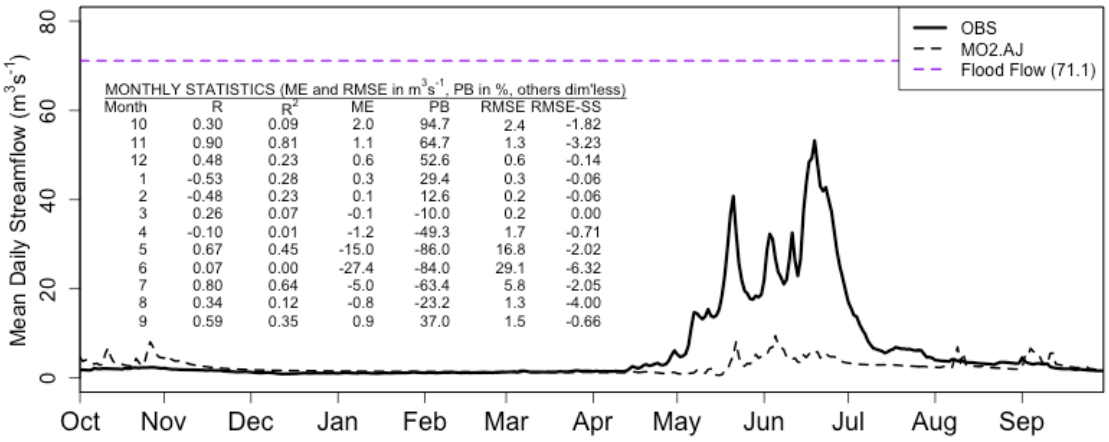

MONTHLY STATISTICS (ME and RMSE in m^3s^{-1}, PB in %, others dim'less)

Month	R	R^2	ME	PB	RMSE	RMSE-SS
10	0.30	0.09	2.0	94.7	2.4	-1.82
11	0.90	0.81	1.1	64.7	1.3	-3.23
12	0.48	0.23	0.6	52.6	0.6	-0.14
1	-0.53	0.28	0.3	29.4	0.3	-0.06
2	-0.48	0.23	0.1	12.6	0.2	-0.06
3	0.26	0.07	-0.1	-10.0	0.2	0.00
4	-0.10	0.01	-1.2	-49.3	1.7	-0.71
5	0.67	0.45	-15.0	-86.0	16.8	-2.02
6	0.07	0.00	-27.4	-84.0	29.1	-6.32
7	0.80	0.64	-5.0	-63.4	5.8	-2.05
8	0.34	0.12	-0.8	-23.2	1.3	-4.00
9	0.59	0.35	0.9	37.0	1.5	-0.66

Figure 34: WY2008 observed (bold) and MO2.AJ simulated (dashed) of streamflow for OAWU1

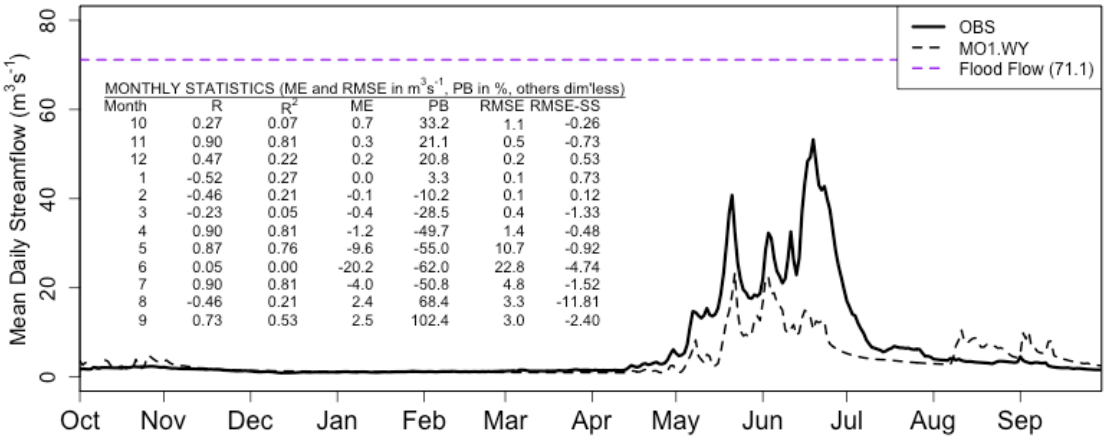

MONTHLY STATISTICS (ME and RMSE in m^3s^{-1}, PB in %, others dim'less)

Month	R	R^2	ME	PB	RMSE	RMSE-SS
10	0.27	0.07	0.7	33.2	1.1	-0.26
11	0.90	0.81	0.3	21.1	0.5	-0.73
12	0.47	0.22	0.2	20.8	0.2	0.53
1	-0.52	0.27	0.0	3.3	0.1	0.73
2	-0.46	0.21	-0.1	-10.2	0.1	0.12
3	-0.23	0.05	-0.4	-28.5	0.4	-1.33
4	0.90	0.81	-1.2	-49.7	1.4	-0.48
5	0.87	0.76	-9.6	-55.0	10.7	-0.92
6	0.05	0.00	-20.2	-62.0	22.8	-4.74
7	0.90	0.81	-4.0	-50.8	4.8	-1.52
8	-0.46	0.21	2.4	68.4	3.3	-11.81
9	0.73	0.53	2.5	102.4	3.0	-2.40

Figure 35: WY2008 observed (bold) and MO1.WY simulated (dashed) of streamflow for OAWU1

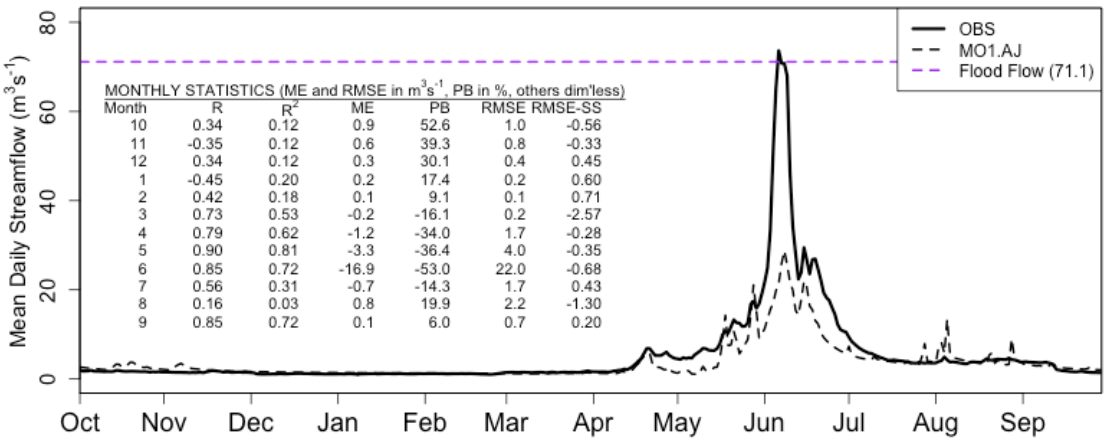

MONTHLY STATISTICS (ME and RMSE in m^3s^{-1}, PB in %, others dim'less)

Month	R	R^2	ME	PB	RMSE	RMSE-SS
10	0.34	0.12	0.9	52.6	1.0	-0.56
11	-0.35	0.12	0.6	39.3	0.8	-0.33
12	0.34	0.12	0.3	30.1	0.4	0.45
1	-0.45	0.20	0.2	17.4	0.2	0.60
2	0.42	0.18	0.1	9.1	0.1	0.71
3	0.73	0.53	-0.2	-16.1	0.2	-2.57
4	0.79	0.62	-1.2	-34.0	1.7	-0.28
5	0.90	0.81	-3.3	-36.4	4.0	-0.35
6	0.85	0.72	-16.9	-53.0	22.0	-0.68
7	0.56	0.31	-0.7	-14.3	1.7	0.43
8	0.16	0.03	0.8	19.9	2.2	-1.30
9	0.85	0.72	0.1	6.0	0.7	0.20

Figure 36: WY2010 observed (bold) and MO1.AJ simulated (dashed) of streamflow for OAWU1

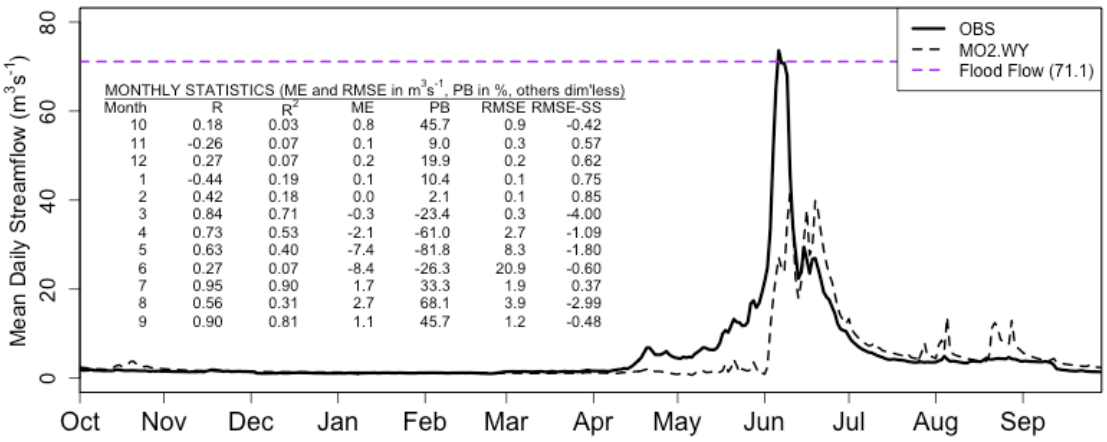

MONTHLY STATISTICS (ME and RMSE in m^3s^{-1}, PB in %, others dim'less)

Month	R	R^2	ME	PB	RMSE	RMSE-SS
10	0.18	0.03	0.8	45.7	0.9	-0.42
11	-0.26	0.07	0.1	9.0	0.3	0.57
12	0.27	0.07	0.2	19.9	0.2	0.62
1	-0.44	0.19	0.1	10.4	0.1	0.75
2	0.42	0.18	0.0	2.1	0.1	0.85
3	0.84	0.71	-0.3	-23.4	0.3	-4.00
4	0.73	0.53	-2.1	-61.0	2.7	-1.09
5	0.63	0.40	-7.4	-81.8	8.3	-1.80
6	0.27	0.07	-8.4	-26.3	20.9	-0.60
7	0.95	0.90	1.7	33.3	1.9	0.37
8	0.56	0.31	2.7	68.1	3.9	-2.99
9	0.90	0.81	1.1	45.7	1.2	-0.48

Figure 37: WY2010 observed (bold) and MO2.WY simulated (dashed) of streamflow for OAWU1

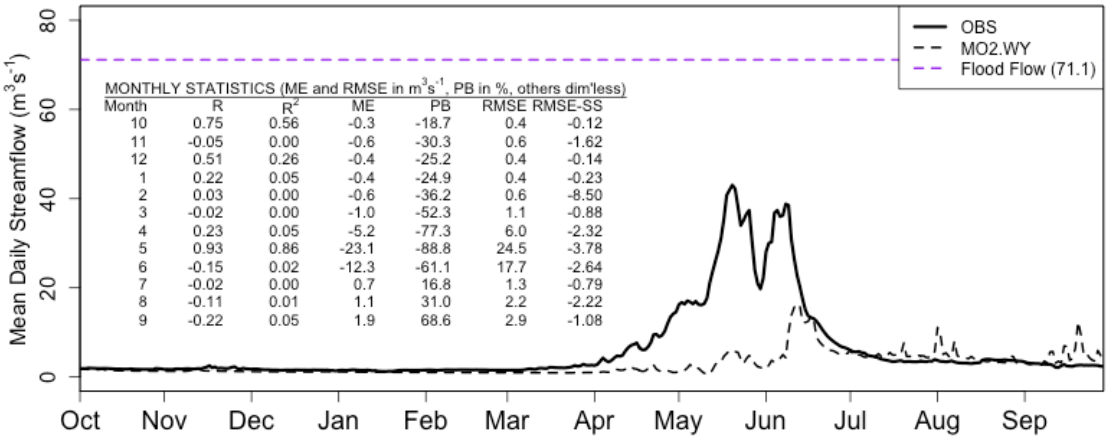

MONTHLY STATISTICS (ME and RMSE in m^3s^{-1}, PB in %, others dim'less)

Month	R	R^2	ME	PB	RMSE	RMSE-SS
10	0.75	0.56	-0.3	-18.7	0.4	-0.12
11	-0.05	0.00	-0.6	-30.3	0.6	-1.62
12	0.51	0.26	-0.4	-25.2	0.4	-0.14
1	0.22	0.05	-0.4	-24.9	0.4	-0.23
2	0.03	0.00	-0.6	-36.2	0.6	-8.50
3	-0.02	0.00	-1.0	-52.3	1.1	-0.88
4	0.23	0.05	-5.2	-77.3	6.0	-2.32
5	0.93	0.86	-23.1	-88.8	24.5	-3.78
6	-0.15	0.02	-12.3	-61.1	17.7	-2.64
7	-0.02	0.00	0.7	16.8	1.3	-0.79
8	-0.11	0.01	1.1	31.0	2.2	-2.22
9	-0.22	0.05	1.9	68.6	2.9	-1.08

Figure 38: WY2006 observed (bold) and MO2.WY simulated (dashed) of streamflow for OAWU1

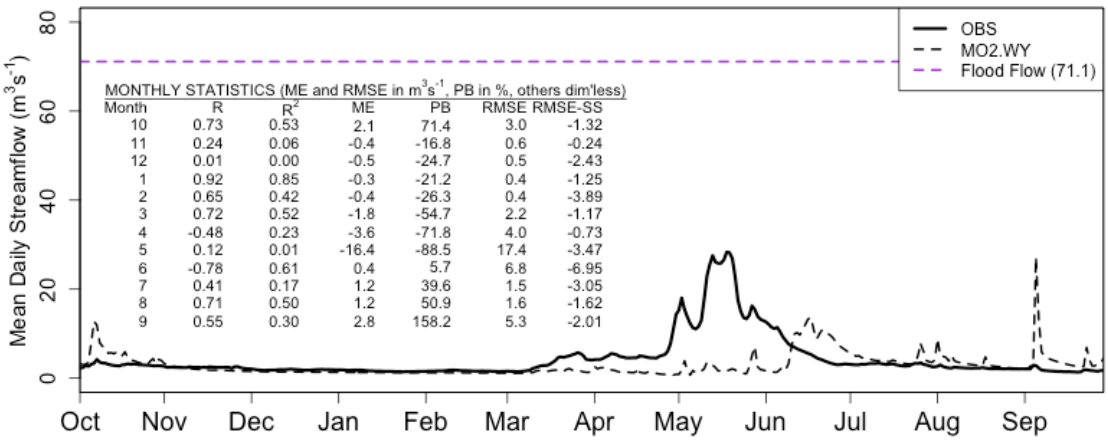

MONTHLY STATISTICS (ME and RMSE in m^3s^{-1}, PB in %, others dim'less)

Month	R	R^2	ME	PB	RMSE	RMSE-SS
10	0.73	0.53	2.1	71.4	3.0	-1.32
11	0.24	0.06	-0.4	-16.8	0.6	-0.24
12	0.01	0.00	-0.5	-24.7	0.5	-2.43
1	0.92	0.85	-0.3	-21.2	0.4	-1.25
2	0.65	0.42	-0.4	-26.3	0.4	-3.89
3	0.72	0.52	-1.8	-54.7	2.2	-1.17
4	-0.48	0.23	-3.6	-71.8	4.0	-0.73
5	0.12	0.01	-16.4	-88.5	17.4	-3.47
6	-0.78	0.61	0.4	5.7	6.8	-6.95
7	0.41	0.17	1.2	39.6	1.5	-3.05
8	0.71	0.50	1.2	50.9	1.6	-1.62
9	0.55	0.30	2.8	158.2	5.3	-2.01

Figure 39: WY2007 observed (bold) and MO2.WY simulated (dashed) of streamflow for OAWU1

5.2 MODEL PERFORMANCE BY QUANTITATIVE METRICS

5.2.1 Overall Performance of Simulations by Quantitative Metrics

5.2.1.1 Control Simulation

The simulated streamflow from the control, which does not include information from the MODIS-derived fSCA values, performs reasonably well (overall errors near zero, biases near zero) over the study period. The mean monthly errors are close to zero outside of the runoff period of April - July (Fig. 40). Within the runoff period (bracketed by red lines in Fig. 40), the control simulation under predicts in some years and over predicts in others, depending on the individual month. The largest errors occur during May (under prediction/negative bias) and June (over prediction/positive bias) of WY2009. The monthly mean errors are most variable in the months of May and June, as shown in Fig. 40.

The monthly RMSE for each water year is low (generally less than 1 m^3s^{-1}, on average for the control simulation) outside of the April – July runoff period (Fig. 41). The RMSE values increase within the runoff period (bracketed in red lines in Figs. 41), with the largest RMSE (13 m^3 s^{-1}) occurring in June 2010. In June 2010, the control simulation does not capture a sharp peak in the observed hydrograph (bold line in Fig. 36), so the monthly RMSE for June 2010 exceeds and is more than double the June RMSE from the other water years. With the exception of WY2010 (where the monthly RMSE value is largest in June), monthly RMSE values are largest for the month of May, indicating that, in general, errors of the largest magnitude occur in May.

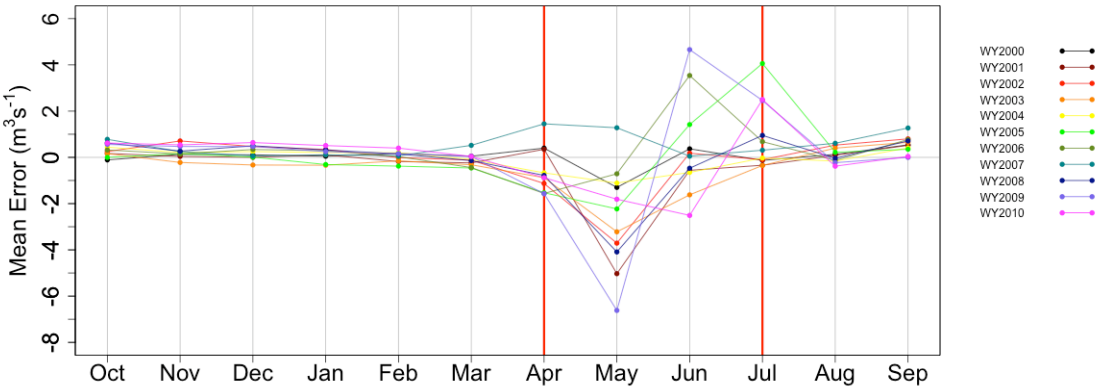

Figure 40: Monthly mean errors for the control simulation, by individual water year of the WY2000 to WY2010 study period. Red lines bracket the spring snowmelt runoff period of April-July.

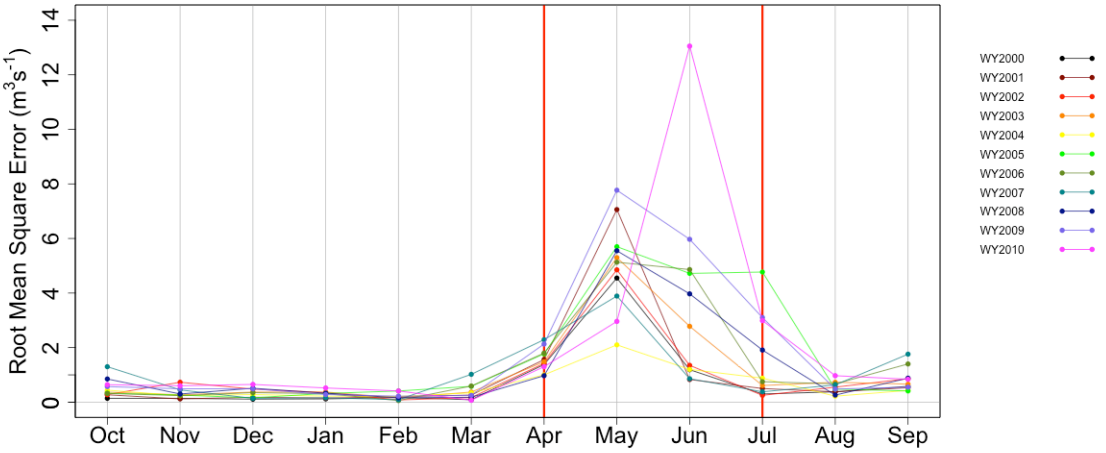

Figure 41: Monthly root mean square error for the control simulation, by individual water year of the WY2000 to WY2010 study period. Red lines bracket the spring snowmelt runoff period of April-July.

5.2.1.2 Direct Insertion Simulations

In contrast to the CTL simulation, the simulated streamflow with active DI has a limited ability to capture characteristics of the observed hydrograph during the study period of WY2000 and WY2010. The simulation accuracy varies with time of year, slightly with the type of MODIS-derived fSCA observations used, and, to a small degree, with the application of DI throughout the full water year (WY simulations) or only during

the April-July runoff season (AJ simulations). Generally, under prediction of the observed flow occurs. Considering the streamflow volumes for each water year, the observed volume is under predicted by the four DI simulations in all but one DI simulation for one year in the study period: WY2007, when the MO2.AJ simulation over predicts the observed volume for the water year by 5% (Fig. 42). More typical patterns of under prediction are shown in Fig. 43, for WY2009, where all four DI simulations under predict the annual streamflow volume by ~30 to ~50%. The resulting under prediction of streamflow by the DI simulation occurs because of the manner in which SNOW17 uses the snow cover extent within its computations (discussed in detail in section 5.3).

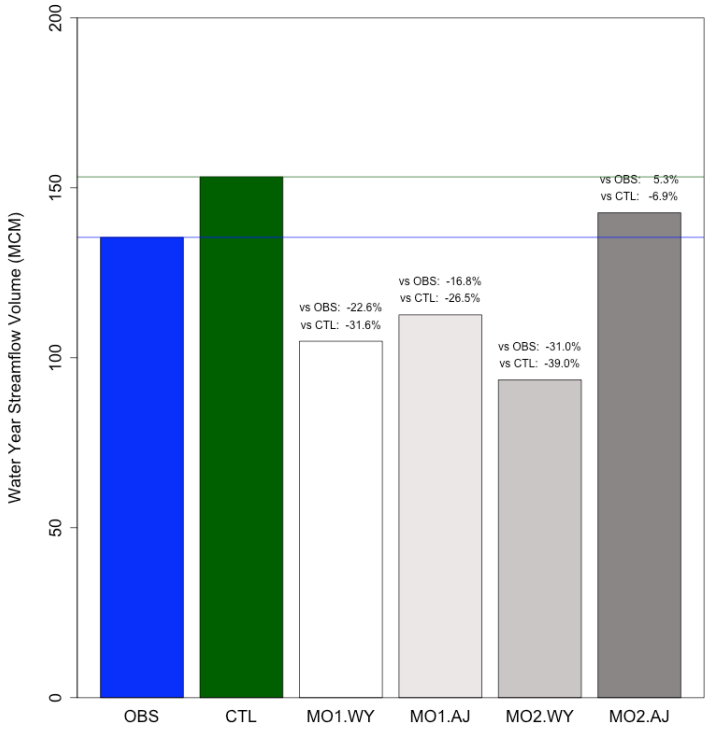

Figure 42: Observed and simulated annual streamflow volumes in million m^3 (MCM) for WY2007. The percent difference in annual streamflow volume between the observed volume and the DI simulations and between the CTL simulation and the DI simulations is also shown.

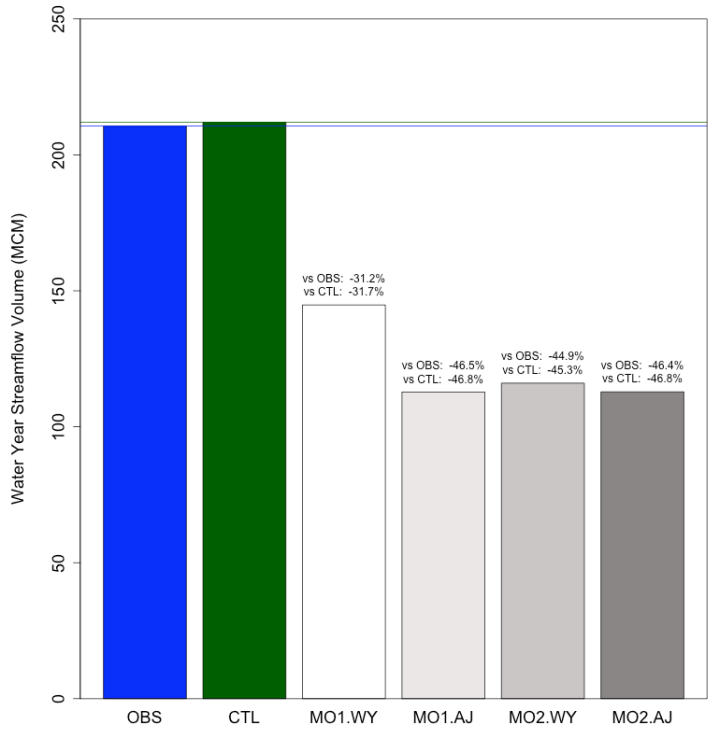

Figure 43: Observed and simulated annual streamflow volumes in million m^3 (MCM) for WY2009. The percent difference in annual streamflow volume between the observed volume and the DI simulations and between the CTL simulation and the DI simulations is also shown.

Severe under prediction occurs regardless of the type of MODIS-derived fSCA used, and regardless of whether the MODIS-derived fSCA is used during the full water year or only during the runoff period of April – July. The most obvious failure of the DI simulations occurs during the runoff season of April – July, the season during which the largest impacts would be anticipated as the snowpack depletes and observed fSCA drops below 100%. Detailed descriptions of the results are organized by seasons of the water year in the next section (5.2.2).

5.2.2 Breakdown of Performance Metrics by Season

The streamflow simulations from the control run and the simulations run with active DI are compared to observed data using the measure of association and error metrics described in section 4.7.2. In addition, a skill score (section 4.7.2.2) is used to compare the performance of the DI simulations to the control simulation. The evaluation metrics were calculated and then averaged on a monthly basis.

Results during the April – July snowmelt runoff period are described first, since this period is the most important period of the year for seasonal streamflow volume with respect to water supplies. During the study period, on average, 75 percent of the annual water volume observed at the USGS gage at the study basin outlet is observed during the months of April – July. The snowpack at the start of the runoff period serves as an indicator of the runoff water volume potentially yielded by the snowpack (McInerney and Alvord, 2007). The runoff period is also the period during which DI of MODIS-derived fSCA most dramatically impacts the streamflow simulations. Descriptions of results from other seasons of the water year follow the description of the runoff period results.

5.2.2.1 Ablation/Runoff Season (April – July)

The OAWU1 watershed has a distinct ablation season. Snowmelt is the primary driver of flows in the spring, and the highest flows of the water year are observed in the April-July runoff period (Fig. 15). The spring and early summer runoff season is when snowmelt-driven high flows can occur and when water managers must make decisions

about their operations, so it is the most important period of the water year with respect to streamflow prediction accuracy.

As discussed in section 5.1, during the melt period, the control (CTL) simulation predicts the observed hydrograph in most water years of the study. The most prominent exception is the under prediction of the sharp snowmelt runoff peak for WY2010, which occurred in June 2010 (Fig. 36).

Unfortunately, the DI of MODIS-derived fSCA observations mostly results in drastic under prediction of the observed streamflow during the April – July melt season. Tables 21-23 show the values of the error statistics by month of the April – July runoff period, averaged over the study period of WY2000 to WY2010. All of the values for the error metrics indicate under prediction during the runoff season when averaged over the study period of WY2000 to WY2010, with the most extensive under prediction occurring in May for all DI simulations.

Table 21: Ablation season (April – July) monthly mean error (ME, units of m^3s^{-1}) for the study period of WY2000 to WY2010, for the five streamflow simulations within the experiment.

Month	WY00-WY10 Mean Error CTL	WY00-WY10 Mean Error MO1.WY	WY00-WY10 Mean Error MO1.AJ	WY00-WY10 Mean Error MO2.WY	WY00-WY10 Mean Error MO2.AJ
4	-0.62	-2.07	-1.90	-3.27	-2.78
5	-2.60	-11.23	-11.90	-15.74	-15.28
6	0.40	-9.19	-10.09	-9.84	-10.39
7	0.91	-0.48	-0.44	-0.42	-0.37

Table 22: Ablation season (April – July) monthly average percent bias (PB, units of %) for the study period of WY2000 to WY2010, for the five streamflow simulations within the experiment.

Month	WY00-WY10 Percent Bias CTL	WY00-WY10 Percent Bias MO1.WY	WY00-WY10 Percent Bias MO1.AJ	WY00-WY10 Percent Bias MO2.WY	WY00-WY10 Percent Bias MO2.AJ
4	-13.39 %	-44.08 %	-40.19 %	-69.40 %	-58.69 %
5	-14.46 %	-61.07 %	-63.40 %	-85.15 %	-82.65 %
6	0.90 %	-51.95 %	-55.56 %	-56.67 %	-52.80 %
7	13.49 %	-5.51 %	-3.28 %	-5.05 %	-1.96 %

Table 23: Monthly average root mean square error (RMSE, units of m^3s^{-1}) for the study period of WY2000 to WY2010, for the five streamflow simulations within the experiment.

Month	WY00-WY10 Root Mean Square Error CTL	WY00-WY10 Root Mean Square Error MO1.WY	WY00-WY10 Root Mean Square Error MO1.AJ	WY00-WY10 Root Mean Square Error MO2.WY	WY00-WY10 Root Mean Square Error MO2.AJ
4	1.55	2.44	2.37	3.74	3.36
5	4.99	13.04	13.89	17.82	17.47
6	3.71	11.64	12.27	13.86	15.00
7	1.49	1.85	2.05	2.47	2.61

Under prediction of the observed streamflow by the DI simulations during the melt season, in terms of percent bias (PB) for individual months, ranges from -4% to -92% among all DI simulations (Fig 44-47). The MOD10A DI simulations suffer from under prediction, -40 to -60% PB (Fig. 44-45), but less severely than the MODSCAG DI runs (Fig. 46-47). The largest under prediction occurs with the MODSCAG DI runs, which commonly have PB values of -50 to -80% (Fig. 46-47), particularly during May. The difference in the degree of under prediction between the MOD10A and MODSCAG DI simulations is related to the fact that MOD10A fSCA is usually greater than MODSCAG's fSCA (e.g., Fig. 20). The low runoff season bias is related to how SNOW17 uses snow-covered area as a multiplier on snowmelt volume initially computed within its snowmelt subroutine. A more detailed explanation of the impacts of SNOW17's use of snow cover extent as a multiplier on meltwater volume is provided in section 5.3.

Over prediction occasionally occurs for individual months in the later part of the runoff period (June and July). Cases of over prediction are more common in July than in June, though a great degree of over prediction can occur in June. For example, the June

2007 PB value is +103.6% for the MO2.AJ simulation (Fig. 47). Causes of the over prediction are discussed in Section 5.3.

In general, the DI simulations do not represent predictions that would be useful to emergency managers or other users of streamflow predictions. The severe under prediction that occurs during the April-July snowmelt runoff period is the primary reason. Explanations of the under prediction/negative bias are offered in section 5.3.

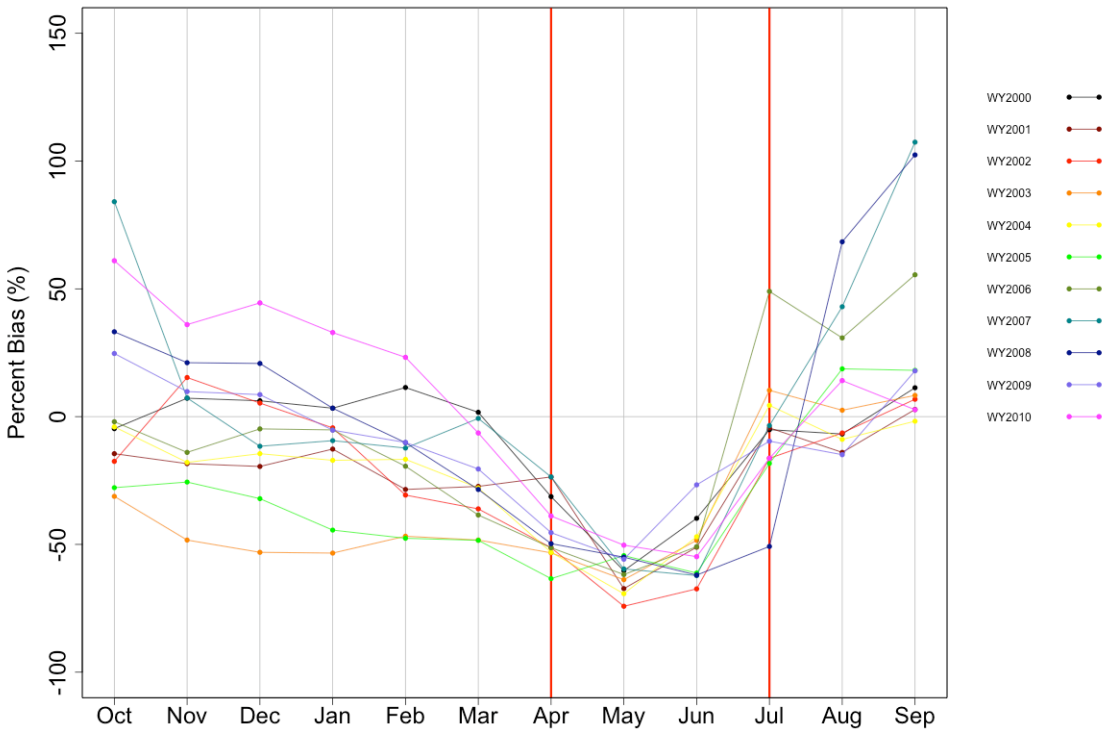

Figure 44: Monthly average percent bias for individual water years in the study period of WY2000 to WY2010, for the DI simulation MO1.WY

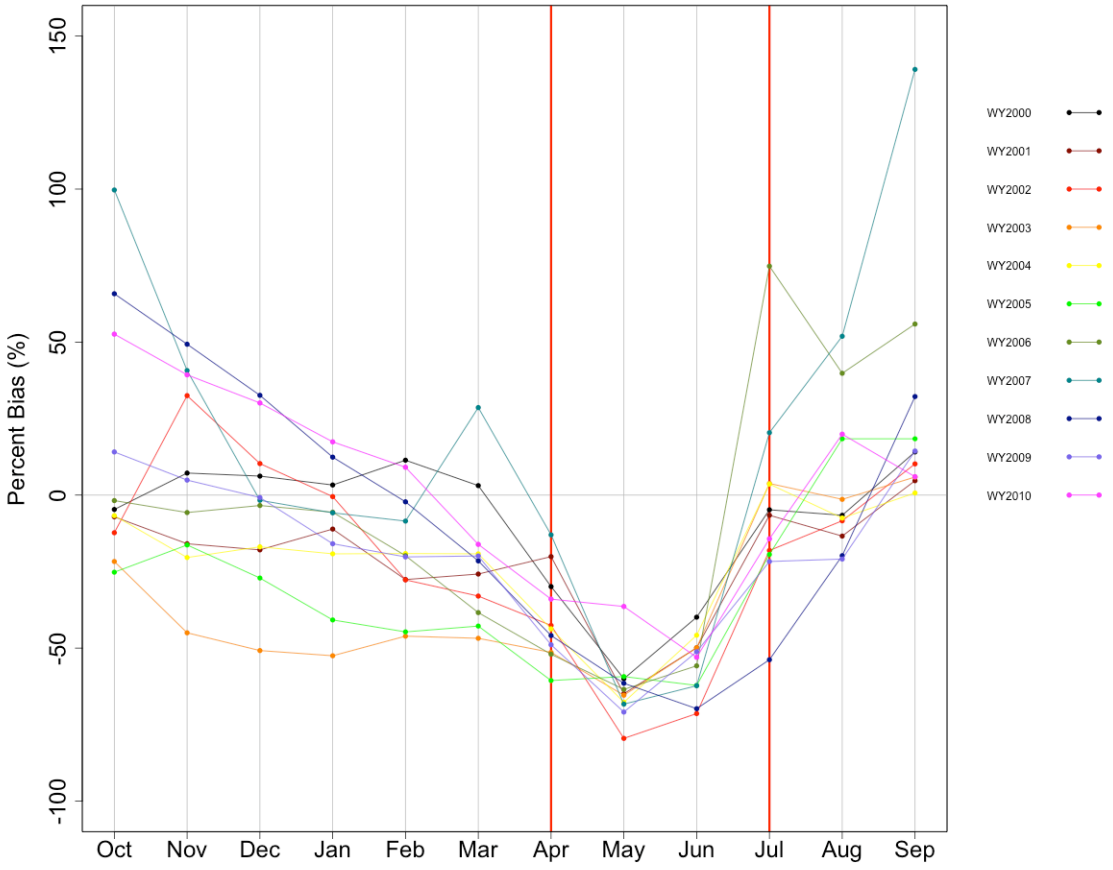

Figure 45: Monthly average percent bias for individual water years in the study period of WY2000 to WY2010, for the DI simulation MO1.AJ

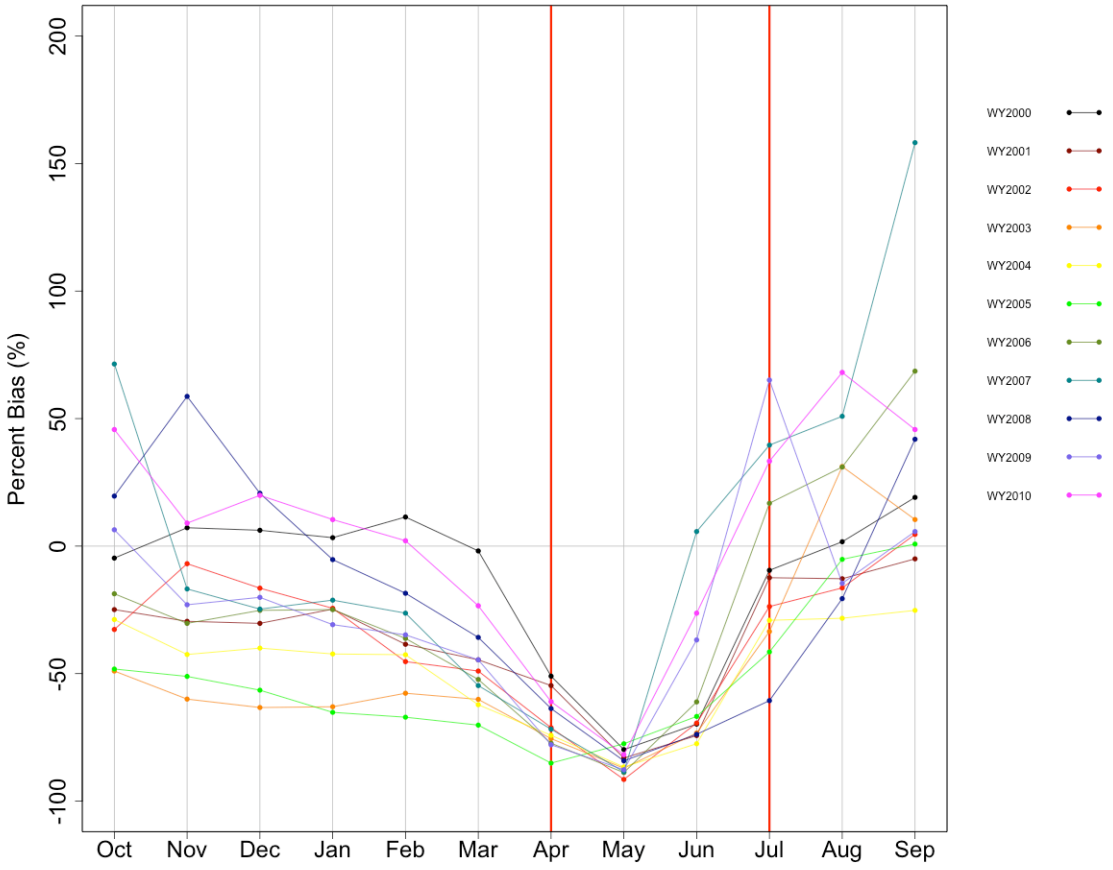

Figure 46: Monthly average percent bias for individual water years in the study period of WY2000 to WY2010, for the DI simulation MO2.WY

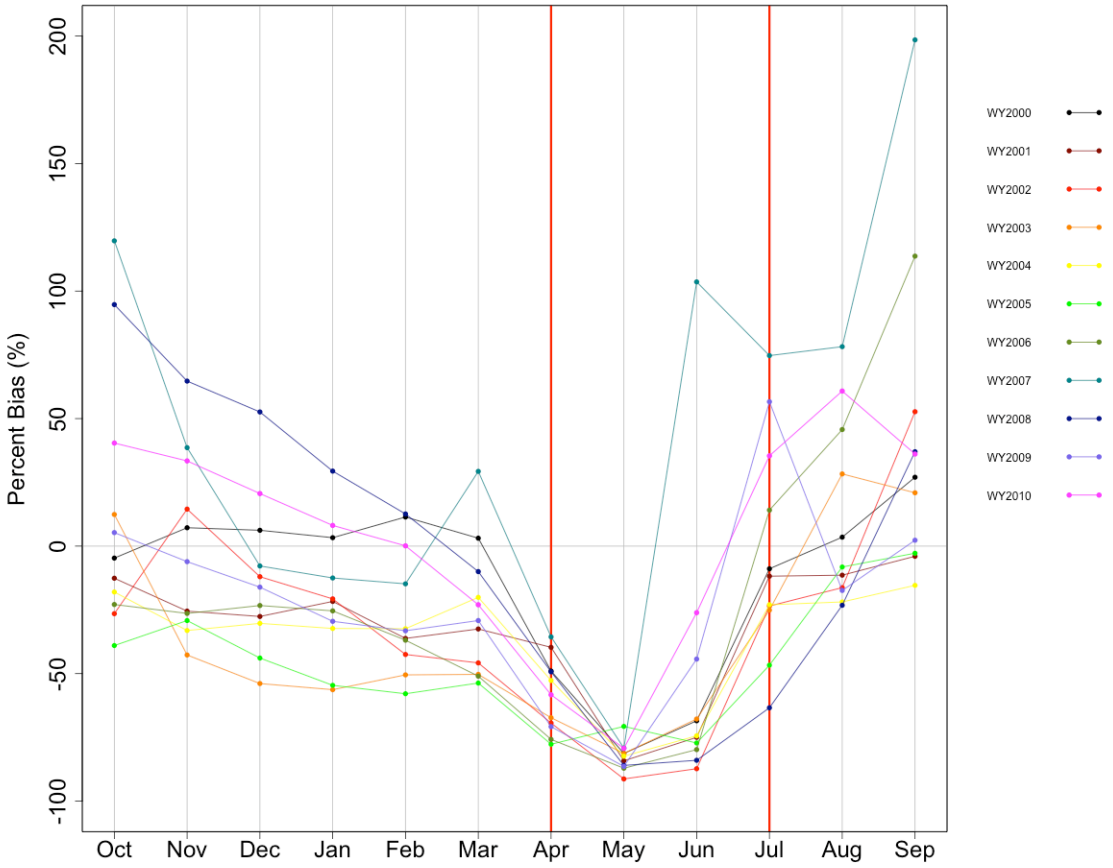

Figure 47: Monthly average percent bias for individual water years in the study period of WY2000 to WY2010, for the DI simulation MO2.AJ

5.2.2.2 Late Summer/Early Fall (August - September)

During the late summer and early fall, a mix of under and over prediction occurs during the month of August, depending on the water year (Fig. 48). All of the simulations (CTL and DI) are more likely to over predict during the month of September (Fig. 49) than in August. OAWU1 streamflow is dominated by baseflow in the late summer and early fall, the seasonal snowmelt runoff has finished, and no floods occur.

The streamflow during this season is small, and errors are often of the same order of magnitude as the observations. Hence, the errors in the DI simulations, even though the PB values in September may approach 200%, are less of a concern in August and September than during the runoff period of April-July, which is more important in terms of flooding and streamflow for water supply. Regardless, causes of the simulations' deviations from the observed streamflow are discussed further in Section 5.3.

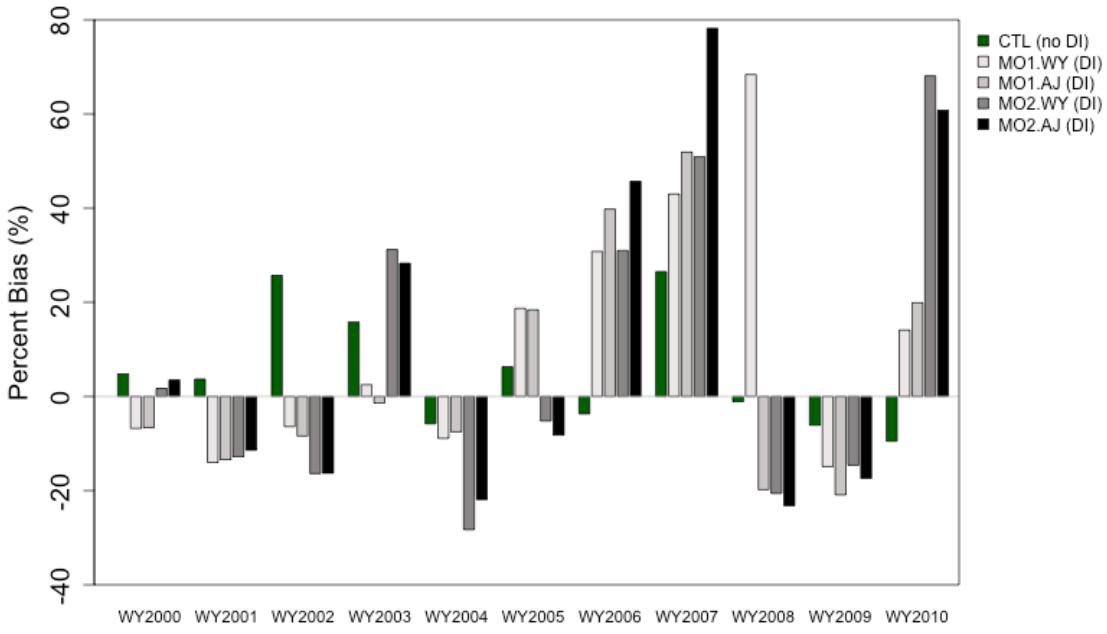

	WY2000	WY2001	WY2002	WY2003	WY2004	WY2005	WY2006	WY2007	WY2008	WY2009	WY2010
CTL	4.8	3.7	25.7	15.8	-5.8	6.3	-3.7	26.5	-1.1	-6.1	-9.5
MO1.WY	-6.8	-14.0	-6.4	2.5	-8.9	18.7	30.8	43.0	68.4	-14.9	14.1
MO1.AJ	-6.6	-13.4	-8.4	-1.4	-7.5	18.4	39.8	51.9	-19.8	-20.9	19.9
MO2.WY	1.7	-12.8	-16.4	31.2	-28.3	-5.2	31.0	50.9	-20.6	-14.6	68.1
MO2.AJ	3.5	-11.4	-16.3	28.3	-21.9	-8.2	45.7	78.2	-23.2	-17.4	60.8

Figure 48: Mean monthly percent bias (PB) for August during the study period of WY00 to WY10, for all simulations (CTL and DI) within the experiment. PB values for individual water years and individual simulations are shown in the table below the plot.

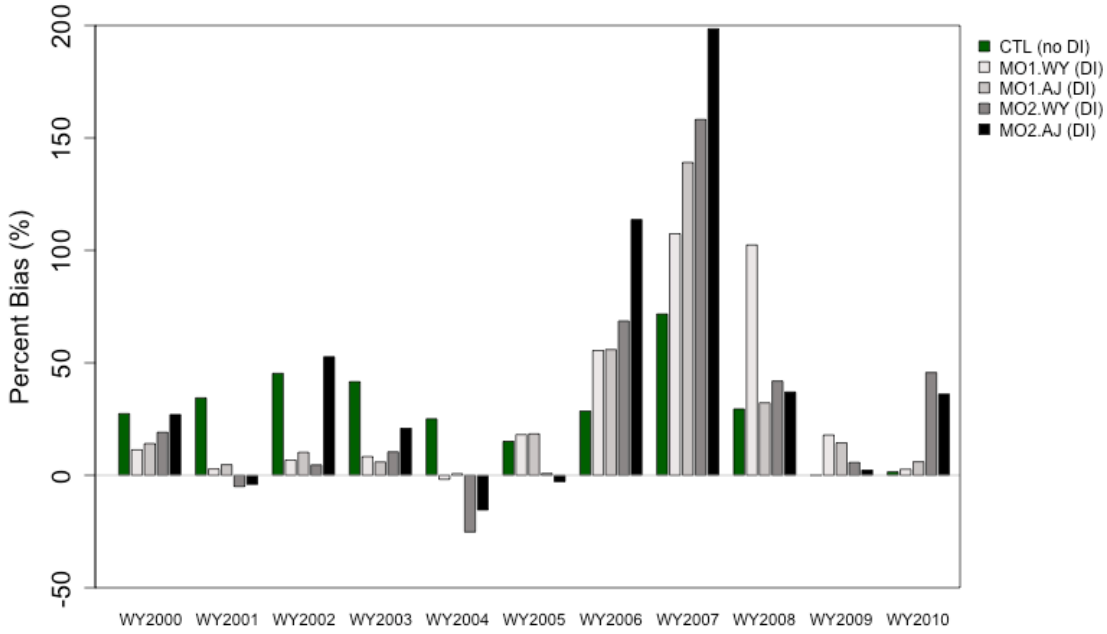

CTL	27.4	34.4	45.3	41.6	25.1	15.1	28.5	71.7	29.5	0.0	1.5
MO1.WY	11.3	2.8	6.8	8.3	-1.8	18.1	55.5	107.4	102.4	17.9	2.7
MO1.AJ	14.1	4.7	10.2	5.9	0.7	18.4	55.9	139.1	32.2	14.4	6.0
MO2.WY	19.1	-5.0	4.6	10.4	-25.2	0.8	68.6	158.2	41.9	5.7	45.7
MO2.AJ	27.0	-4.0	52.7	20.9	-15.4	-2.8	113.7	198.5	37.0	2.3	36.1

Figure 49: Mean monthly percent bias (PB) for September during the study period of WY00 to WY10, for all simulations (CTL and DI) within the experiment. PB values for individual water years and individual simulations are shown in the table below the plot.

5.2.2.3 Fall Baseflow (October – November)

During October, mean error (ME) and root mean square error (RMSE) are all near zero for most years (Figs. 50-51). Notable exceptions are WY2007 (October of calendar year 2006) and WY2008 (October of calendar year 2007), when over prediction occurs, and average errors are three to four times the average October errors of other water years. The over prediction that occurs in October 2006 and October 2007 is related to the availability of MODIS fSCA values of greater than 5% (discussed in section 5.3.3).

The October percent bias (PB) metric generally follows the same patterns as the ME and RMSE, where October 2006 shows the largest errors and the magnitude of the

metric for October is similar among other years. However, for the majority of the years, observed and simulated streamflow are low in October. An error that is small in magnitude may be large, percentage-wise, in situations of low flow. Because streamflow in the OAWU1 watershed is heavily dominated by snowmelt, the large PB values in the month of October (indicating poor model performance) are less concerning than the poor model performance during the runoff period of April – July. Specifically, flows in October are usually low, October streamflow is not of primary importance as a source of water supply, and no flooding occurs in October of the study period. The full set of statistics is available in Appendix A.

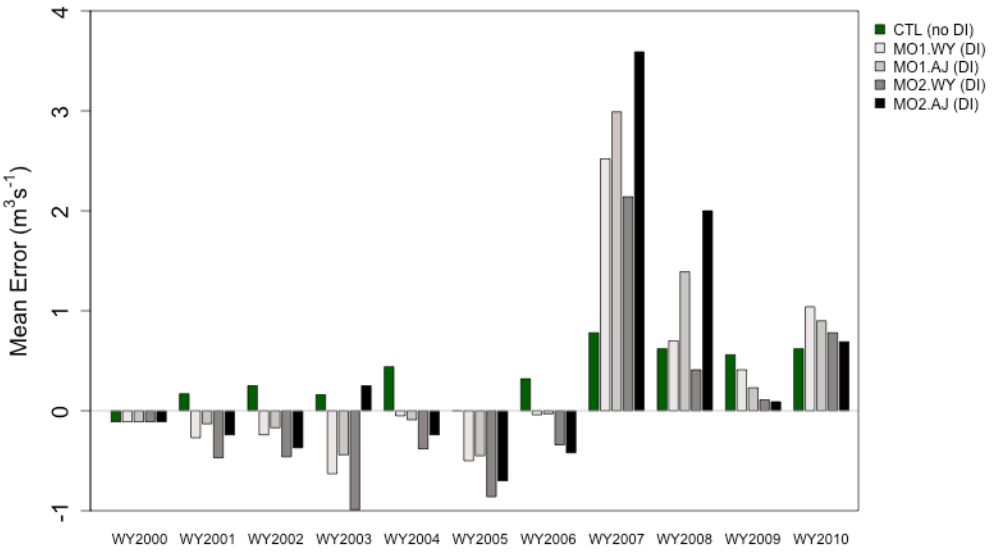

Figure 50: October mean error (m3 s-1) for all simulations during the study period of WY00 to WY10, for all simulations (CTL and DI) within the experiment. ME values for individual water years and individual simulations are shown in the table below the plot.

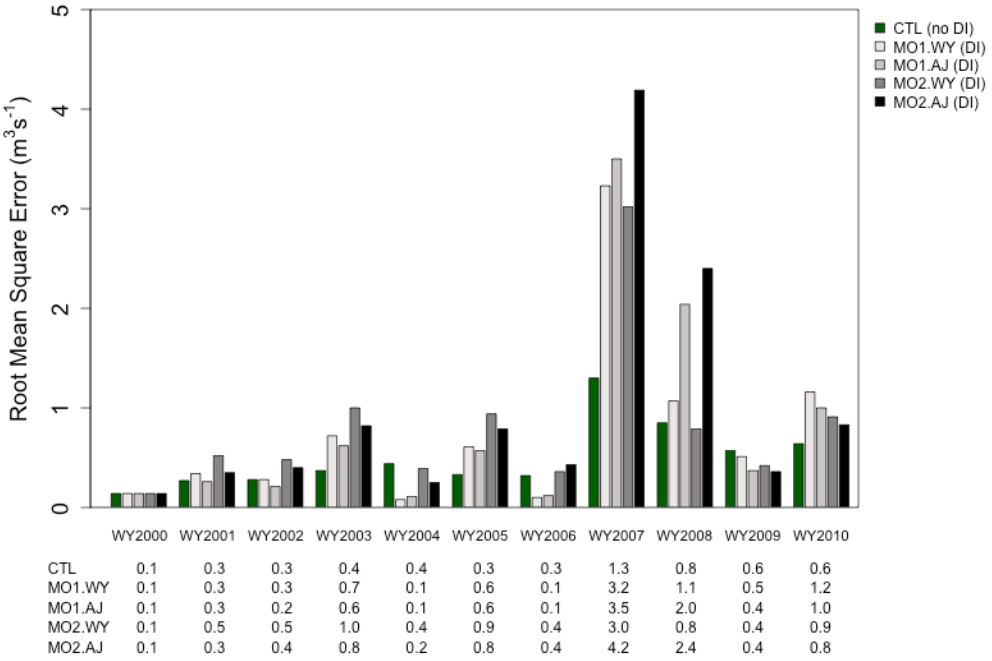

	WY2000	WY2001	WY2002	WY2003	WY2004	WY2005	WY2006	WY2007	WY2008	WY2009	WY2010
CTL	0.1	0.3	0.3	0.4	0.4	0.3	0.3	1.3	0.8	0.6	0.6
MO1.WY	0.1	0.3	0.3	0.7	0.1	0.6	0.1	3.2	1.1	0.5	1.2
MO1.AJ	0.1	0.3	0.2	0.6	0.1	0.6	0.1	3.5	2.0	0.4	1.0
MO2.WY	0.1	0.5	0.5	1.0	0.4	0.9	0.4	3.0	0.8	0.4	0.9
MO2.AJ	0.1	0.3	0.4	0.8	0.2	0.8	0.4	4.2	2.4	0.4	0.8

Figure 51: October monthly root mean square error (m^3 s^{-1}) for all simulations during the study period of WY00 to WY10, for all simulations (CTL and DI) within the experiment. RMSE values for individual water years and individual simulations are shown in the table below the plot.

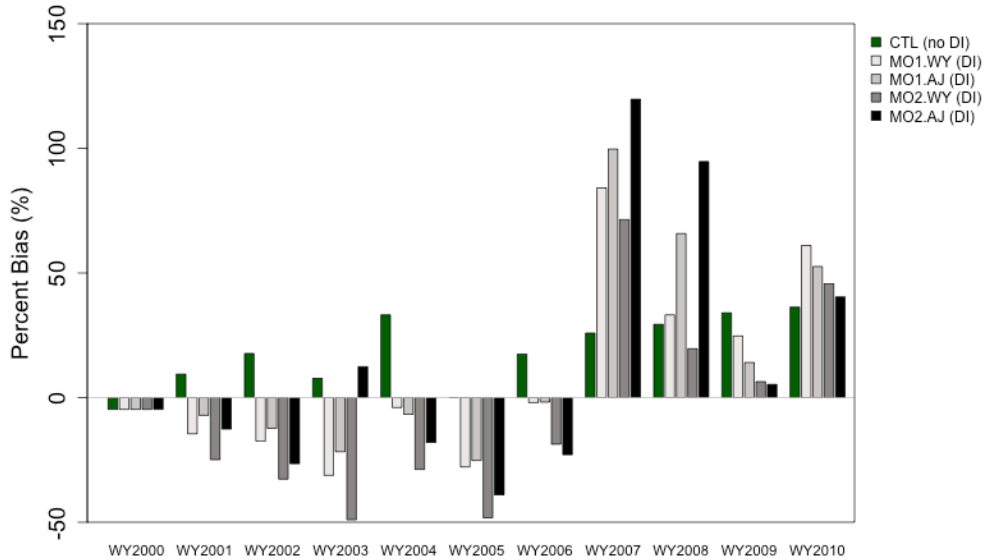

	WY2000	WY2001	WY2002	WY2003	WY2004	WY2005	WY2006	WY2007	WY2008	WY2009	WY2010
CTL	-4.7	9.4	17.7	7.7	33.2	0.0	17.4	25.9	29.4	34.0	36.3
MO1.WY	-4.7	-14.5	-17.5	-31.2	-4.0	-27.8	-2.0	84.1	33.2	24.7	61.0
MO1.AJ	-4.7	-7.1	-12.3	-21.7	-6.7	-25.2	-1.8	99.7	65.8	14.1	52.6
MO2.WY	-4.7	-24.9	-32.7	-49.0	-28.8	-48.2	-18.7	71.4	19.6	6.4	45.7
MO2.AJ	-4.7	-12.6	-26.5	12.4	-18.0	-39.0	-22.9	119.7	94.7	5.3	40.4

Figure 52: October monthly percent bias during the study period of WY00 to WY10, for all simulations (CTL and DI) within the experiment. PB values for individual water years and individual simulations are shown in the table below the plot.

During the month of November, the mean error and root mean square error performance metrics are near zero and similar for the control simulation and the DI simulations. Following a pattern consistent throughout the study results, the CTL simulation usually has better performance than the DI simulations. Though they are nonzero, monthly mean errors and root mean square errors for the DI simulations are low in November, compared to other seasons of the water year. For November, the magnitudes of both the monthly mean error and monthly RMSE values for the simulations are less than 1.5 $m^3 s^{-1}$ for all water years in the study (Figs. 53-54). The average magnitudes of these error metrics can be ten times greater during the runoff season months of April - July (see Tables 21 and 23) than during November. Therefore, the monthly ME and RMSE of November, for all simulations, are considered to be minor.

Even though the ME and RMSE values are low, the percent bias (PB) values are seemingly large (generally +/-40-60%) in November for the DI simulations in some years (Fig. 55). The CTL simulation exhibits monthly PB values that are mostly lower than those of the DI simulations, except in one year (WY2002). Despite the seemingly high PB values in some of the water years, the differences in percent bias are less of a concern during the baseflow period of November than during the runoff period of April - July. In the OAWU1 basin at this time of year, flows are low as winter approaches. No flooding occurred in the fall during WY2000 to WY2010, and fall streamflow is not used as a major source of reservoir inflow. Since the majority of the annual runoff occurs between April and July, and the spring and early summer runoff is used to fill reservoirs, efforts to diagnose poor streamflow prediction performance should first focus on the April-July

period. Hence, the large PB values during October and November are not investigated in detail at this time.

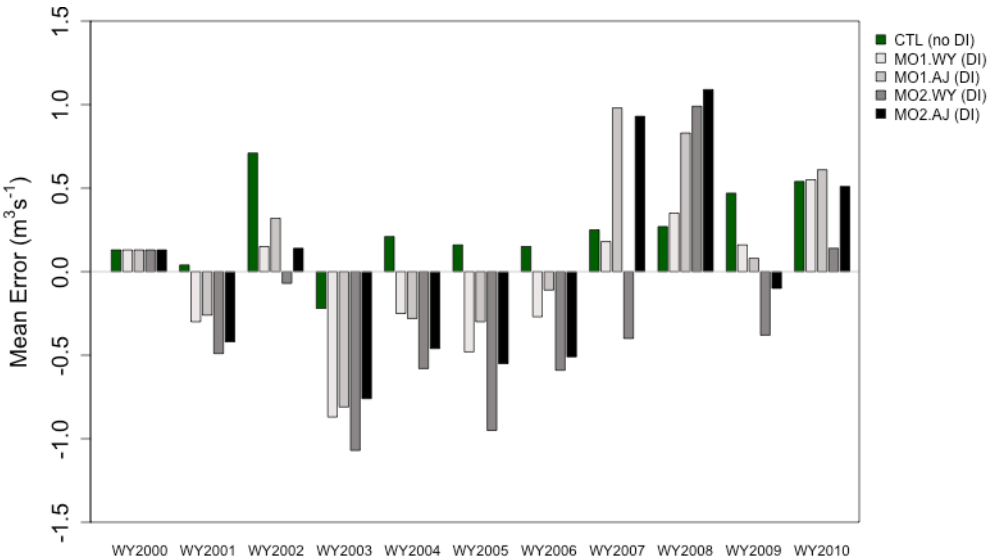

Figure 53: November mean error ($m^3 s^{-1}$) for all simulations during the study period of WY00 to WY10, for all simulations (CTL and DI) within the experiment. ME values for individual water years and individual simulations are shown in the table below the plot.

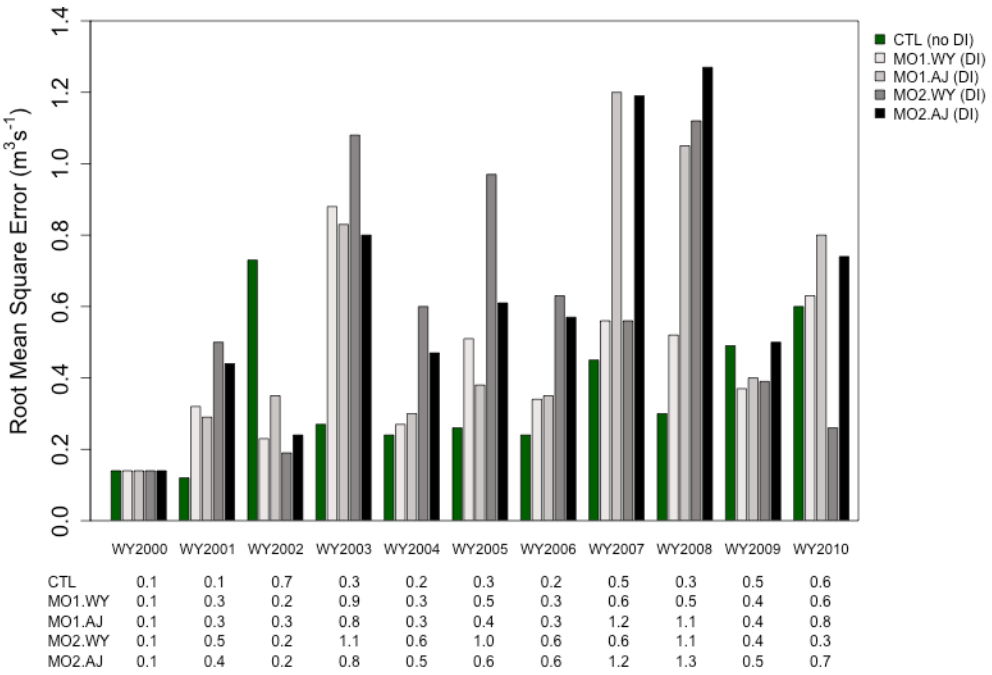

Figure 54: November monthly root mean square error (m3 s-1) for all simulations during the study period of WY00 to WY10, for all simulations (CTL and DI) within the experiment. RMSE values for individual water years and individual simulations are shown in the table below the plot.

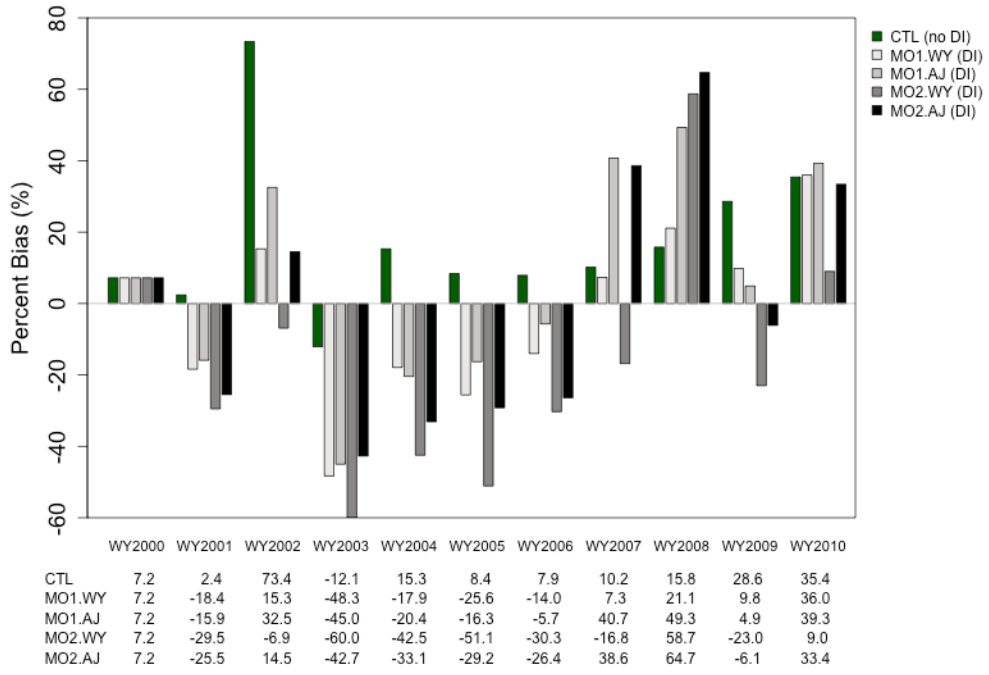

Figure 55: November monthly percent bias during the study period of WY00 to WY10, for all simulations (CTL and DI) within the experiment. PB values for individual water years and individual simulations are shown in the table below the plot

5.2.2.4 Accumulation Season/Winter Baseflow (December – March)

During the winter months, the majority of the precipitation in the OAWU1 basin falls as snow and temperatures are low, so little melt occurs. Streamflow typically remains low, although it increases slightly in March in some years as the melt season approaches. Performance metrics for this season are mixed and vary among the water years of the study period.

For some months, R indicates a strong and rational linear relationship between the observed and simulated streamflow (e.g. near +1.0, as in December for WY2001, January for WY2007, and in March of most water years – see Figs. 56-59). In other months, R is negative (sometimes approaching -1.0), indicating an inverse and irrational relationship between observed and simulated streamflow. The most prominent examples of negative R values during the accumulation period occur in December for WY2002 and WY2005, January of WY2001, and February of WY2002 and WY2008.

The negative Pearson R values indicate an irrational relationship between the observed and simulated streamflow values; as the observed hydrograph is rising, the simulated hydrograph is receding, or vice versa. Pearson's R as an indicator of an inverse relationship between observed and simulation streamflow may be related to timing problems within the simulations. If hydrograph peaks are simulated correctly in magnitude but not with respect to timing, the simulated streamflow may exhibit opposite characteristics of the observed streamflow over short durations (e.g., the simulation may indicate a rise in the hydrograph while the observed streamflow indicates recession).

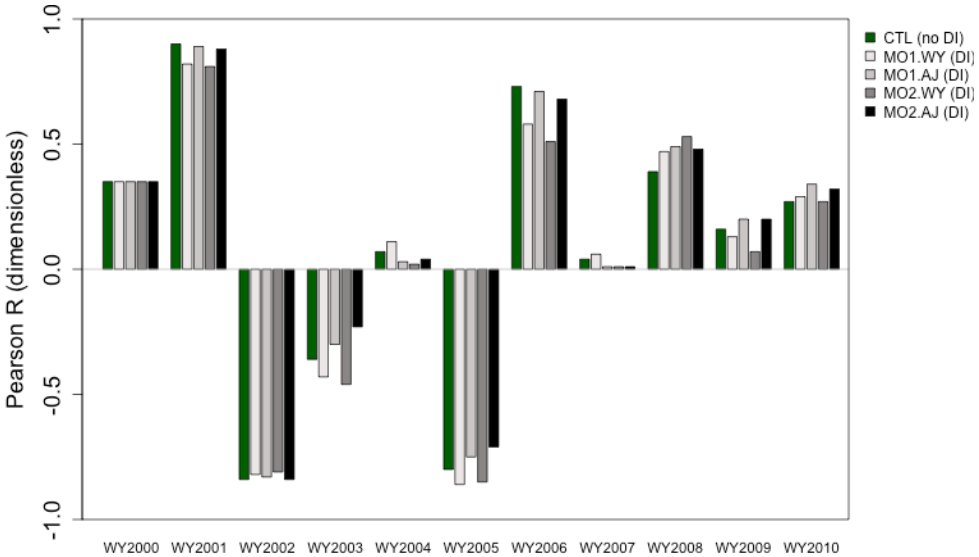

CTL	0.35	0.90	-0.84	-0.36	0.07	-0.80	0.73	0.04	0.39	0.16	0.27
MO1.WY	0.35	0.82	-0.82	-0.43	0.11	-0.86	0.58	0.06	0.47	0.13	0.29
MO1.AJ	0.35	0.89	-0.83	-0.30	0.03	-0.75	0.71	0.01	0.49	0.20	0.34
MO2.WY	0.35	0.81	-0.81	-0.46	0.02	-0.85	0.51	0.01	0.53	0.07	0.27
MO2.AJ	0.35	0.88	-0.84	-0.23	0.04	-0.71	0.68	0.01	0.48	0.20	0.32

Figure 56: December monthly mean Pearson R values for all simulations during the study period of WY00 to WY10, for all simulations (CTL and DI) within the experiment. R values for individual water years and individual simulations are shown in the table below the plot.

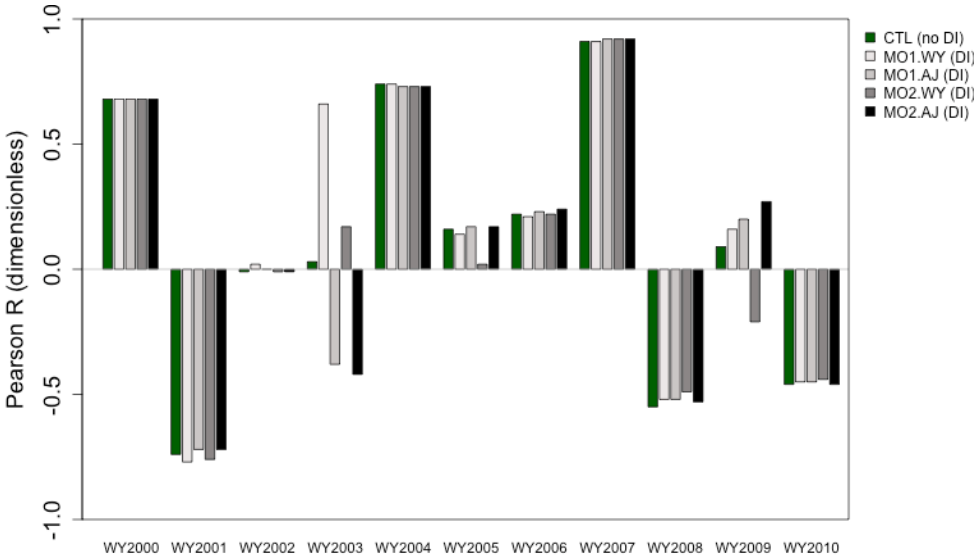

CTL	0.68	-0.74	-0.01	0.03	0.74	0.16	0.22	0.91	-0.55	0.09	-0.46
MO1.WY	0.68	-0.77	0.02	0.66	0.74	0.14	0.21	0.91	-0.52	0.16	-0.45
MO1.AJ	0.68	-0.72	0.00	-0.38	0.73	0.17	0.23	0.92	-0.52	0.20	-0.45
MO2.WY	0.68	-0.76	-0.01	0.17	0.73	0.02	0.22	0.92	-0.49	-0.21	-0.44
MO2.AJ	0.68	-0.72	-0.01	-0.42	0.73	0.17	0.24	0.92	-0.53	0.27	-0.46

Figure 57: January monthly mean Pearson R values for all simulations during the study period of WY00 to WY10, for all simulations (CTL and DI) within the experiment. R values for individual water years and individual simulations are shown in the table below the plot.

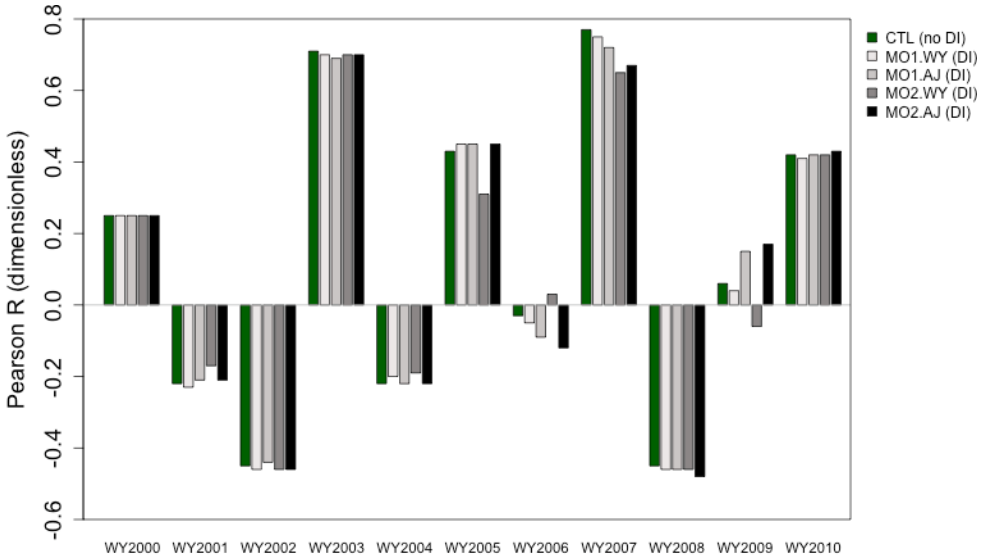

CTL	0.25	-0.22	-0.45	0.71	-0.22	0.43	-0.03	0.77	-0.45	0.06	0.42
MO1.WY	0.25	-0.23	-0.46	0.70	-0.20	0.45	-0.05	0.75	-0.46	0.04	0.41
MO1.AJ	0.25	-0.21	-0.44	0.69	-0.22	0.45	-0.09	0.72	-0.46	0.15	0.42
MO2.WY	0.25	-0.17	-0.46	0.70	-0.19	0.31	0.03	0.65	-0.46	-0.06	0.42
MO2.AJ	0.25	-0.21	-0.46	0.70	-0.22	0.45	-0.12	0.67	-0.48	0.17	0.43

Figure 58: February monthly mean Pearson R values for all simulations during the study period of WY00 to WY10, for all simulations (CTL and DI) within the experiment. R values for individual water years and individual simulations are shown in the table below the plot.

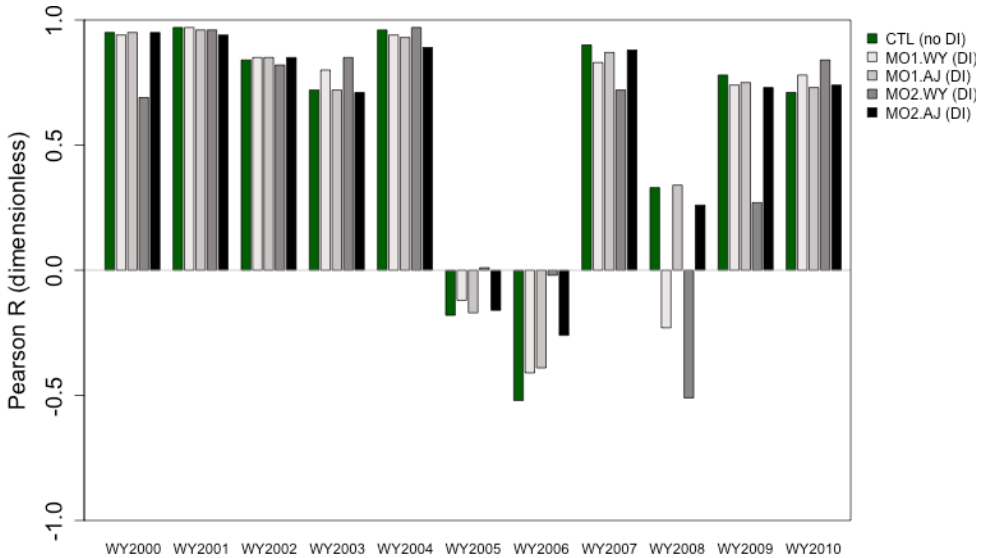

CTL	0.95	0.97	0.84	0.72	0.96	-0.18	-0.52	0.90	0.33	0.78	0.71
MO1.WY	0.94	0.97	0.85	0.80	0.94	-0.12	-0.41	0.83	-0.23	0.74	0.78
MO1.AJ	0.95	0.96	0.85	0.72	0.93	-0.17	-0.39	0.87	0.34	0.75	0.73
MO2.WY	0.69	0.96	0.82	0.85	0.97	0.01	-0.02	0.72	-0.51	0.27	0.84
MO2.AJ	0.95	0.94	0.85	0.71	0.89	-0.16	-0.26	0.88	0.26	0.73	0.74

Figure 59: March monthly mean Pearson R values for all simulations during the study period of WY00 to WY10, for all simulations (CTL and DI) within the experiment. R values for individual water years and individual simulations are shown in the table below the plot.

During the mid winter months (December, January, February), average ME and PB values over the study period of WY2000 to WY2010 show that the DI simulations under predict flows on average by –0.09 to -0.46 $m^3 s^{-1}$ or -4 to -32% (Tables 24 and 25). The CTL simulation tends to over predict in the mid winter months by 0.04 to 0.23 $m^3 s^{-1}$ or 4 to 20% when averaged over the study period (Tables 24 and 25).

For March, the CTL simulation under predicts on average during the study period (ME of -0.11 $m^3 s^{-1}$ on average over the study period), but to a lesser extent than the DI simulations, for which the study period average ME ranges from -0.33 to -0.89 $m^3 s^{-1}$, depending on the DI simulation (Table 24). Percent bias values, averaged over the study period, for the DI simulations range from -21 to -45% for the month of March (Table 25). The average percent bias for the study period for the CTL simulation is -7% (Table 25). RMSE values (Table 26) overall indicate larger magnitudes of error in the accumulation period over the study period of WY 2000 to WY2010 in the DI simulations than in the CTL simulation. The study period average RMSE value for the CTL simulation is lower (0.36 $m^3 s^{-1}$) in March than RMSE values of the DI simulations (0.59 to 0.98 $m^3 s^{-1}$) (Table 26).

Figures 60-63 show the monthly mean error for the months in the accumulation period. The magnitude of the monthly mean errors is low during the accumulation period for most water years in the study period for all simulations (CTL and DI). During December and January, the CTL simulation slightly over predicts while the DI simulations usually under predict (Figs. 60 and 61). The monthly mean error for February indicates a mix of over and under prediction by the CTL simulation and consistent under prediction by the DI simulations (Fig. 62). In March, as the

accumulation season transitions into the spring runoff season, the CTL under predicts more often, and the DI simulations continue a tendency of under prediction and negative bias (Fig. 63). The monthly RMSE values (Figs. 64-67) also show low error magnitudes for the accumulation period).

Table 24: Average streamflow error for the WY2000 to WY2010 study period, for all five simulations, by month of the December – March accumulation season

	Mean Error ($m^3 s^{-1}$) for the Overall Study Period				
Month	CTL	MO1.WY	MO1.AJ	MO2.WY	MO2.AJ
12	0.23	-0.11	-0.09	-0.33	-0.21
1	0.14	-0.17	-0.18	-0.38	-0.29
2	0.04	-0.25	-0.26	-0.46	-0.37
3	-0.11	-0.45	-0.33	-0.89	-0.41

Table 25: Average percent bias for the WY2000 to WY2010 study period, for all five simulations, by month of the December – March accumulation season

	Overall Percent Bias (%) for the Study Period				
Month	CTL	MO1.WY	MO1.AJ	MO2.WY	MO2.AJ
12	20%	-5%	-4%	-21%	-12%
1	13%	-10%	-11%	-26%	-19%
2	4%	-17%	-18%	-32%	-25%
3	-7%	-26%	-21%	-45%	-26%

Table 26: Average streamflow root mean square error for the WY2000 to WY2010 study period, for all five simulations, by month of the December – March accumulation season

	Overall Root Mean Square Error ($m^3 s^{-1}$) for the Study Period				
Month	CTL	MO1.WY	MO1.AJ	MO2.WY	MO2.AJ
12	0.34	0.32	0.30	0.45	0.41
1	0.28	0.29	0.28	0.43	0.40
2	0.20	0.34	0.32	0.50	0.44
3	0.36	0.59	0.64	0.98	0.74

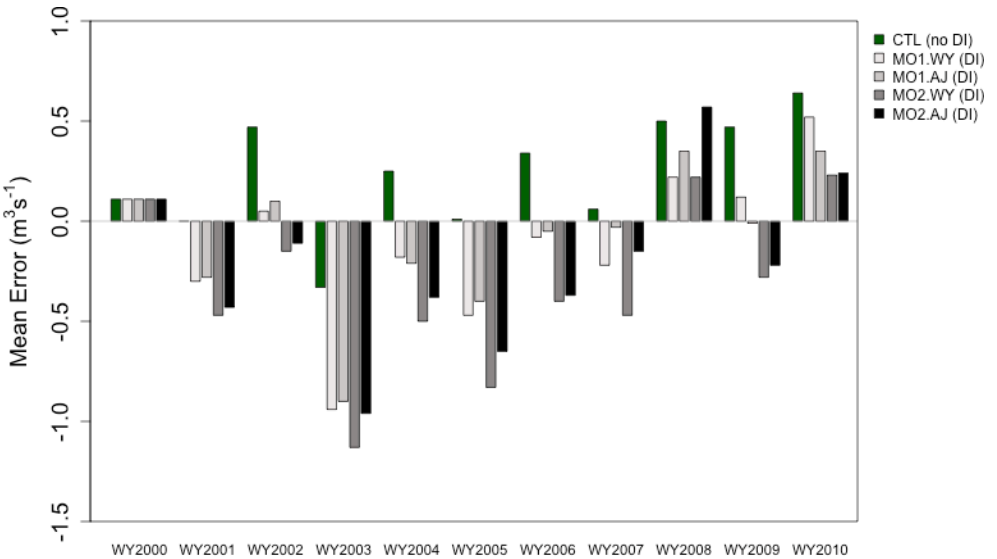

CTL	0.1	0.0	0.5	-0.3	0.2	0.0	0.3	0.1	0.5	0.5	0.6
MO1.WY	0.1	-0.3	0.1	-0.9	-0.2	-0.5	-0.1	-0.2	0.2	0.1	0.5
MO1.AJ	0.1	-0.3	0.1	-0.9	-0.2	-0.4	-0.1	-0.0	0.3	-0.0	0.3
MO2.WY	0.1	-0.5	-0.1	-1.1	-0.5	-0.8	-0.4	-0.5	0.2	-0.3	0.2
MO2.AJ	0.1	-0.4	-0.1	-1.0	-0.4	-0.7	-0.4	-0.1	0.6	-0.2	0.2

Figure 60: December mean error ($m^3 s^{-1}$) for all simulations during the study period of WY00 to WY10, for all simulations (CTL and DI) within the experiment. ME values for individual water years and individual simulations are shown in the table below the plot.

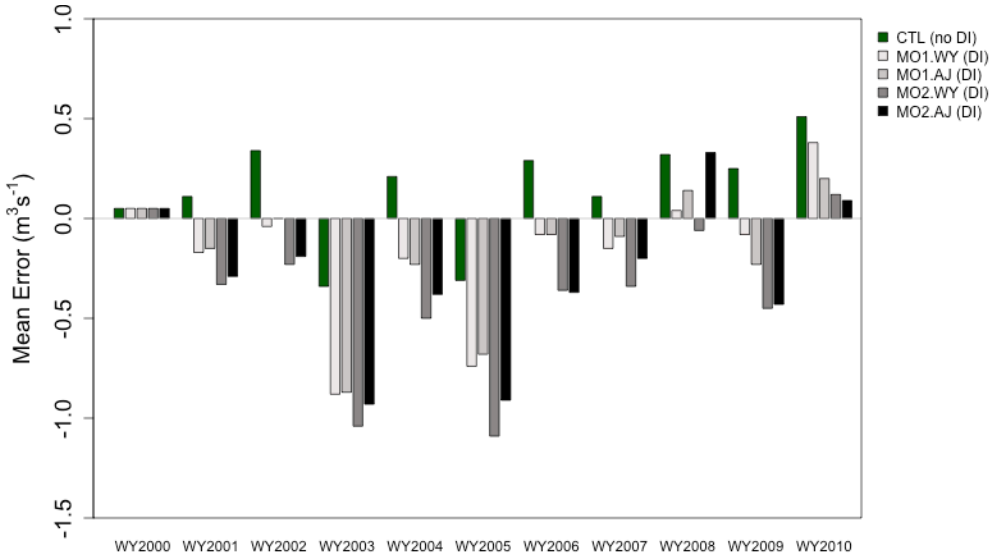

CTL	0.1	0.1	0.3	-0.3	0.2	-0.3	0.3	0.1	0.3	0.2	0.5
MO1.WY	0.1	-0.2	-0.0	-0.9	-0.2	-0.7	-0.1	-0.1	0.0	-0.1	0.4
MO1.AJ	0.1	-0.1	0.0	-0.9	-0.2	-0.7	-0.1	-0.1	0.1	-0.2	0.2
MO2.WY	0.1	-0.3	-0.2	-1.0	-0.5	-1.1	-0.4	-0.3	-0.1	-0.5	0.1
MO2.AJ	0.1	-0.3	-0.2	-0.9	-0.4	-0.9	-0.4	-0.2	0.3	-0.4	0.1

Figure 61: January mean error ($m^3 s^{-1}$) for all simulations during the study period of WY00 to WY10, for all simulations (CTL and DI) within the experiment. ME values for individual water years and individual simulations are shown in the table below the plot.

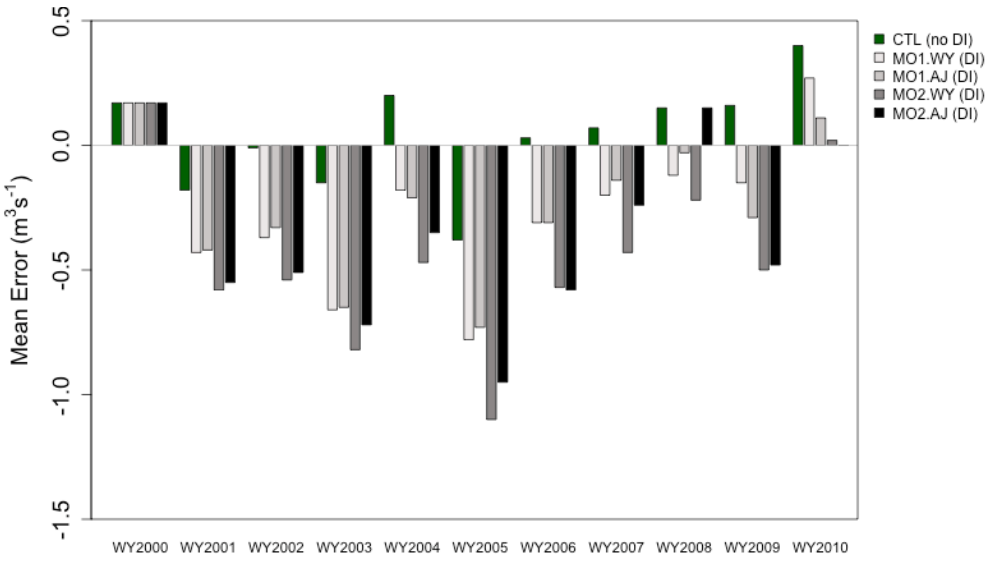

CTL	0.2	-0.2	-0.0	-0.1	0.2	-0.4	0.0	0.1	0.1	0.2	0.4
MO1.WY	0.2	-0.4	-0.4	-0.7	-0.2	-0.8	-0.3	-0.2	-0.1	-0.1	0.3
MO1.AJ	0.2	-0.4	-0.3	-0.7	-0.2	-0.7	-0.3	-0.1	-0.0	-0.3	0.1
MO2.WY	0.2	-0.6	-0.5	-0.8	-0.5	-1.1	-0.6	-0.4	-0.2	-0.5	0.0
MO2.AJ	0.2	-0.6	-0.5	-0.7	-0.3	-0.9	-0.6	-0.2	0.1	-0.5	0.0

Figure 62: February mean error (m^3 s^{-1}) for all simulations during the study period of WY00 to WY10, for all simulations (CTL and DI) within the experiment. ME values for individual water years and individual simulations are shown in the table below the plot.

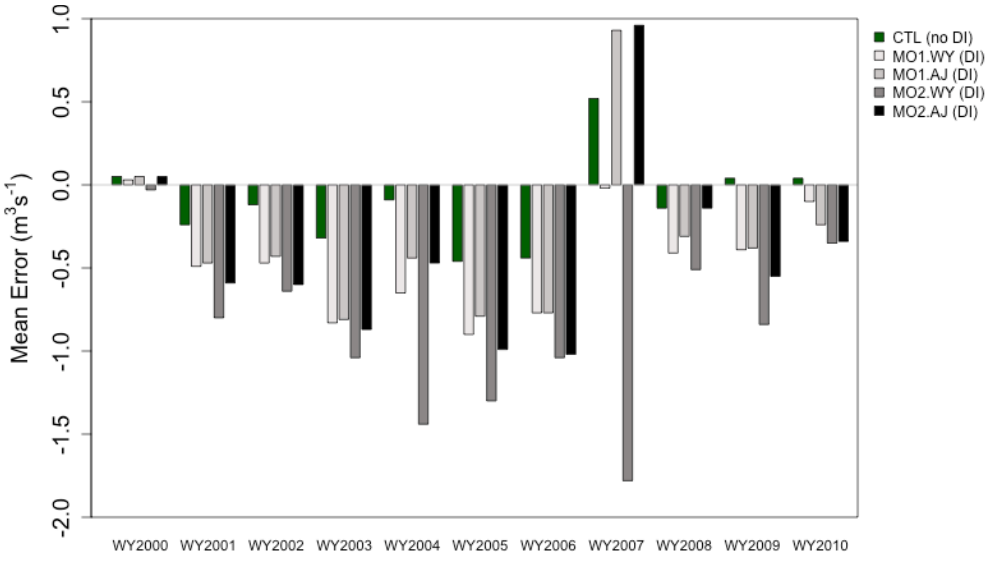

CTL	0.1	-0.2	-0.1	-0.3	-0.1	-0.5	-0.4	0.5	-0.1	0.0	0.0
MO1.WY	0.0	-0.5	-0.5	-0.8	-0.7	-0.9	-0.8	-0.0	-0.4	-0.4	-0.1
MO1.AJ	0.1	-0.5	-0.4	-0.8	-0.4	-0.8	-0.8	0.9	-0.3	-0.4	-0.2
MO2.WY	-0.0	-0.8	-0.6	-1.0	-1.4	-1.3	-1.0	-1.8	-0.5	-0.8	-0.3
MO2.AJ	0.1	-0.6	-0.6	-0.9	-0.5	-1.0	-1.0	1.0	-0.1	-0.6	-0.3

Figure 63: March mean error (m^3 s^{-1}) for all simulations during the study period of WY00 to WY10, for all simulations (CTL and DI) within the experiment. ME values for individual water years and individual simulations are shown in the table below the plot.

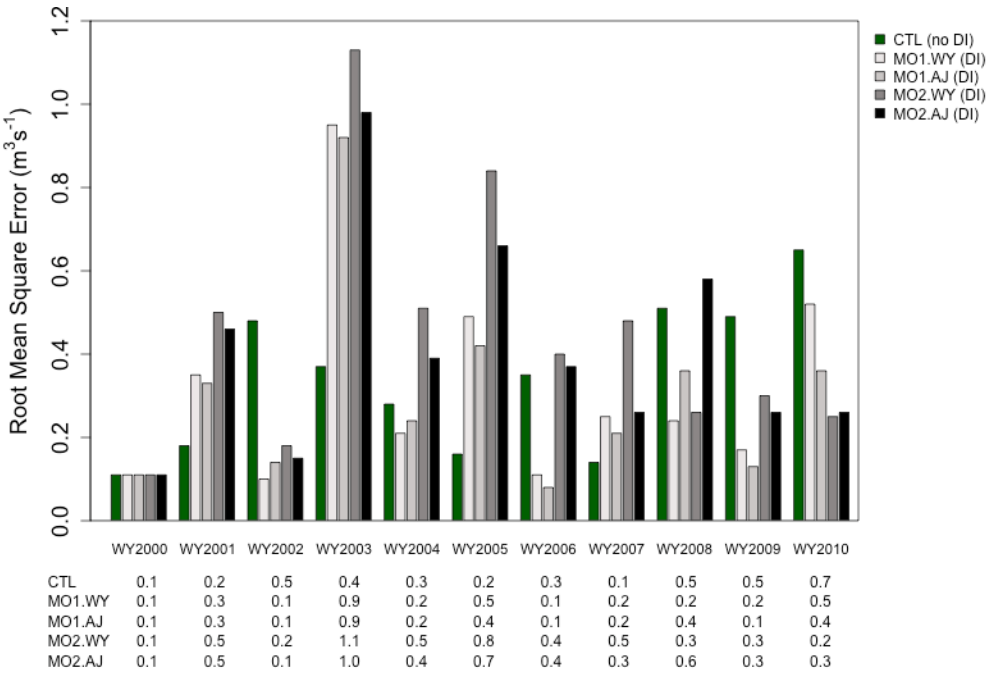

Figure 64: December root mean square error (m3 s-1) for all simulations during the study period of WY00 to WY10, for all simulations (CTL and DI) within the experiment. RMSE values for individual water years and individual simulations are shown in the table below the plot.

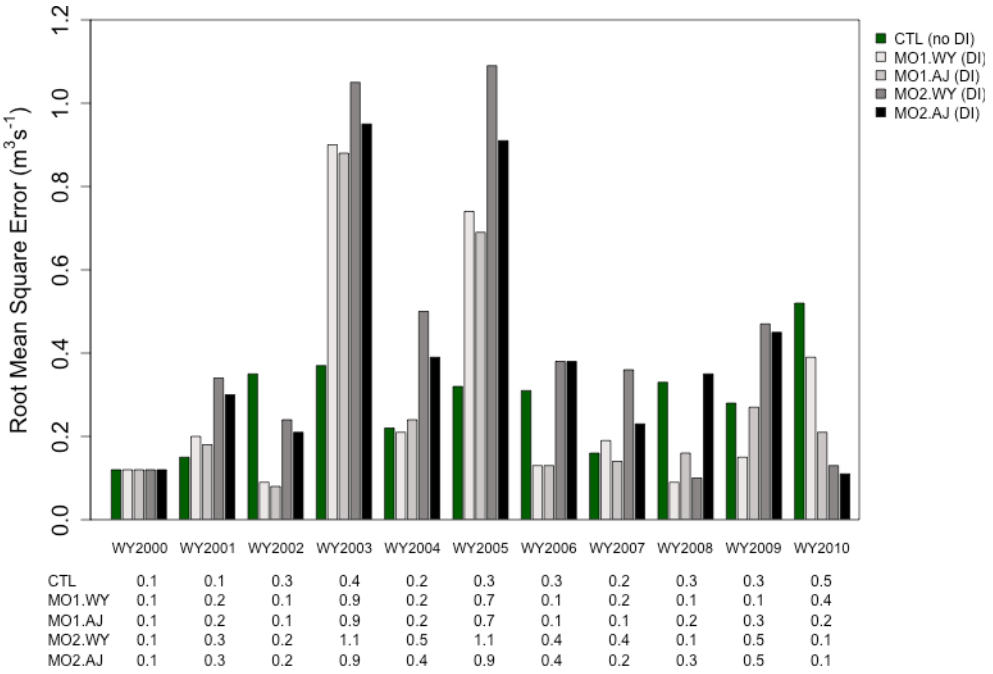

Figure 65: January root mean square error ($m^3 s^{-1}$) for all simulations during the study period of WY00 to WY10, for all simulations (CTL and DI) within the experiment. RMSE values for individual water years and individual simulations are shown in the table below the plot.

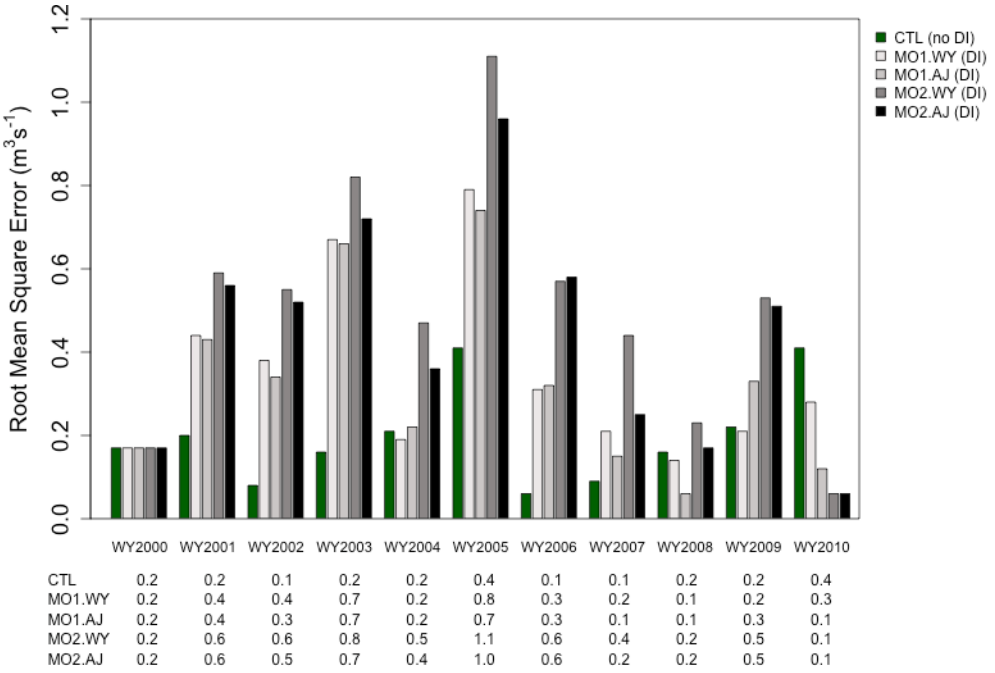

Figure 66: February root mean square error (m^3 s^{-1}) for all simulations during the study period of WY00 to WY10, for all simulations (CTL and DI) within the experiment. RMSE values for individual water years and individual simulations are shown in the table below the plot.

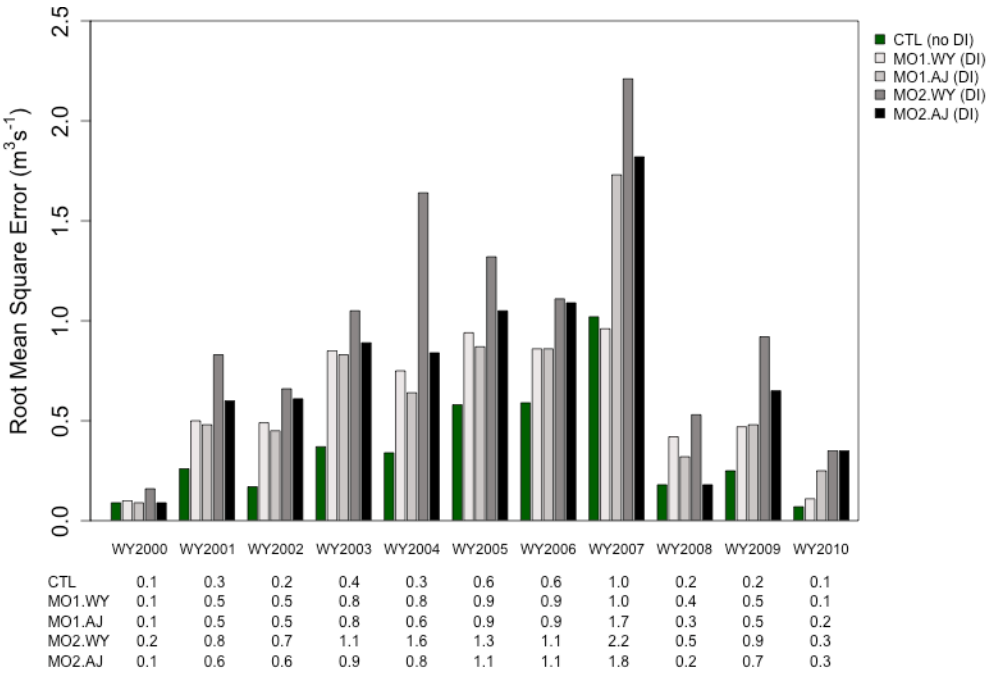

Figure 67: March root mean square error (m^3 s^{-1}) for all simulations during the study period of WY00 to WY10, for all simulations (CTL and DI) within the experiment. RMSE values for individual water years and individual simulations are shown in the table below the plot.

5.2.3 Comparison of April – July DI and CTL Simulations via Skill Scores

For the most important season of the water year (April – July), the RMSE skill score (RMSE-SS) for the water years in the study quantifies the difference between the error metrics for the CTL and DI simulations. The DI simulations mostly have poorer performance with respect to streamflow predictions when compared to the CTL simulation. The majority of the monthly RMSE-SS values during the runoff period of April-July are negative, indicating that use of MODIS-derived fSCA via DI degrades the streamflow simulations when compared to the CTL simulation. Figures 68-71 show that RMSE-SS values are commonly less than -2 during months of the runoff period (April – July), with the largest negative value of -14.3 in June 2007. For the month of May, throughout the water years in the study period, the RMSE-SS values are all negative, indicating that none of the DI simulations improve upon the performance of the CTL simulation, in terms of RMSE (Fig. 69). The MOD10A DI simulations result in small improvements over the CTL simulation (RMSE-SS is positive but less than or equal to 0.5, generally 0.2 to 0.4) in April of WY2001 and WY2007 (Fig. 68), and in July of WY2005, WY2009, and WY2010 (Fig. 71). Direct insertion of the MODSCAG data set results in improved model performance when compared to the CTL simulation in July of WY2010 only (Fig. 71).

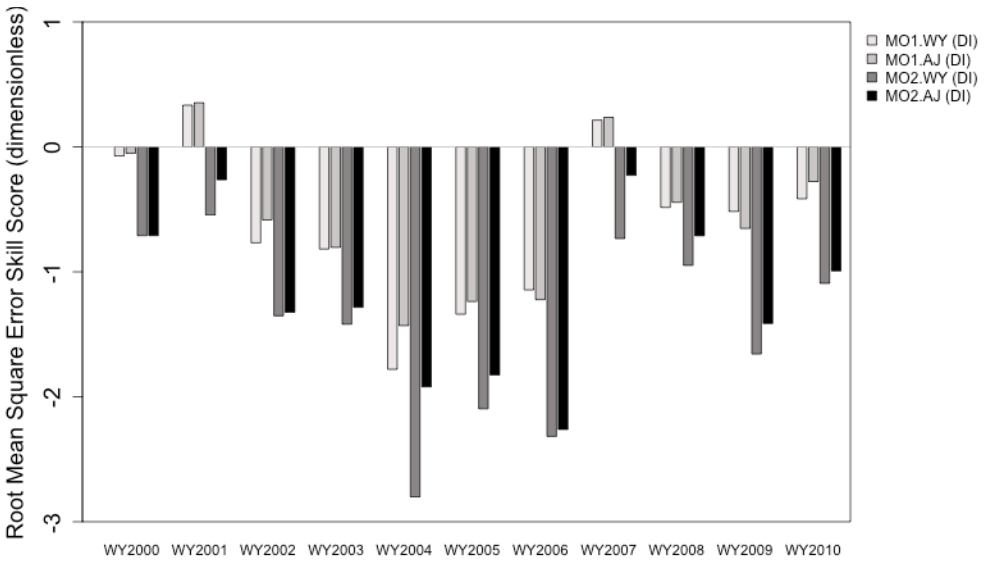

	WY2000	WY2001	WY2002	WY2003	WY2004	WY2005	WY2006	WY2007	WY2008	WY2009	WY2010
MO1.WY	-0.1	0.3	-0.8	-0.8	-1.8	-1.3	-1.1	0.2	-0.5	-0.5	-0.4
MO1.AJ	-0.1	0.4	-0.6	-0.8	-1.4	-1.2	-1.2	0.2	-0.4	-0.7	-0.3
MO2.WY	-0.7	-0.5	-1.4	-1.4	-2.8	-2.1	-2.3	-0.7	-0.9	-1.7	-1.1
MO2.AJ	-0.7	-0.3	-1.3	-1.3	-1.9	-1.8	-2.3	-0.2	-0.7	-1.4	-1.0

Figure 68: April root mean square error skill score for all DI simulations within the experiment during the study period of WY00 to WY10. RMSE-SS values for individual water years and individual simulations are shown in the table below the plot.

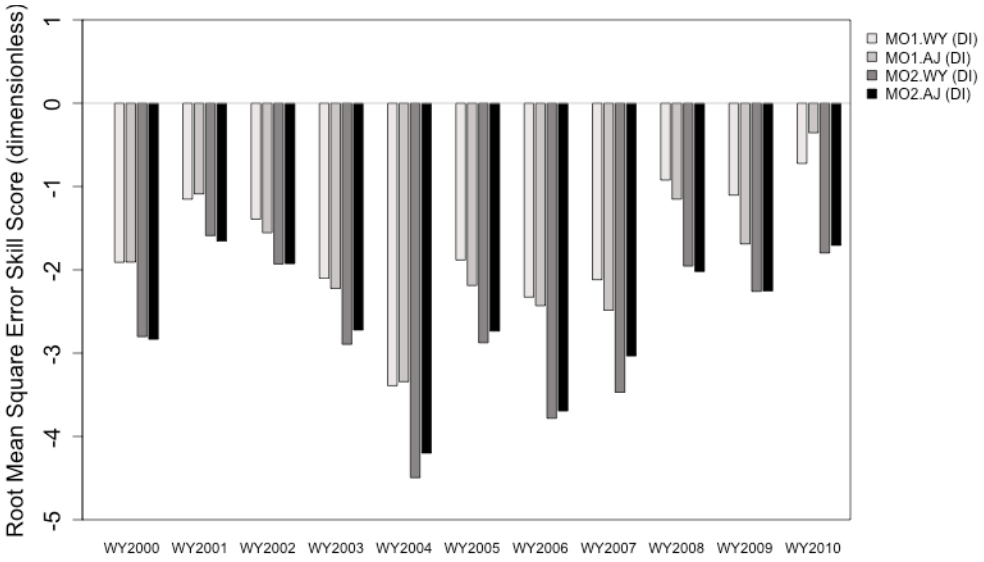

	WY2000	WY2001	WY2002	WY2003	WY2004	WY2005	WY2006	WY2007	WY2008	WY2009	WY2010
MO1.WY	-1.9	-1.2	-1.4	-2.1	-3.4	-1.9	-2.3	-2.1	-0.9	-1.1	-0.7
MO1.AJ	-1.9	-1.1	-1.6	-2.2	-3.3	-2.2	-2.4	-2.5	-1.2	-1.7	-0.4
MO2.WY	-2.8	-1.6	-1.9	-2.9	-4.5	-2.9	-3.8	-3.5	-2.0	-2.3	-1.8
MO2.AJ	-2.8	-1.7	-1.9	-2.7	-4.2	-2.7	-3.7	-3.0	-2.0	-2.3	-1.7

Figure 69: May root mean square error skill score for all DI simulations within the experiment during the study period of WY00 to WY10. RMSE-SS values for individual water years and individual simulations are shown in the table below the plot.

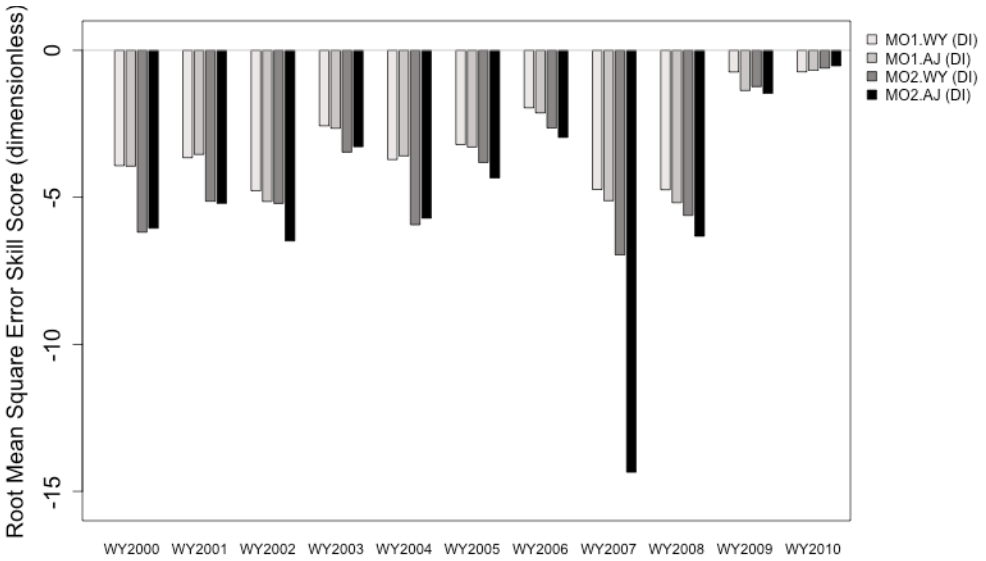

MO1.WY	-3.9	-3.7	-4.8	-2.6	-3.7	-3.2	-2.0	-4.7	-4.7	-0.7	-0.7
MO1.AJ	-3.9	-3.5	-5.1	-2.7	-3.6	-3.3	-2.1	-5.1	-5.2	-1.4	-0.7
MO2.WY	-6.2	-5.1	-5.2	-3.5	-5.9	-3.8	-2.6	-7.0	-5.6	-1.2	-0.6
MO2.AJ	-6.1	-5.2	-6.5	-3.3	-5.7	-4.3	-3.0	-14.3	-6.3	-1.5	-0.5

Figure 70: June root mean square error skill score for all DI simulations within the experiment during the study period of WY00 to WY10. RMSE-SS values for individual water years and individual simulations are shown in the table below the plot.

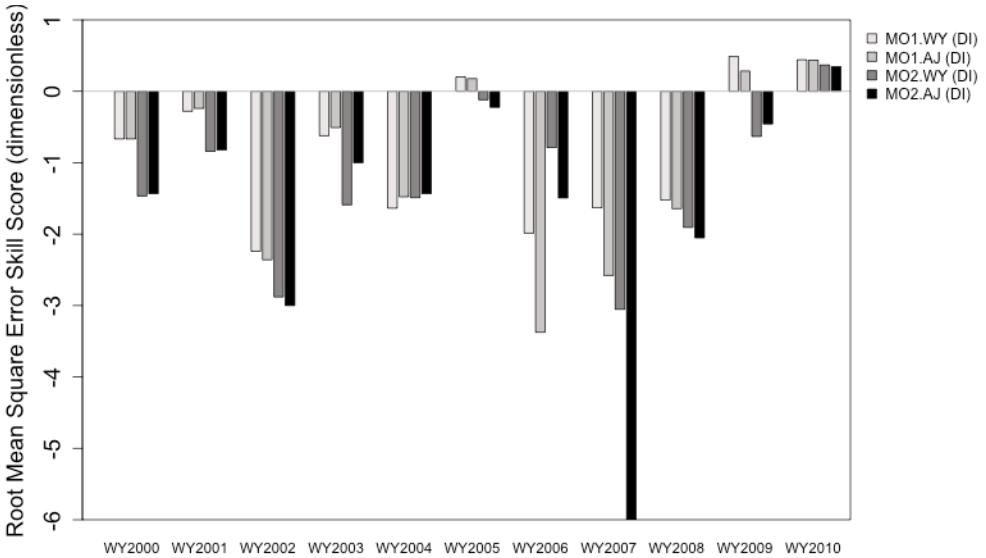

MO1.WY	-0.7	-0.3	-2.2	-0.6	-1.6	0.2	-2.0	-1.6	-1.5	0.5	0.4
MO1.AJ	-0.7	-0.2	-2.4	-0.5	-1.5	0.2	-3.4	-2.6	-1.6	0.3	0.4
MO2.WY	-1.5	-0.8	-2.9	-1.6	-1.5	-0.1	-0.8	-3.1	-1.9	-0.6	0.4
MO2.AJ	-1.4	-0.8	-3.0	-1.0	-1.4	-0.2	-1.5	-6.0	-2.1	-0.5	0.3

Figure 71: July root mean square error skill score for all DI simulations within the experiment during the study period of WY00 to WY10. RMSE-SS values for individual water years and individual simulations are shown in the table below the plot.

Figures 72 and 73 show the RMSE-SS values for individual months of each water year in the study period, for two selected DI simulations, MO1.AJ (DI of MOD10A during the April – July runoff period only) and MO2.AJ. (DI of MODSCAG during the April – July runoff period). In the majority of individual months of all water years, the DI of MODIS-derived fSCA results in poorer streamflow predictions, in terms of RMSE, when compared to the CTL simulation. The degradation in prediction performance of the DI runs is particularly apparent during the runoff period of April – July, specifically in May and June. Outside of March and the runoff period of April – July, use of MODIS-derived fSCA via DI results in improved predictions (RMSE-SS for individual months of ~ +0.5) compared to the CTL simulation in some months of some water years, though not all. The DI simulations that use MODSCAG (Fig. 74) generally show worse performance than the DI simulations that use MOD10A (Fig. 73).

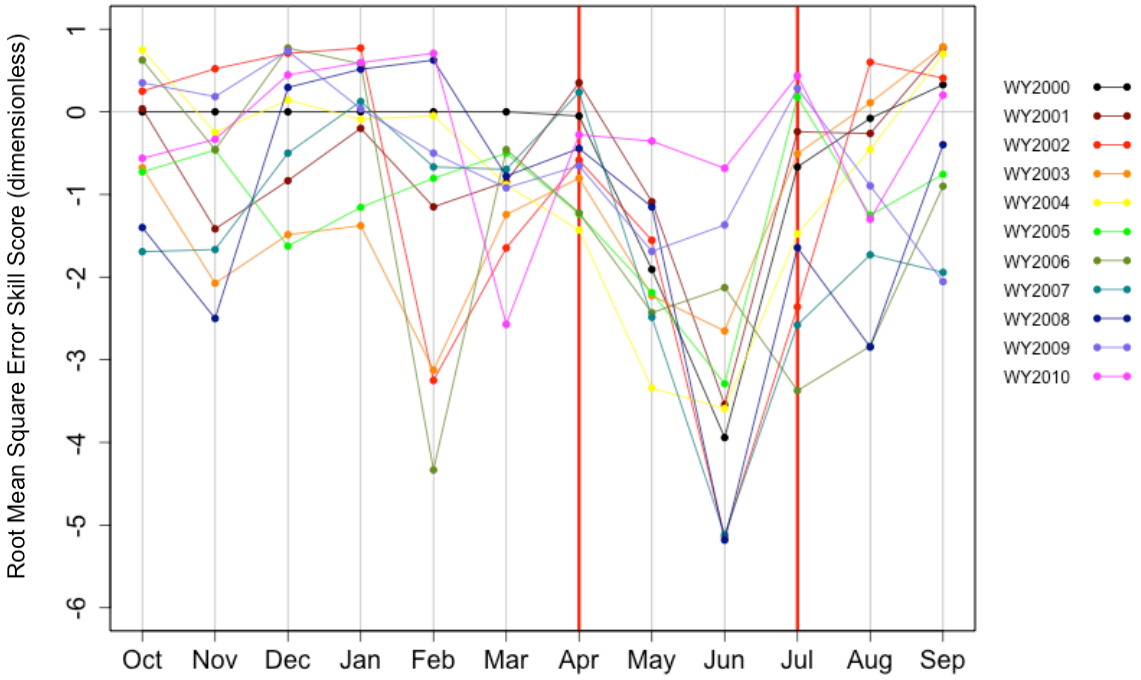

Figure 72: Monthly RMSE-SS for MO1.AJ DI simulation for study period of WY2000 to WY2010

Table 27: Monthly RMSE-SS values for MO1.AJ DI simulation for study period of WY00 to WY10

Water Year	OCT	NOV	DEC	JAN	FEB	MAR	APR	MAY	JUN	JUL	AUG	SEP
2000	0.00	0.00	0.00	0.00	0.00	0.00	-0.05	-1.91	-3.94	-0.67	-0.08	0.33
2001	0.04	-1.42	-0.83	-0.20	-1.15	-0.85	0.35	-1.09	-3.54	-0.24	-0.26	0.77
2002	0.25	0.52	0.71	0.77	-3.25	-1.65	-0.58	-1.55	-5.14	-2.36	0.60	0.41
2003	-0.68	-2.07	-1.49	-1.38	-3.12	-1.24	-0.80	-2.22	-2.65	-0.51	0.11	0.79
2004	0.75	-0.25	0.14	-0.09	-0.05	-0.88	-1.43	-3.34	-3.59	-1.48	-0.45	0.70
2005	-0.73	-0.46	-1.62	-1.16	-0.80	-0.50	-1.24	-2.19	-3.29	0.18	-1.25	-0.76
2006	0.62	-0.46	0.77	0.58	-4.33	-0.46	-1.22	-2.43	-2.13	-3.37	-2.84	-0.90
2007	-1.69	-1.67	-0.50	0.12	-0.67	-0.70	0.24	-2.49	-5.12	-2.58	-1.73	-1.94
2008	-1.40	-2.50	0.29	0.52	0.62	-0.78	-0.44	-1.15	-5.18	-1.64	-2.85	-0.40
2009	0.35	0.18	0.73	0.04	-0.50	-0.92	-0.65	-1.69	-1.37	0.28	-0.90	-2.05
2010	-0.56	-0.33	0.45	0.60	0.71	-2.57	-0.28	-0.35	-0.68	0.43	-1.30	0.20

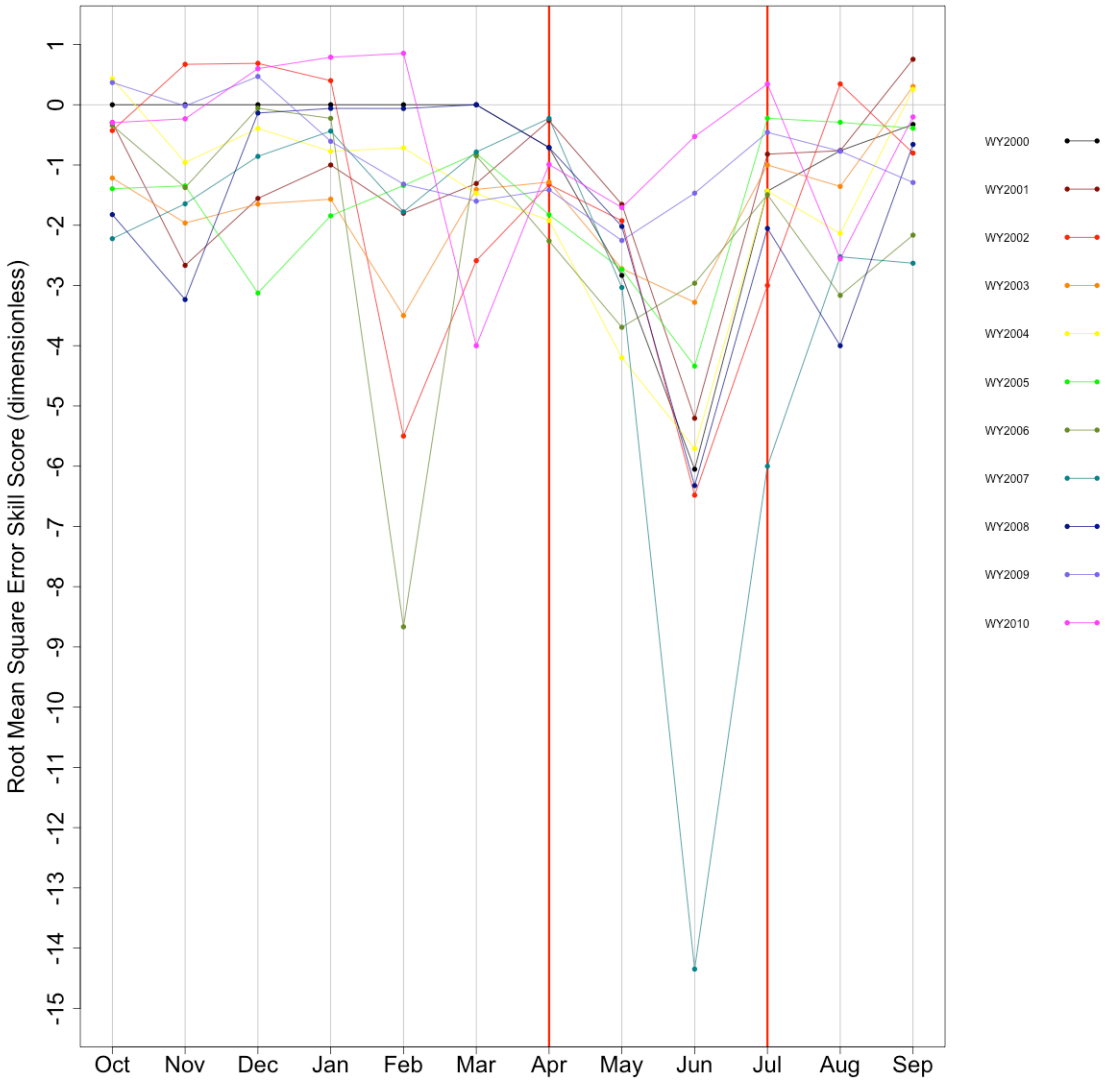

Figure 73: Monthly RMSE-SS for MO2.AJ DI simulation for study period of WY2000 to WY2010

Table 28: Monthly RMSE-SS values for MO2.AJ DI simulation for study period of WY00 to WY10

Water Year	OCT	NOV	DEC	JAN	FEB	MAR	APR	MAY	JUN	JUL	AUG	SEP
2000	0.00	0.00	0.00	0.00	0.00	0.00	-0.71	-2.83	-6.05	-1.43	-0.76	-0.33
2001	-0.30	-2.67	-1.56	-1.00	-1.80	-1.31	-0.26	-1.65	-5.20	-0.82	-0.76	0.75
2002	-0.43	0.67	0.69	0.40	-5.50	-2.59	-1.32	-1.93	-6.48	-3.00	0.35	-0.80
2003	-1.22	-1.96	-1.65	-1.57	-3.50	-1.41	-1.28	-2.72	-3.28	-1.00	-1.36	0.30
2004	0.43	-0.96	-0.39	-0.77	-0.71	-1.47	-1.92	-4.20	-5.71	-1.43	-2.14	0.26
2005	-1.39	-1.35	-3.12	-1.84	-1.34	-0.81	-1.82	-2.74	-4.34	-0.22	-0.29	-0.39
2006	-0.34	-1.38	-0.06	-0.23	-8.67	-0.85	-2.26	-3.69	-2.96	-1.49	-3.16	-2.16
2007	-2.22	-1.64	-0.86	-0.44	-1.78	-0.78	-0.23	-3.03	-14.35	-6.00	-2.52	-2.63
2008	-1.82	-3.23	-0.14	-0.06	-0.06	0.00	-0.71	-2.02	-6.32	-2.05	-4.00	-0.66
2009	0.37	-0.02	0.47	-0.61	-1.32	-1.60	-1.41	-2.25	-1.47	-0.46	-0.77	-1.29
2010	-0.30	-0.23	0.60	0.79	0.85	-4.00	-0.99	-1.71	-0.53	0.34	-2.56	-0.20

5.3 DISCUSSION OF SIMULATIONS AND STUDY RESULTS

Understanding the reasons why the inclusion of observed fSCA does not improve streamflow predictions using the data and modeling system of this study requires examination of the SNOW17 algorithm and the physical interpretation of the depletion curve. Treatment of fSCA within SNOW17 and its impacts on snowmelt rates are discussed in this section.

5.3.1 Impacts of MODIS fSCA via DI on Simulated SWE

SNOW17 uses snow cover extent as a multiplier on the melt volume computed within the MELT19 subroutine, in which a melt volume is computed assuming 100% snow cover across the elevation zone. A SNOW17 AESC value close to 1.0 will deplete

the snowpack fastest because the melt volume, after it is multiplied by the AESC value, would be closest to the melt volume that assumes 100% snow cover. The largest melt volume value available in a single timestep would be the volume computed assuming 100% snow cover, then multiplied by 1.0. Use of a MODIS-derived fSCA value of less than 1.0 would result in a lower melt volume being deducted from the snowpack, and the simulated SWE would deplete more slowly. When MODIS-derived fSCA (less than what SNOW17 would expect) is forced into SNOW17 in place of the model's estimate of snow cover extent, the rate at which the snowpack melts drastically slows. In some years, the simulated snowpack unrealistically does not melt off in the summer in the upper and middle elevation zones. For example, SNOTEL SWE data for WY2006 indicate that the snowpack depleted between early May and early June, depending on the SNOTEL site (Fig. 74). However, Figures 75-82 show that, in most of the DI simulations, the simulated snowpack persists though the summer of 2006 carrying over into WY2007, in the middle elevation zone and often the upper elevation as well (e.g., WY2005-2006, 2009-2010).

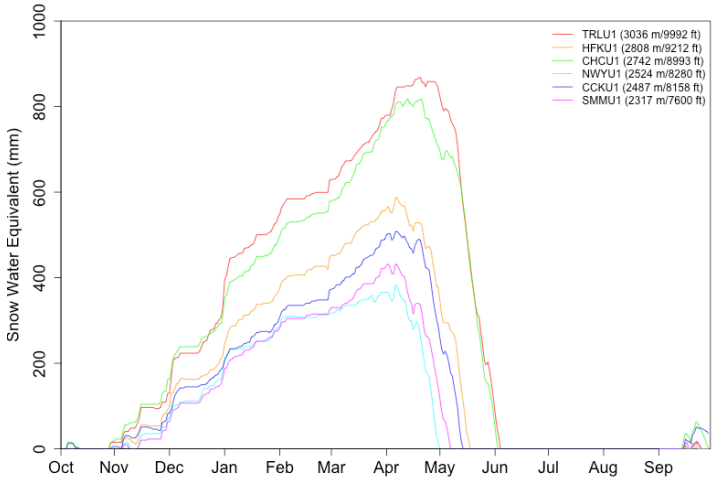

Figure 74: WY2006 SWE (mm) for SNOTEL stations near and within the OAWU1 basin

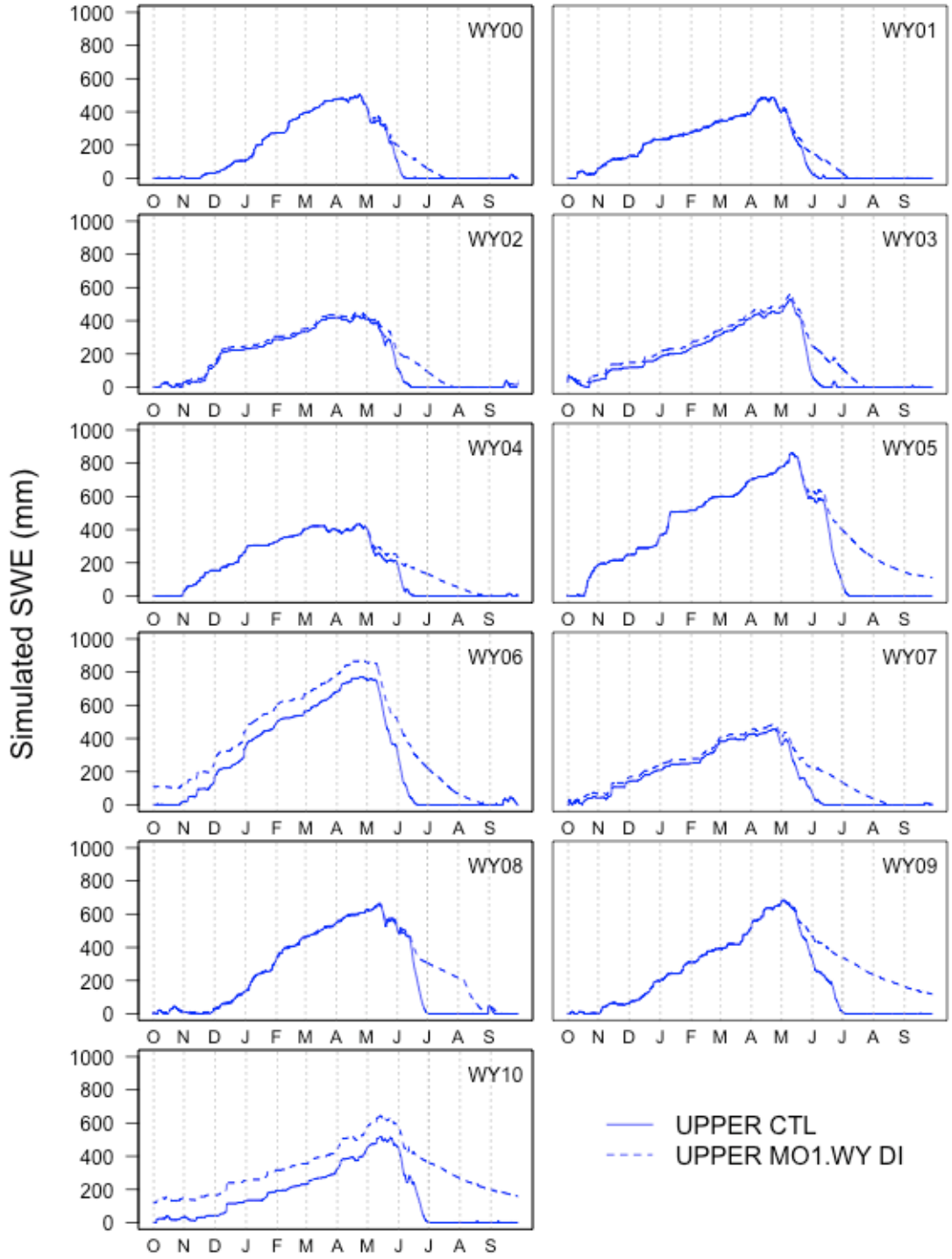

Figure 75: CTL (solid line) and MO1.WY (dashed line) simulated SWE for upper (blue) elevation zone for study period

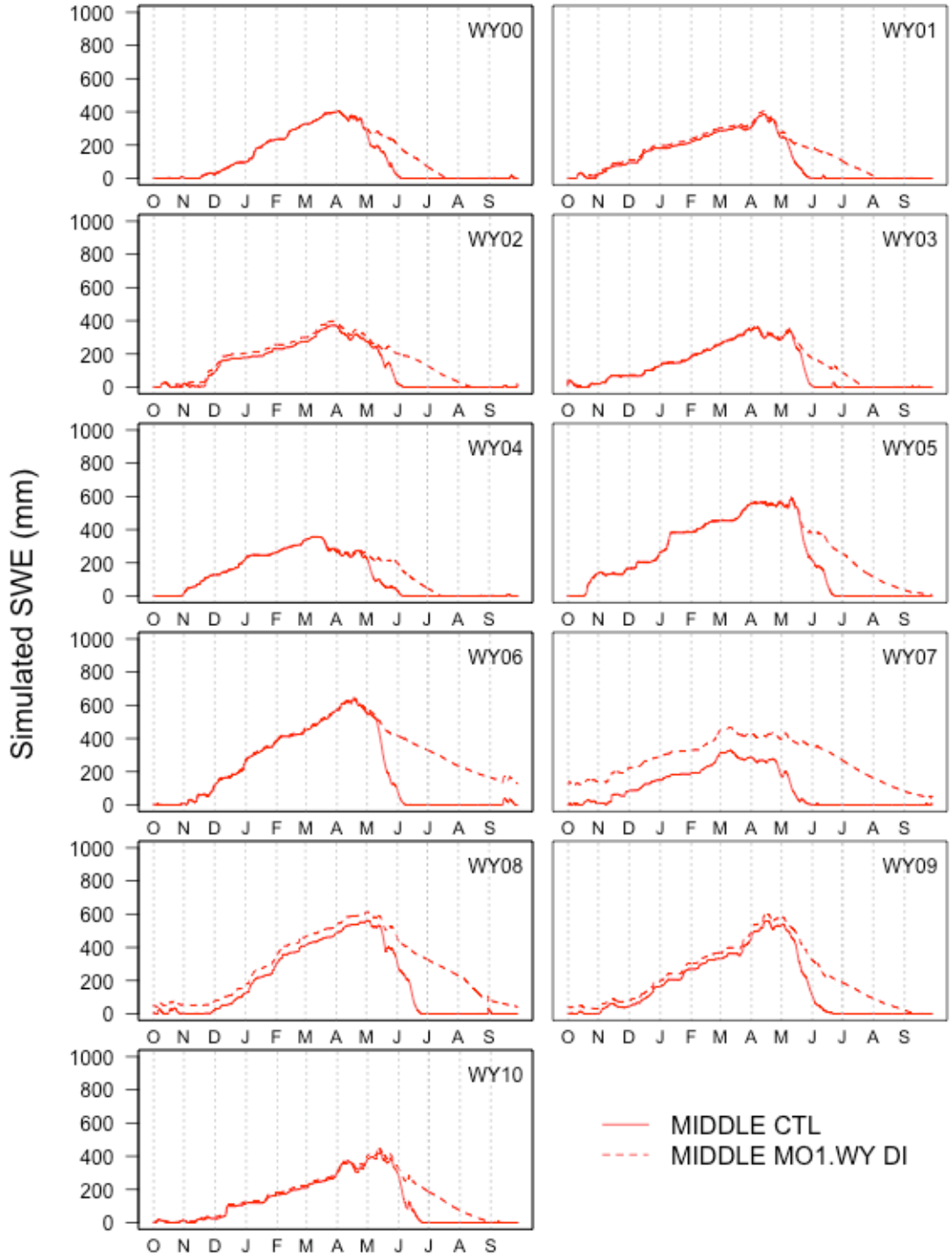

Figure 76: CTL (solid line) and MO1.WY (dashed line) simulated SWE for middle (red) elevation zone for study period

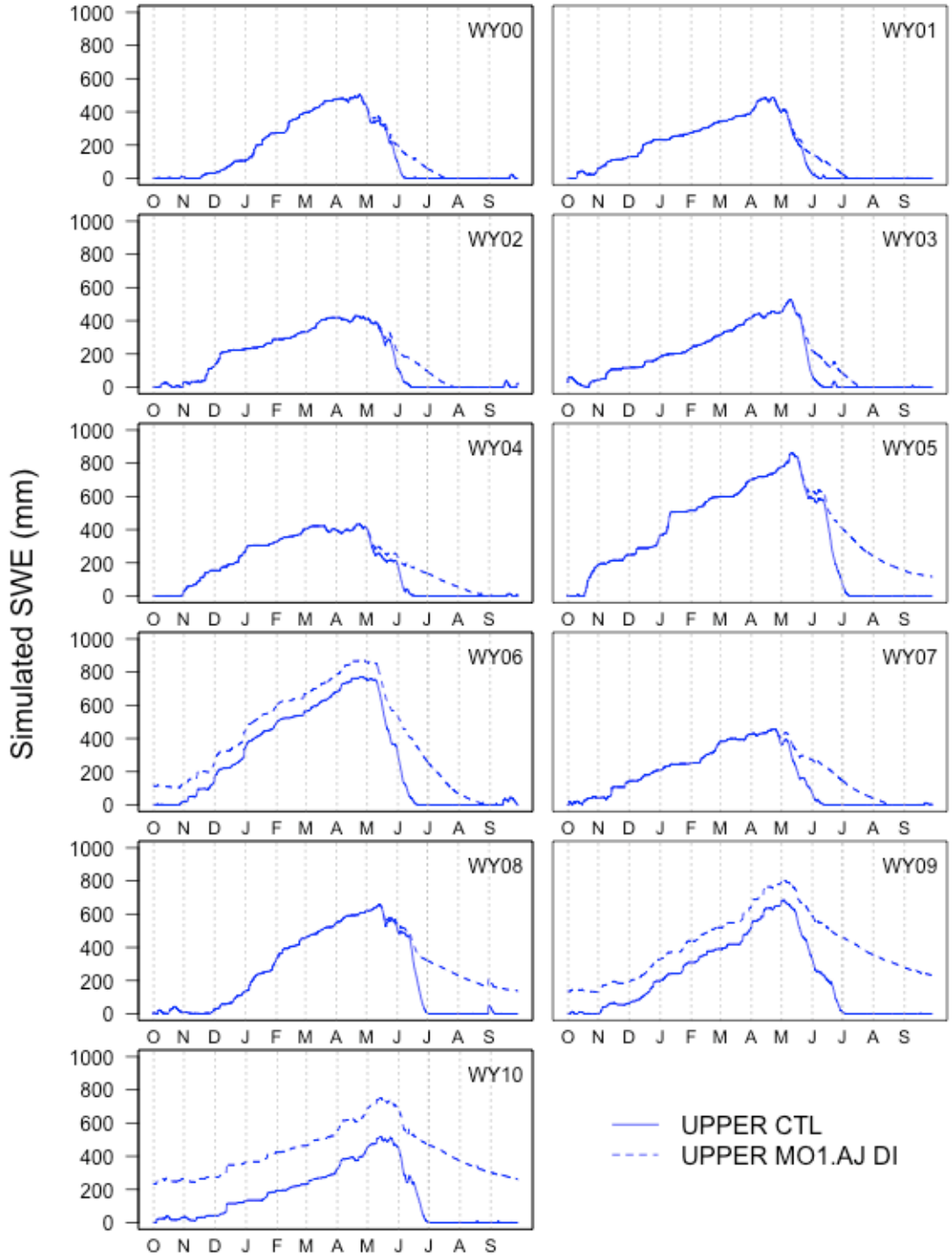

Figure 77: CTL (solid line) and MO1.AJ (dashed line) simulated SWE for upper (blue) elevation zone for study period

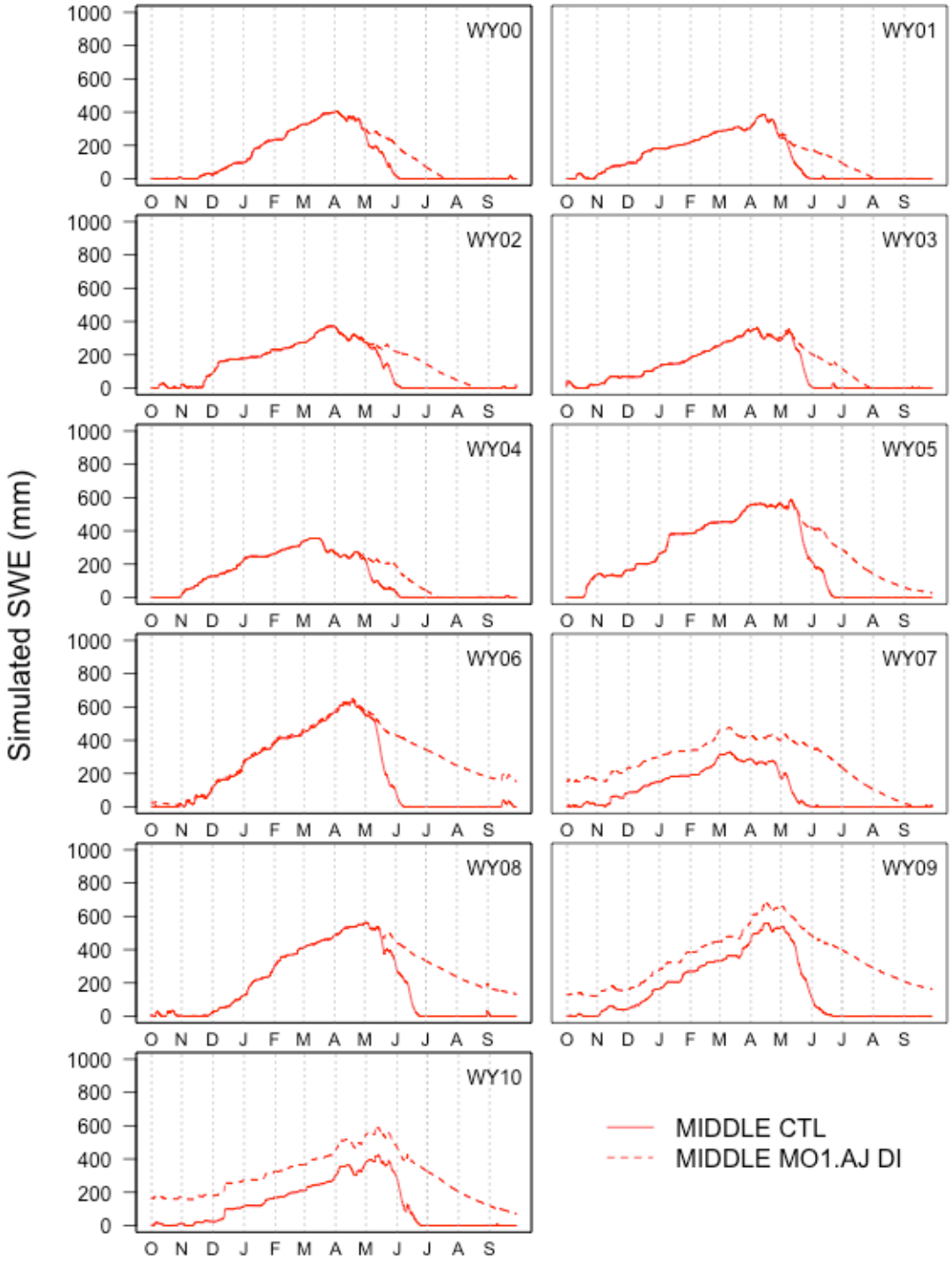

Figure 78: CTL (solid line) and MO1.AJ (dashed line) simulated SWE for middle (red) elevation zone for study period

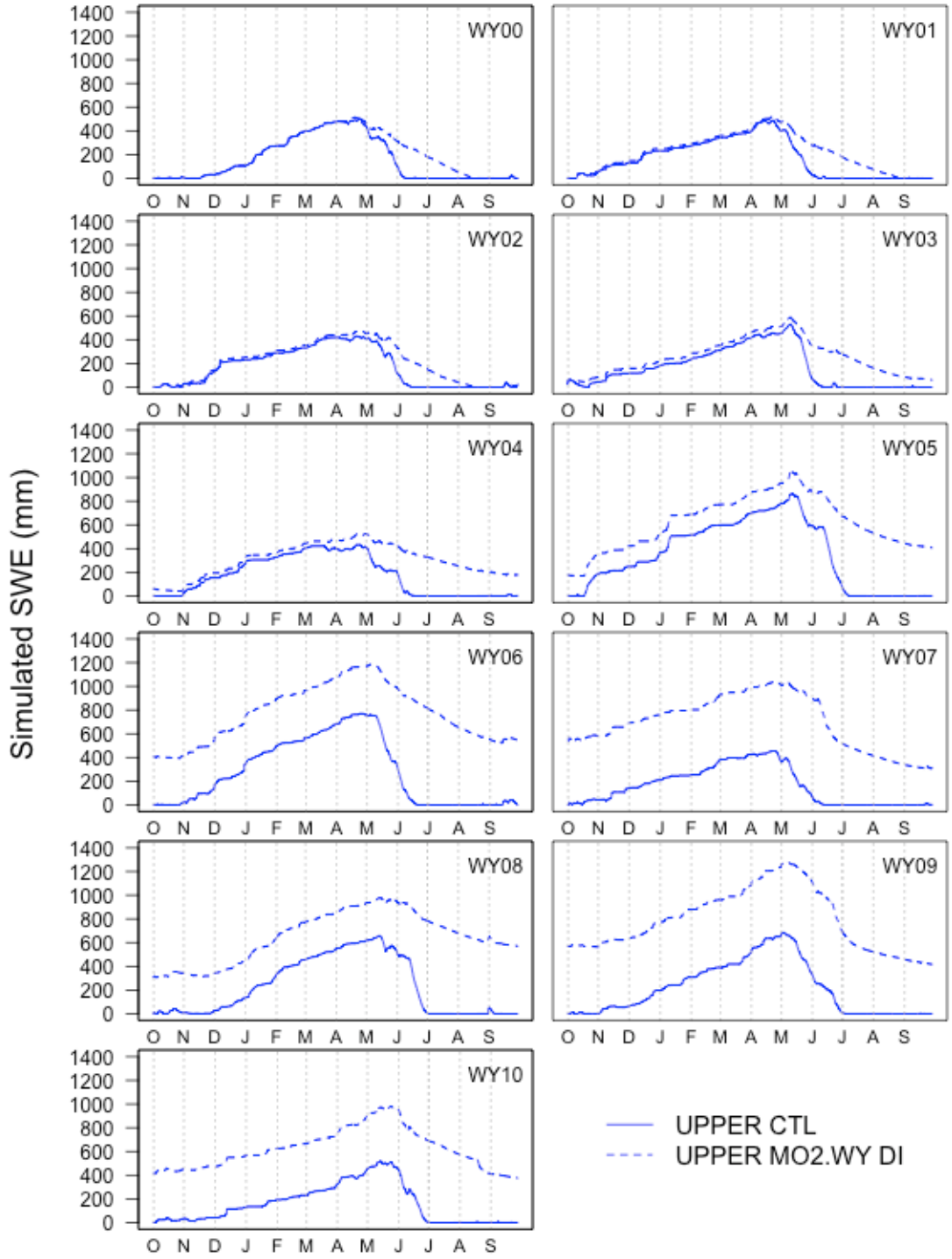

Figure 79: CTL (solid line) and MO2.WY (dashed line) simulated SWE for upper (blue) elevation zone for study period

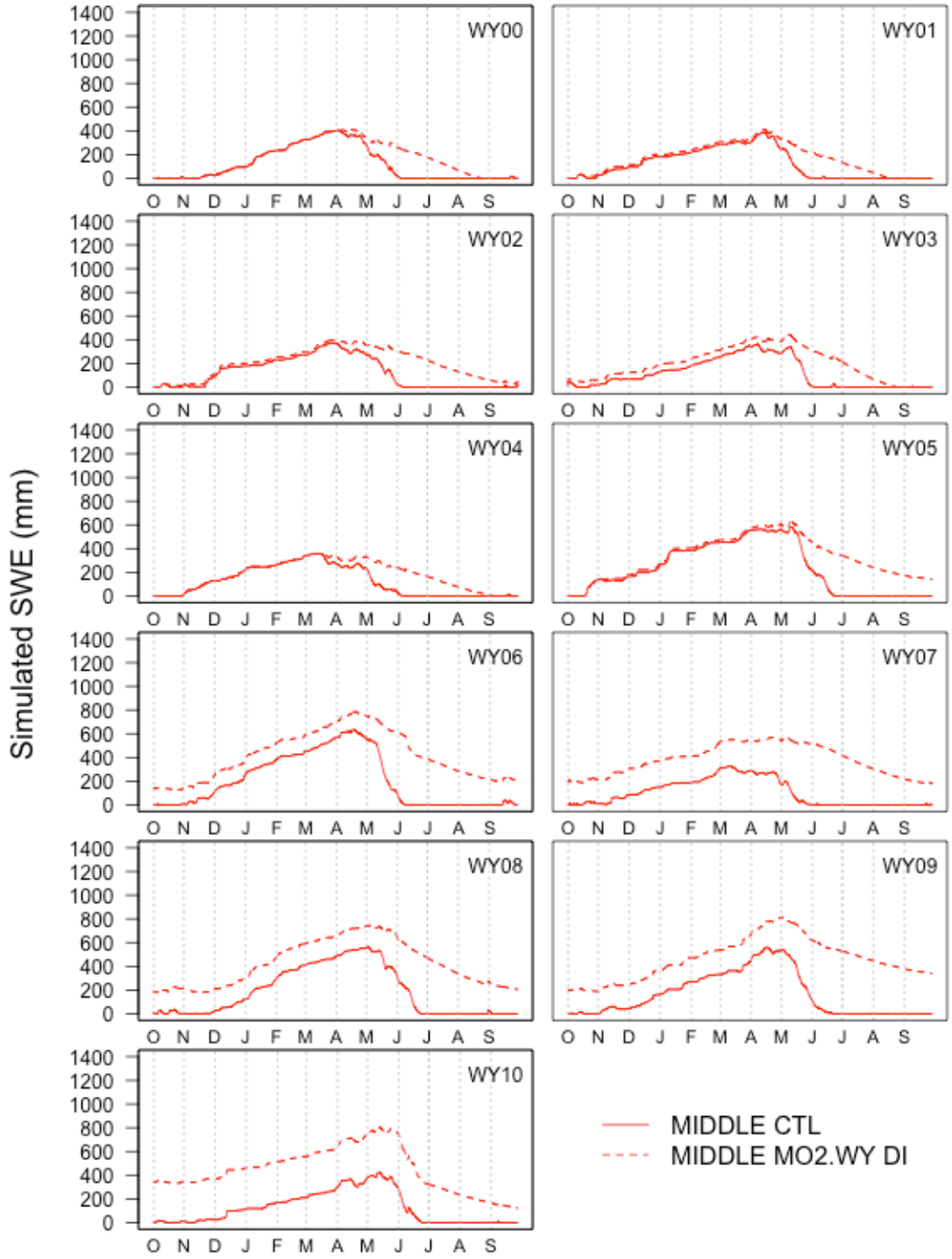

Figure 80: CTL (solid line) and MO2.WY (dashed line) simulated SWE for middle (red) elevation zone for study period

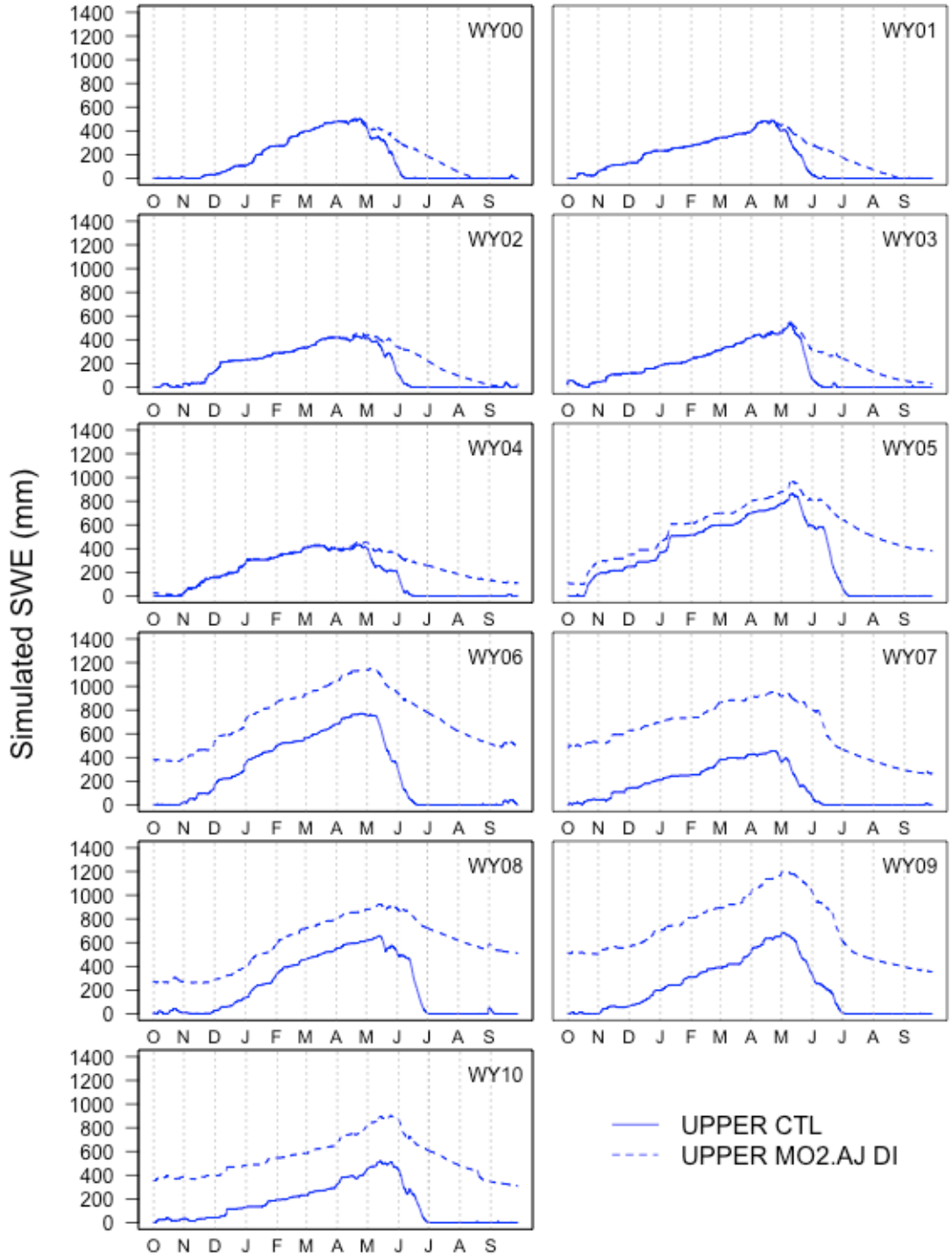

Figure 81: CTL (solid line) and MO2.AJ (dashed line) simulated SWE for upper (blue) elevation zone for study period

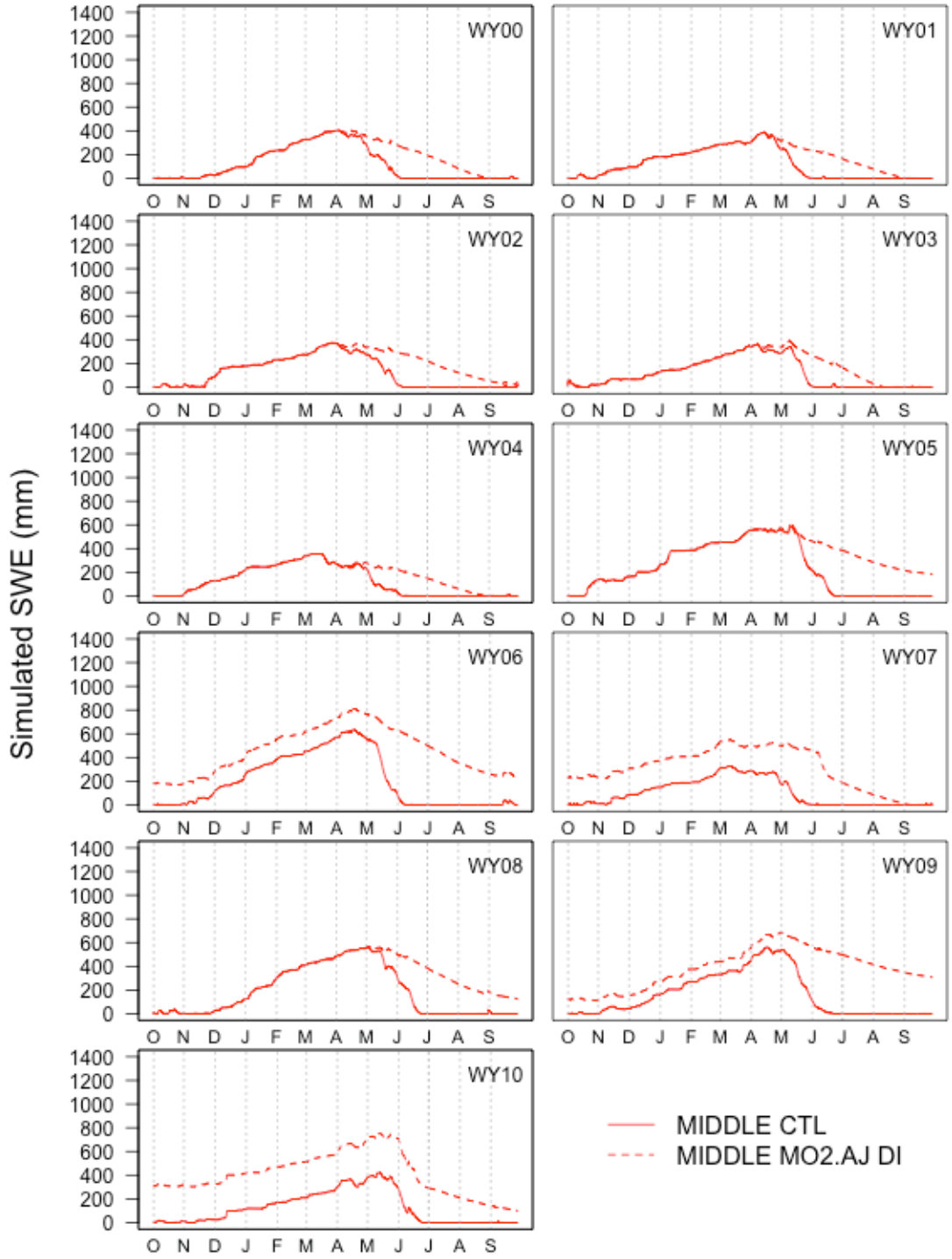

Figure 82: CTL (solid line) and MO2.AJ (dashed line) simulated SWE for middle (red) elevation zone for study period

Complete depletion of the snowpack in SNOW17 depends on the *SWE* approaching and reaching zero, not the value of AESC (snow cover extent used by the model). In SNOW17, SWE is a model state variable and AESC is a diagnostic variable (not a model state variable) that is a function of SWE. In the operational version of the SNOW17 source code, the snowpack cannot be "zeroed out" by setting the AESC value to zero (either via direct insertion of an fSCA value of 0% or set to 0% manually by a forecaster). A check within the code (UPDT19 subroutine) ensures that SNOW17 ignores any directly inserted fSCA value of 5% or less. The check was included in SNOW17 so that, in cases where DI is *not* used (which is always the case in the current operational configuration of SNOW17 in NWS hydro operations), the snowpack would not linger into the summer due to an AESC multiplier of nearly zero being applied, rendering the melt volume within a single timestep very small. In other words, if simulated SWE is nonzero and the modeled snowpack exists, only AESC values that exceed 5% will be allowed in SNOW17 computations. Once simulated SWE reaches zero, *then* the AESC (a diagnostic variable) in the operations version of SNOW17 is permitted to go to zero. So, even if MODIS-derived fSCA values of 0% snow cover are available, which would indicate complete snowpack depletion by the observations, they cannot be used within the operational version of the SNOW17 code. The fact that AESC is used as an indicator of melt rate more than physical snow covered area in SNOW17 is apparent after thorough examination of the results of this study as well as of the source code (NWS/OHD, 2012).

When an observed MODIS-derived fSCA value is directly inserted into SNOW17, the SWE value is not altered *within the same timestep*. SNOW17 aims to

conserve simulated mean areal SWE (a state variable) for the elevation zone when the AESC value is changed via direct insertion of an observed fSCA value. As stated previously, the snow cover extent (AESC) is not considered a state variable but rather a diagnostic variable in SNOW17. While the simulated SWE value does not change *within* the timestep when an observed fSCA value replaces the model AESC estimate, the simulated SWE *is* impacted in future timesteps. Details are explained below.

Direct insertion of MODIS-derived fSCA usually slows the snowpack melt rate over the ablation season, regardless of whether the MOD10A or MODSCAG fSCA data set is used, because the inserted fSCA is almost always less than the AESC that the model would calculate as a function of SWE from the depletion curve. In SNOW17, accounting of the simulated SWE occurs after SNOW17 makes the adjustment by AESC to the melt volume that is initially computed assuming 100% snow cover. Direct insertion of observed fSCA effectively reduces the melt volume that is actually deducted from the snowpack in each SNOW17 timestep. Because the mean areal fSCA from MODSCAG is usually less than that from MOD10A (Fig. 20), the DI runs that use MODSCAG have even slower melt rates than the DI runs that use the MOD10A fSCA data.

While the snowpack carries over through the summer and from water year to water year in the upper and middle elevation zones at some point in all of the DI simulations (Figs. 75-82), it carries over through the summer more often in simulations that directly insert MODSCAG mean areal fSCA estimates (Fig. 79=82). The snowpack in the lower elevation zone melts off every year in all of the DI simulations (not shown). Figures 79-82 show that snowpack carryover in the MODSCAG DI simulations starts

earlier in the study period (as early as 2003) than in the MOD10A DI simulations. Overall, DI of MODSCAG mean areal fSCA into SNOW17 results in slower melt rates in the simulated SWE, and the slower melt rates often lead to the model erroneously sustaining the snowpack through summers in the study period when it should deplete completely.

5.3.2 Impacts of MODIS fSCA via DI on Simulated Snow Cover Extent

In almost all cases, DI of observed fSCA into SNOW17 results in a simulated AESC time series that is less than the AESC time series from the CTL run. Figure 83 shows MODIS-derived fSCA (observed snow cover extent), simulated AESC (modeled snow cover extent based on the depletion curve), simulated SWE, and streamflow time series for WY2002 when DI of the MOD10A data is active for the full water year. The fSCA/AESC subpanels show that the DI simulation (dashed line) is usually less than the CTL simulation (solid line). Figure 84 shows the difference between the CTL and DI simulated AESC, where orange indicates that the predicted AESC from the DI simulation is less than that from the CTL simulation. Purple indicates that the predicted AESC from the DI simulation is greater than that from the CTL. The instances where the DI-simulated AESC is less than the CTL-simulated AESC clearly outnumber the opposite case.

Since SNOW17 uses the AESC value (either entirely model-driven, or influenced by observed fSCA in the DI simulations) as a multiplier on a melt volume computed assuming 100% snow cover, the negative fSCA innovations (difference or residual between model estimate and the observation) result in a slower rate of snowpack melt.

The slower melt rate translates to reduced streamflow in the DI simulations as well as negative bias and negative errors when the DI simulations are compared to observed streamflow.

In addition to the fact that the AESC from the DI simulation (impacted by use of observed fSCA from MODIS) is usually less than the AESC from the CTL simulation, it should be noted that predicted AESC from the DI simulation plateaus at 0.05 in the summer in all three elevation zones. This pattern is due to the operational version of SNOW17 ignoring any directly-inserted, observed fSCA value of less than 5%. As discussed previously, "zeroing out" the snowpack via an observed fSCA value of 0% snow cover is not currently encoded into the operational version of SNOW17. In this case, the observed fSCA data (when it is 0%) cannot be used to clear out an abnormally large simulated snowpack that has built up over multiple water years due to very slow melt rates.

The SNOW17 source code could be altered to "zero out" the snowpack if the snow cover extent is entirely depleted according to observations of MODIS-derived fSCA. However, this change would not address larger issues inherent in the simulations that utilize unadjusted MODIS-derived fSCA via DI. Differences between SNOW17 AESC and unadjusted MODIS-derived fSCA, and the fact that SNOW17 does not include full representation of the energy balance should be addressed before implementing a fix that simply "zeroes out" the snowpack when the observations indicate full depletion of the snowpack. If more prominent problems with DI of unadjusted MODIS-derived fSCA can be addressed and solved first, then implementation of such a fix would seem more reasonable.

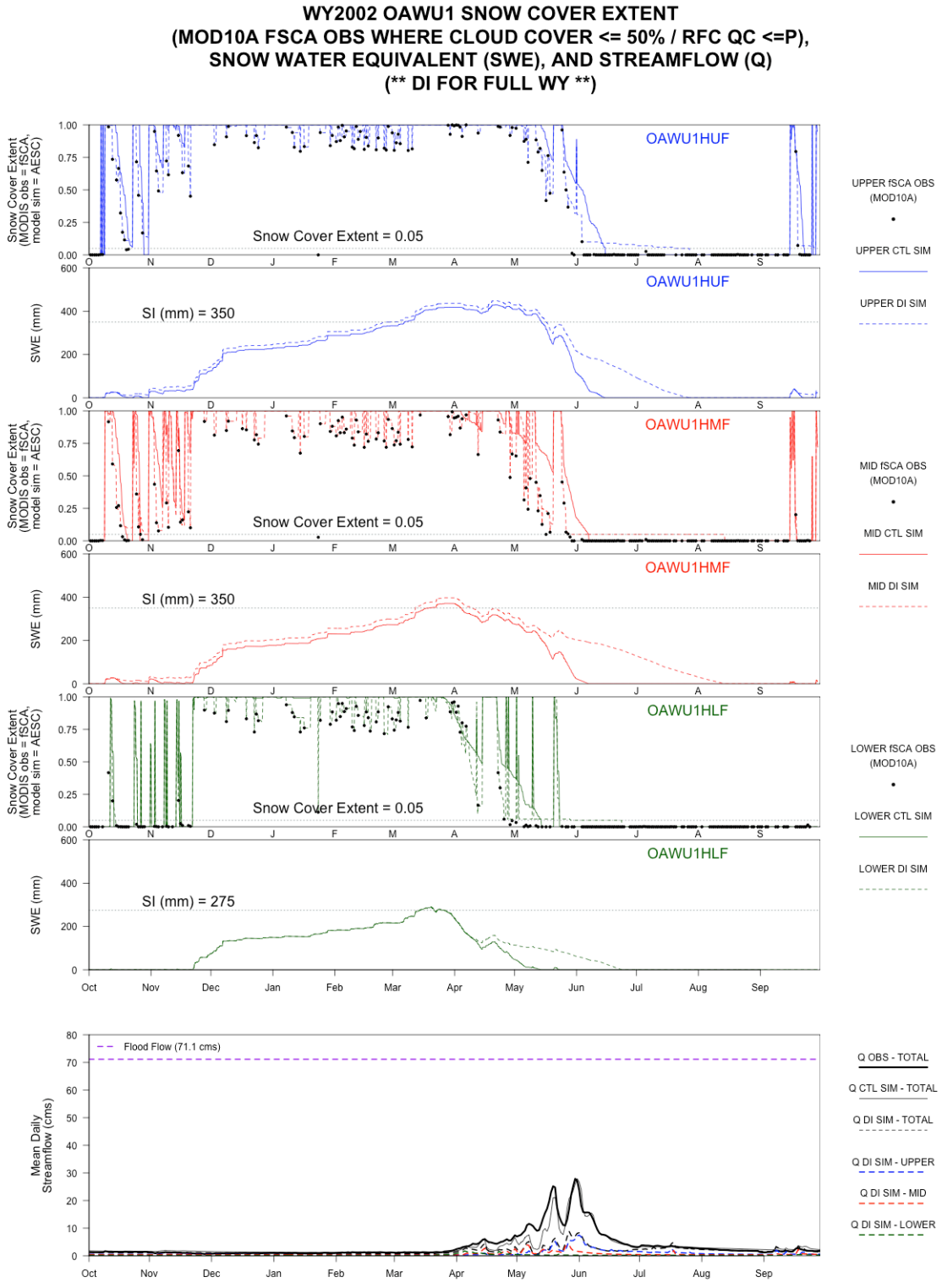

Figure 83: WY2002 CTL and MO1.WY snow cover extent, SWE, and streamflow simulations (DI using MODIS fSCA where cloud cover less than or equal to 50%)

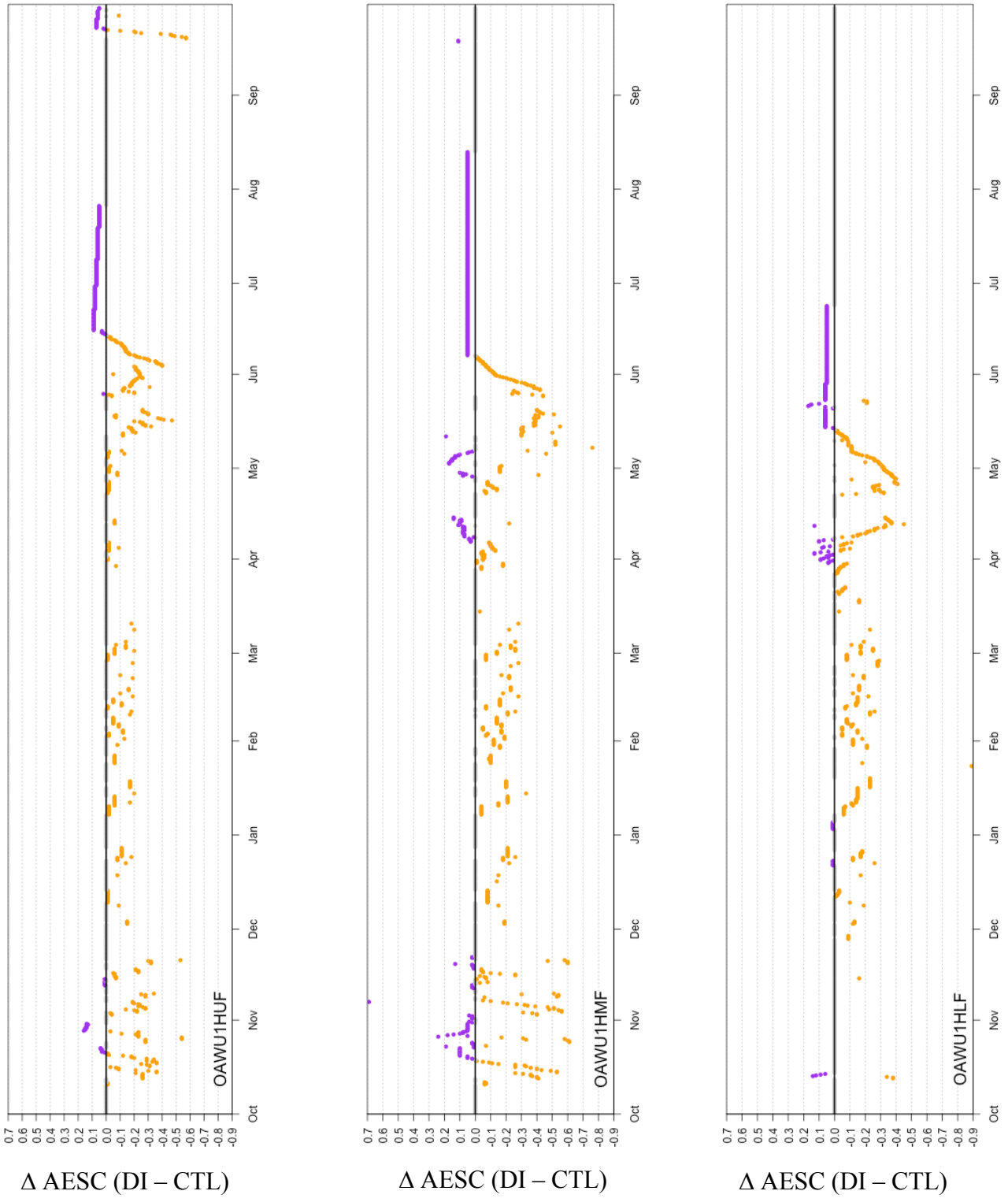

Figure 84: WY2002 OAWU1 fSCA differences (DI Sim – CTL Sim) for DI simulation MO1.WY

5.3.3 Impacts of MODIS fSCA Availability on Streamflow Predictions

While most of the DI simulations under predict streamflow with respect to both volumes and peak flow magnitude and timing, over prediction occurs occasionally. Over prediction occurs due to a combination of events: (1) when the simulated snowpack persists into the middle and late summer and (2) the MODIS-derived fSCA indicates snow cover depletion below a threshold of 5% earlier than normal. Two water years (WY2007 and WY2008) from the MO2.AJ simulation are used to illustrate an example.

The streamflow in June 2007 was over predicted by +104% by the MO2.AJ DI simulation. In contrast, the streamflow in June 2008 was under predicted to nearly the same degree (under prediction of -84%). Yet, WY2007 was a much drier year with a lower April – July runoff volume (88.36 MCM) than WY2008 (158.38 MCM).

The difference between the model performance for June streamflow between these two years is related to snowpack carryover in the middle to late summer and the timing of when the MODIS-derived fSCA values indicate snow cover depletion. In the MO2.AJ DI simulation, the simulated snowpack began to carryover in earnest during the summer of 2005 in both the upper and middle zones (Figs. 81 and 82). WY2007 was a dry year in the OAWU1 basin, but the simulated SWE in the upper and middle elevation zones, as predicted by the DI simulation, was nonzero for the entire 2007 water year due to carryover from WY2006. Because WY2007 was actually a dry year in terms of observed streamflow, the MODIS-derived fSCA values indicated that the snow cover depleted by ~June 1 in the upper elevation zone (Fig. 87, top subpanel) and by mid-May in the middle elevation zone (Fig. 87, third panel from the top). By these times, the

MODIS-derived fSCA values dropped below 5% and were ignored by SNOW17 in the simulations with active DI. From mid-May forward in the middle elevation zone and from early June forward in the upper elevation zone, SNOW17 modeled the snowpack *without influence of the MODIS-derived fSCA* observations. The SWE melt rates were no longer forcibly slowed by DI of the MODIS fSCA data.

In contrast, the MODIS-derived fSCA during WY2008 reached a threshold of 5% approximately a month later than in 2007 (Fig. 86). In WY2008, MODIS-derived fSCA data slowed the melt rate of the simulated SWE over a much longer time period, leading to lower simulated melt rates and streamflow in June of 2008, despite WY2008 being wetter overall than WY2007.

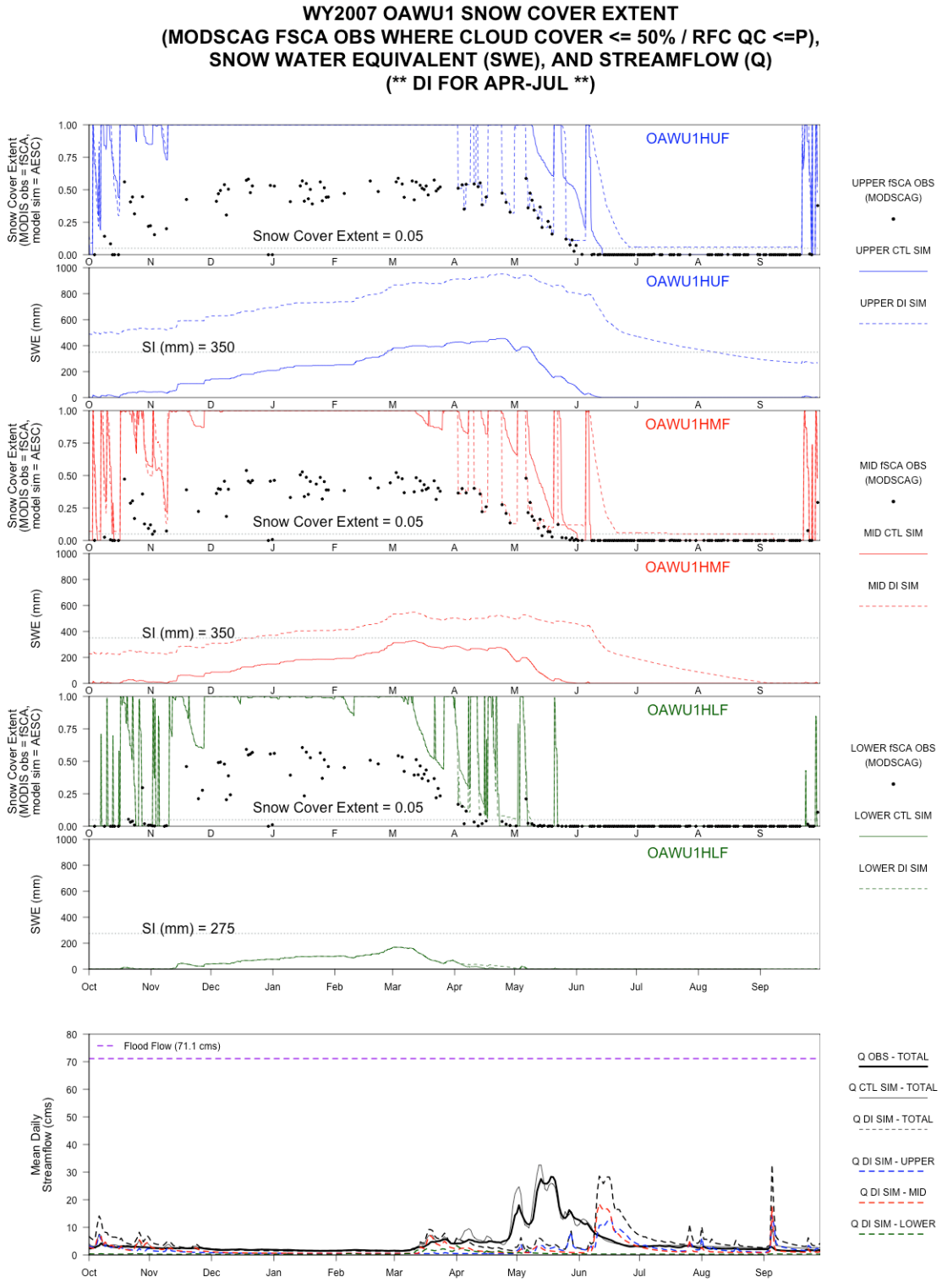

Figure 85: WY2007 CTL and MO2.AJ snow cover extent, SWE, and streamflow simulations (DI using MODIS fSCA where cloud cover less than or equal to 50%)

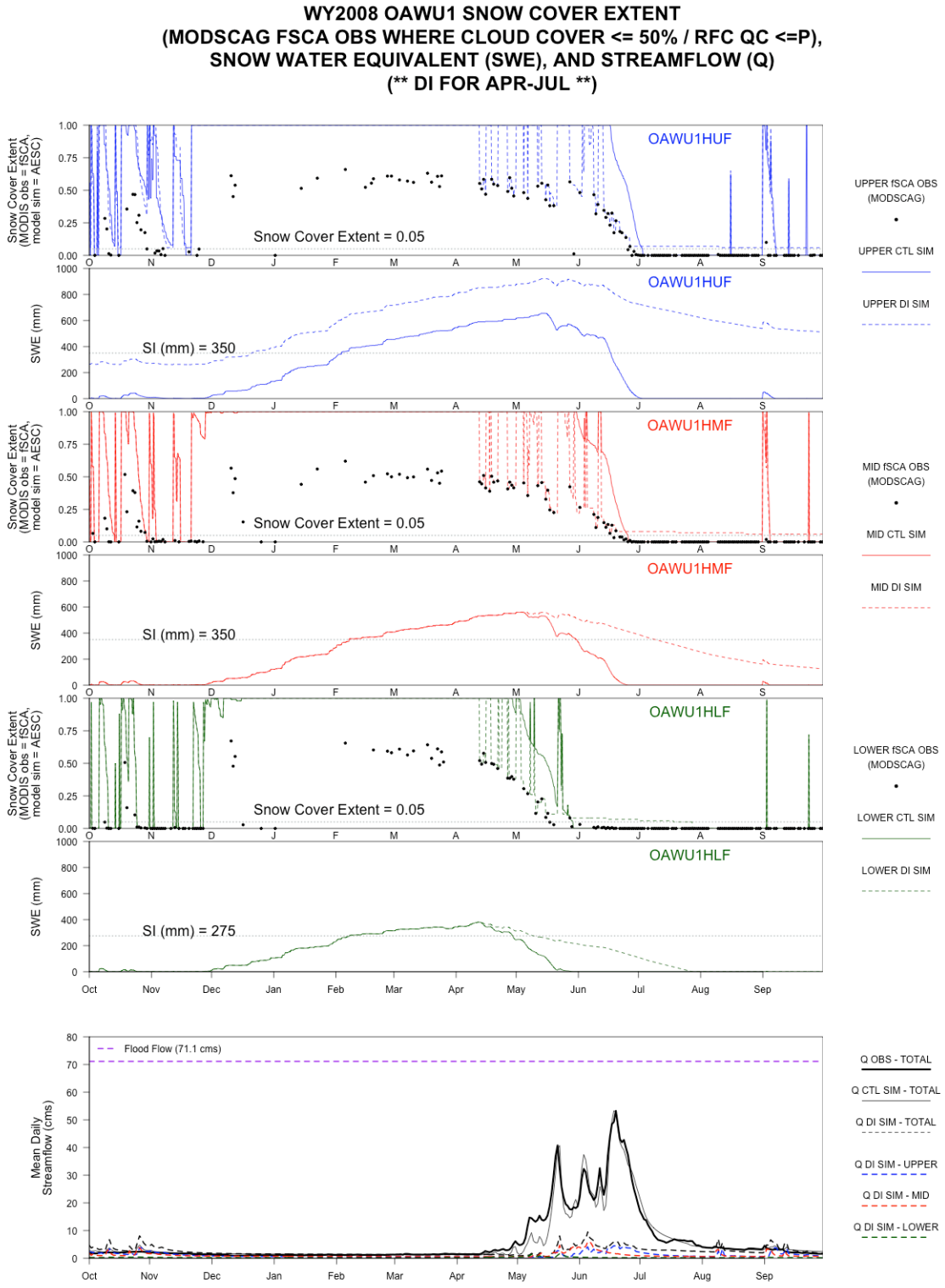

Figure 86: WY2008 CTL and MO2.AJ snow cover extent, SWE, and streamflow simulations (DI using MODIS fSCA where cloud cover less than or equal to 50%)

5.3.4 Apparent Lack of Mass Conservation

Throughout this report, many examples of under prediction of observed streamflow by the DI simulations have been shown. The poor performance of the DI simulations is a result of under prediction of peak flows as well as streamflow volumes.

The under prediction of streamflow volumes is partially explained by the reduced snowmelt rates apparent in the DI simulations (see Figs. 75-82). However, reduced snowmelt rates do not entirely explain the severe under prediction of the streamflow volumes. Even in years when the simulated snowpack completely depletes and the simulated SWE reaches zero before the end of the water year, the streamflow volumes are still under predicted. For example, in WY2001, the simulated snowpack was completely depleted during the summer of 2001 in all elevation zones in the CTL and in all of the DI simulations (Figs. 75-82). Yet, the streamflow volumes for the April – July period and the streamflow volume for the 2001 water year as a whole are still severely under predicted by the DI simulations. The streamflow volumes for the April – July runoff period are under predicted by 50 to 70% when compared to observations (Fig. 88) and for the full water year by 40 to 60%, depending on the DI simulation (Figs. 87-88).

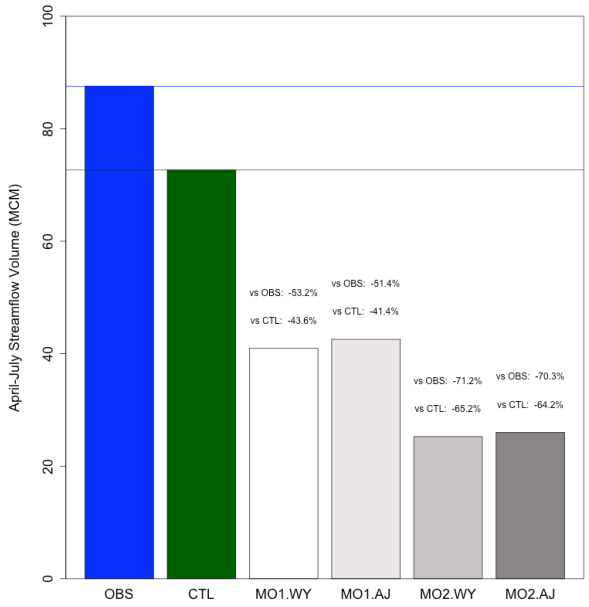

Figure 87: Observed and simulated streamflow volumes for the runoff period of April – July 2001. The percent difference in annual streamflow volume between the observed volume and the DI simulations and between the CTL simulation and the DI simulations is also shown.

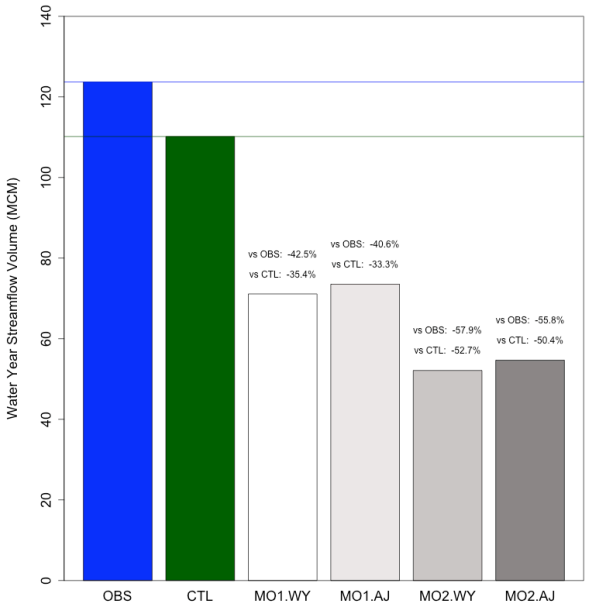

Figure 88: Observed and simulated annual streamflow volumes for WY2001. The percent difference in annual streamflow volume between the observed volume and the DI simulations and between the CTL simulation and the DI simulations is also shown.

The streamflow is also under predicted by the DI simulations in years when the maximum SWE is larger than the maximum SWE in the CTL simulation. In these cases, even though the peak SWE attained by the DI simulations is greater than the peak SWE of the CTL simulation, under prediction of the streamflow still occurs. An example of this case occurs in WY2007 in the MO1.AJ DI simulation, which is discussed below.

In WY2007, the simulated peak SWE in the MO1.AJ DI simulation is the same as in the CTL simulation for the upper and lower elevation zones, but larger than the peak SWE of the CTL simulation in the middle elevation zone, where the snowpack has carried over from the previous water year (Figs. 89-91). Because the middle elevation zone is the largest elevation zone by area in the OAWU1 basin (Table 12), and because a larger peak SWE occurs in the middle elevation zone in the DI simulation than in the CTL, larger streamflow volumes would be expected from the DI simulation than the CTL simulation. One might even expect *over* prediction of streamflow by the DI simulation in a case like this. Contrary to expected results, the DI simulation actually predicts less streamflow volume than the CTL simulation does for not only the runoff period of April-July (54% less than observed) but also for WY2007 as a whole (27% less) (Table 25).

The DI feature of SNOW17 is not used in the operational RFC environment to make official operational predictions, and it has rarely been used as part of an experiment conducted in-house by an RFC. The possibility of an undiagnosed software bug or an unaddressed minute detail of configuration that actually has a large impact on snow model outflow may be affecting the results of this study. The current schedule and IT

configuration at CBRFC prevents detailed troubleshooting of the source code, though the code should be examined in detail once resources are available.

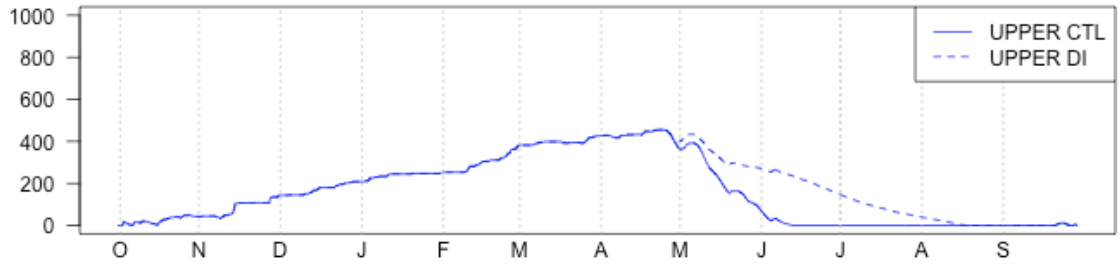

Figure 89: WY2007 CTL and MO1.AJ simulated SWE (mm) for OAWU1 upper elevation zone

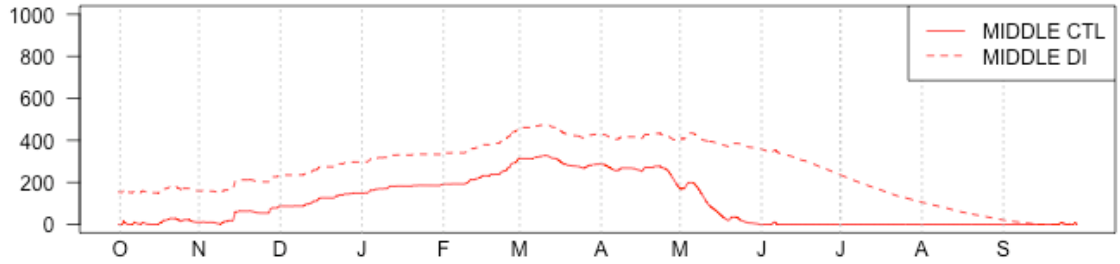

Figure 90: WY2007 CTL and MO1.AJ simulated SWE (mm) for OAWU1 middle elevation zone

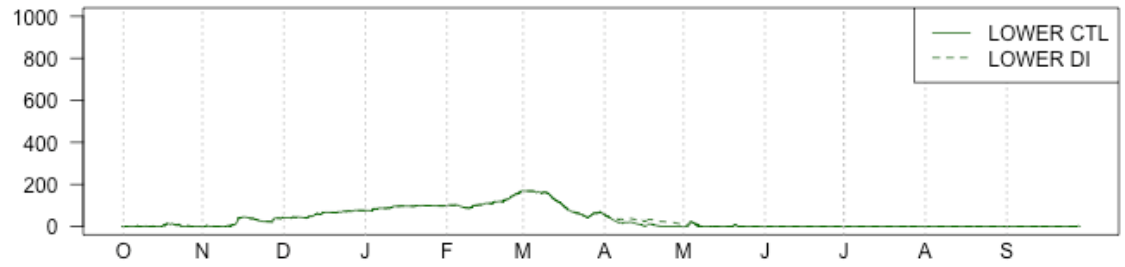

Figure 91: WY2007 CTL and MO1.AJ simulated SWE (mm) for OAWU1 lower elevation zone

Table 29: Comparison of multi-month streamflow volumes for WY2007

	April – July Streamflow Volume (MCM)	WY2007 Streamflow Volume (MCM)
Observed	88.3	135.4
CTL Simulation	94.5	153.2
MO1.AJ (DI simulation)	43.6 (-51% vs. obs, -54% vs. CTL)	112.6 (-17% vs. obs, -27% vs. CTL)

5.4 SUMMARY OF RESULTS

The results of this study found negative impacts on streamflow predictions when DI of observed fSCA is used. The negative impacts are particularly evident when DI simulations are compared to control simulations from a well-calibrated set of snow and soil moisture models.

The DI simulations are heavily impacted by the differences in MODIS-derived observed snow cover extent (fSCA) and modeled snow cover extent by SNOW17 (AESC). MODIS-derived fSCA is "viewable" snow cover extent; it represents what the sensor observes. This viewable extent may or may not agree with the model's meaning of AESC and its relationship to SWE through the depletion curve. Cloud cover affects the availability of MODIS-derived fSCA. In addition, on clear days when cloud cover is not a factor, vegetation impacts the MODIS fSCA retrieval depending on whether or not the vegetation is covered with fresh snow. In contrast, the AESC value represented within SNOW17 is not modeled with consideration of cloud cover or fresh snow (or lack of fresh snow) on vegetation.

SNOW17 uses snow cover extent as a multiplier on melt volume that is initially computed assuming 100% snow cover. The use of snow cover extent as a multiplier directly affects the amount of melt water that is routed through the snowpack and eventually made available to the soil moisture model. Because MODIS-derived fSCA observations are almost always less than the snow cover extent expected by SNOW17, direct insertion of the MODIS-derived fSCA results in a smaller volume of melt water being made available to other modules in the hydrologic modeling system. As a result, the streamflow predictions that use MODIS-derived fSCA via DI exhibit a negative bias compared to the streamflow predictions from the CTL simulation. SNOW17 does not adjust the model SWE state to be consistent with the inserted fSCA.

In its simplest configuration (no adjustment of MODIS data, no recalibration of snow model), use of MODIS-derived fSCA via DI degrades CBRFC streamflow predictions. Methods by which the degradation could be alleviated are discussed in section 6.3.

CHAPTER 6: CONCLUSIONS AND RECOMMENDATIONS

6.1 SUMMARY

While DI is an objective, quantitative way to use MODIS-derived fSCA observations in an operational hydrologic model, it does not improve streamflow predictions under the assumptions and conditions of this study. The streamflow predictions from the DI simulations are impacted by the initial assumption that MODIS-derived fSCA represents a value of snow cover extent that is similar to the snow cover extent as represented by SNOW17 (AESC). After investigation of and comparison of the simulations that are included in this study, as well as investigation of how SNOW17 uses snow cover extent, this initial assumption is incorrect. In most cases, the differences between MODIS-derived fSCA and SNOW17 AESC lead to negative impacts on the streamflow predictions. The experiment results show that DI without recalibration of model parameters, and without bias adjustment or transformation of MODIS-derived fSCA to an equivalent SNOW17 AESC value, is not a viable method by which MODIS-derived snow covered area observations can be quantitatively incorporated into SNOW17 and the NWS hydrologic modeling and streamflow forecasting systems.

In SNOW17, the snow cover extent value (AESC) is used as a multiplier on the melt volume computed assuming 100% snow cover. Essentially, AESC is used as way to control the melt volume within a single timestep, and in turn, the melt rate of the snowpack as the model moves forward in time. In this study, observed fSCA derived from MODIS is almost always less than what SNOW17 simulates; this lower value of

observed fSCA leads to slower melt of the snowpack when the observed (MODIS-derived) fSCA is used in SNOW17 via DI without any adjustments to either the MODIS-derived fSCA values or to the model configuration. The reduced snowmelt translates to reduced streamflow.

Although the areal depletion curve in SNOW17 is described as a relationship between SWE and snow cover extent, it was not developed from observations of snow cover, but rather as a set of parameters inferred in calibration. This inferred SWE-AESC function that was derived during the calibration process may need adjustment.

Even if observed fSCA was compatible with SNOW17's representation of snow cover extent, there are still uncertainties inherent in the observations that need to be addressed. Cloud cover is one of the major drawbacks of using MODIS-derived fSCA in hydrologic models. Methods of estimating fSCA for cloudy pixels vary; there is no one method that works well all of the time. Vegetation also impacts the fSCA retrievals from satellite-borne instrumentation. Adjusting viewable fSCA values for vegetation is another challenge. Studies that verify methods of canopy adjustment with ground observations are very limited at this time.

6.2 IMPLICATIONS OF THE RESULTS

As of June 2013, a way to quantitatively utilize MODIS-derived, observed fSCA on a routine basis in operations at NWS RFCs (including CBRFC) is lacking. DI is available to the RFCs as an option in the current operational system, but this study shows

that use of observed fSCA in SNOW17 via DI results in poor streamflow simulations when existing model parameters, calibrated to streamflow without snow cover observations, are used. The DI technique, at least without recalibration of SNOW17, and possibly SAC-SMA parameters as well, and/or adjustment of the MODIS fSCA data, is currently not a viable option for quantitatively updating SNOW17 snowpack conditions in NWS operations. Modifications to this study's methodology will be necessary if MODIS-derived fSCA observations are to be quantitatively utilized in operational streamflow forecasting and modeling systems within the NWS.

6.3 RECOMMENDATIONS FOR FUTURE RESEARCH

Results of this study show that the DI technique, when used with MODIS-derived fSCA that is unadjusted for vegetation and not transformed to a SNOW17 equivalent AESC, does not improve streamflow predictions. While the combination of the simple DI technique and MODIS-derived fSCA used as-is, with no adjustments, results in poor streamflow predictions, there are many methods by which the predictions could potentially be improved. Several proposals for future work related to modeling of snowmelt-driven flow are described below.

Lumped hydrologic modeling systems (including SNOW17 as the snow model) have been used operationally by the NWS for decades. While lumped models perform reasonably well under average or near average conditions of the historical period to which their parameters were calibrated, their performance is limited by the quality of the calibration, as well as the range of conditions within the historical calibration period.

Alternatives such as distributed hydrologic models and snow models that contain a more explicit representation of snowpack physics than SNOW17 are now commonly available. In mountainous basis with spatially varying topography and highly variable vegetation patterns, a distributed hydrologic model is likely to more accurately account for spatial variability in basin conditions, including radiant energy, temperature, and precipitation. A snow model that includes a more explicit representation of snowpack physics and relies less on tuned model parameters than SNOW17 does may also improve predictions of snowmelt-driven streamflow. To gain large improvements in prediction of snowmelt-driven streamflow, models that are more advanced than those currently used in NWS RFC operations are likely needed. The lumped approach of SNOW17 was appropriate and expedient for forecasting when observational data were scarce and computers slow; recent advances are eliminating these barriers.

As an intermediate step between the lumped models currently used in NWS hydrologic operations and a fully distributed hydrologic model, the relationships among snow cover extent, SWE distribution, and melt rate described by Liston (1999) could be used to transfer information from MODIS-derived fSCA to the snow model state variables (including SWE). An effort such as this would require further historical analysis of MODIS fSCA data and historical model patterns. Such an analysis would be useful in other capacities, such as analysis of uncertainty in the historical observations and model characteristics.

Data assimilation schemes beyond simple DI, schemes that consider uncertainties in the model, in the forcing data, and in the observations, and that are capable of propagating uncertainty information to other model states, could improve the streamflow

simulations. A more detailed study of relationships between errors in observed fSCA from MODIS and errors in SNOW17 simulated AESC could provide more complete information that would enable more sophisticated data assimilation techniques to be tested in the NWS operational hydrologic environment.

New data sets and improvements to existing data sets are always in progress. For example, NASA/GSFC is reprocessing the MODIS record into "Collection 6", which will include an improved fSCA data set (Riggs and Hall, 2012). The primary improvement in this new fSCA data set will be more accurate identification of clouds from snow. NASA/JPL is also in progress of reprocessing the MODIS record into a new version of MODSCAG with a new cloud identification algorithm; they are also generating a canopy-adjusted MODSCAG product. The canopy-adjusted products are expected to be closer to the AESC values that SNOW17 would expect and may prove more useful than the unadjusted MODIS-derived data sets used in this study. NASA/JPL's MODIS Dust Radiative Forcing in Snow (MODDRFS) product, which indicates how much energy is absorbed by and input to the snowpack due to impurities on the snow surface and reduced albedo, is an additional remotely sensed data set that may potentially inform hydrologic predictions.

In addition to the available alternatives described above, DI might still be pursued as the quantitative, objective method by which MODIS-derived fSCA is used in a lumped model. Additional statistics to describe the results of this study, such as the modified R, normalized root mean square error and standard error, should be computed in order to further diagnose data and model shortcomings. Also, differences between the MODIS-derived fSCA observations and AESC as the model expects would need to be resolved.

Development of a transformation (via regression, perhaps) between MODIS-derived fSCA and SNOW17 AESC could enable the MODIS-derived observations to be adjusted to a SNOW17 equivalent prior to being used in SNOW17 via DI.

The DI technique used in this study could be expanded to a rule-based scheme, where a small amount of SWE is added to or subtracted from the model, depending on the conditions indicated by the MODIS fSCA observations. This technique would be helpful only during times of the year when and in areas where fSCA drops below 100% and is changing.

The test basin could be recalibrated and a new set of SNOW17 parameters derived, either manually or with a numerical optimization program, using snow cover extent as a performance variable alone. The recalibration should initially focus on derivation of a new areal depletion curve after more detailed analysis of physiographic characteristics of the watershed, SWE patterns within the watershed, and fSCA patterns across the watershed. Recalibration work should also include using snow cover extent and streamflow jointly as performance variables to derive an additional set of SNOW17 parameters.

Because cloud cover heavily impacts the availability of MODIS data, studies of the sensitivity of predicted streamflow, as well as model parameters, to a variety of cloud cover thresholds would be helpful. When CBRFC processes gridded MODIS data into the mean areal fSCA across the elevation zones that the RFC models, the fraction of the area that is cloud-covered is also computed. These cloud cover fractions could be used in sensitivity tests that investigate the impact of variation in the cloud cover fraction on streamflow simulations.

The soil moisture model, SAC-SMA, was not recalibrated in any way for this study. SAC-SMA parameters from the CBRFC's most recent recalibration were used. The impacts on soil moisture states of this study are mostly unknown, though these impacts should be investigated. Determination of these impacts would augment the understanding of how DI of observed fSCA values impacts the overall modeling and forecasting systems at CBRFC, not just the simulated snowpack.

This study focused on one basin in northern Utah. Climate, snowpack characteristics, terrain characteristics, and latitude/solar radiation vary widely across the Colorado River Basin and the eastern Great Basin. The study could be expanded to additional watersheds in the western U.S. to gain a better understanding of the spatial variability of DI impacts on streamflow simulations.

These recommendations (particularly the expanded use of remote sensing science, the pursuit of distributed hydrologic modeling with energy-balance snow models, and data assimilation) are consistent with research directions and needs recognized by the CBRFC. Several initiatives within CBRFC and collaborative projects between CBRFC and its research partners, aimed at improving the CBRFC operational forecasting and modeling process specifically in the areas mentioned above, are already underway or will soon commence over the next several months of 2013. These efforts are expected to extend into the next three to five years and beyond.

WORKS CITED

Adams, R. M., L. L. Houston, and R. F. Weiher (2004). *The Value of Snow and Snow Information Services.* Chanhassen, MN: NOAA's National Operational Hydrological Remote Sensing Center.

Anderson, E.A. (2002). "Calibration of Conceptual Hydrologic Models for Use in River Forecasting." *NOAA Technical Report*, NWS 45. 372 pp.

Anderson, E.A. (2006). Snow Accumulation and Ablation Model – SNOW17. *NWSRFS User Manual, Chapter II.2.* 43 pp.

Armstrong, R. L. and E. Brun (2008). *Snow and Climate.* Cambridge University Press, New York. 222 pp.

CBRFC (2004). "Statistical Analysis of Two Time Series." Accessed 7/6/2012. http://www.cbrfc.noaa.gov/present/rdhm/STAT-Q_User_manual.pdf.

CBRFC (2010). "CBRFC Postmortem Analysis on June 2010 Flooding in UT and CO." Accessed 3/16/2011. http://www.cbrfc.noaa.gov/present/2010/jun10postmortem.pptx

COMET (2008). *Introduction to Verification of Hydrologic Forecasts*. Accessed 3/26/2012. https://www.meted.ucar.edu/training_module.php?id=486.

Committee on Earth Observation Satellites (CEOS) (2012). *The Earth Observation Handbook.* Accessed 10/08/2012. http://database.eohandbook.com/index.aspx.

Clark, M. P., A. G. Slater, A. P. Barrett, L. E. Hay, G. J. McCabe, B. Rajagopalan, and G. H. Leavesley (2006). "Assimilation of snow covered area information into hydrologic and land-surface models." *Advances in Water Resources*, 29: 1209-1221.

Demargne, J., M. Mullusky, K. Werner, T. Adams, S. Lindsey, N. Schwein, W. Marosi, and E. Welles (2009). "Application of Forecast Verification Science to Operational River Forecasting in the U.S. National Weather Service." *Bulletin of the American Meteorological Society,* 90:779-784.

Daly, S.F., R. Davis, E. Ochs, and T. Pangburn (2000). "An approach to spatially distributed snow modeling of the Sacramento and San Joaquin basins, California." *Hydrological Processes,* 14: 3257-3271.

DeWalle, D.R., and A. Rango (2008). *Principles of Snow Hydrology*. Cambridge University Press, New York. 410 pp.

Derksen, C., A. Walker, and B. Goodison (2003). "A comparison of 18 winter seasons of in situ and passive microwave-derived snow water equivalent estimates in Western Canada. *Remote Sensing of Environment*, 88: 271-282.

DigitalGlobe, Inc. (2006). *QuickBird Imagery Products: Product Guide, Revision 4.7.1*. Colorado: Longmont.

Dozier, J. (1989). "Spectral Signature of Alpine Snow Cover from the Landsat Thematic Mapper." *Remote Sensing of Environment,* 28:9-22.

Dozier, J. and J. Frew (2009). "Computational provenance in hydrologic science: a snow mapping example." *Philosophical Transactions of the Royal Society A*, 367: 1021-1033.

Dozier, J., T.H. Painter, K. Rittger, and J.E. Frew (2008). "Time-space continuity of daily maps of fractional snow cover and albedo from MODIS." *Advances in Water Resources,*31: 1515-1526.

Fletcher, S.J., G.E. Liston, C.A.Hiemestra, and S.D. Miller (2012). "Assimilating MODIS and AMSR-E Snow Observations in a Snow Evolution Model." *Journal of Hydrometeorology*, 13:1475-1492.

Franz, K.J., T.S. Hogue, and S. Sorooshian (2008). "Operational snow modeling: Addressing the challenges of an energy balance model for National Weather Service forecasts." *Journal of Hydrology*, 360: 48-66.

Franz, K.J., and L.R. Karsten, (2013). "Calibration of a distributed snow model using MODIS snow covered area data." *Journal of Hydrology.* Accepted manuscript.

Frankenstein, S., A. Sawyer, and J. Koeberle (2008). "Comparison of FASST and SNTHERM in Three Snow Accumulation Regimes." *Journal of Hydrometeorology,* 9: 1443-1463.

Fry, J., G. Xian, S. Jin, J. Dewitz, C. Homer, L. Yang, C. Barnes, N. Herold, and J. Wickham (2011). "Completion of the 2006 National Land Cover Database for the Conterminous United States", *Photographic Engineering and Remote Sensing*, 77(9): 858-864.

Gao, Y., H. Xie, N. Lu, T. Yao, and T. Liang (2010). "Toward advanced daily cloud-free snow cover and snow water equivalent products from Terra-Aqua MODIS and Aqua AMSR-E measurements." *Journal of Hydrology,* 385: 23-35.

Hall, D.K., G.A. Riggs, J.L. Foster, and S.V. Kumar (2010). "Development and evaluation of a cloud-gap-filled MODIS daily snow-cover product." *Remote Sensing of Environment*, 114: 496-503

He, M., T.S. Hogue, K.J. Franz, S.A. Margulis, and J. A. Vrugt (2011). "Corruption of parameter behaviour and regionalization by model and forcing data errors: A Bayesian example using the SNOW17 model." *Water Resources Research*, 47(7): 1-17.

Hock, R. (2003). "Temperature index melt modelling in mountain areas." *Journal of Hydrology,* 282: 104-115.

Klein, A. G., D. K. Hall, and G. A. Riggs (1998). "Improving snow cover mapping in forests through the use of a canopy reflectance model." *Hydrological Processes,* 12: 1723-1744.

Liston, G. (1999). "Interrelationships among Snow Distribution, Snowmelt, and Snow Cover Depletion: Implications for Atmospheric, Hydrologic, and Ecologic Modeling." *Journal of Applied Meteorology,* 38:1474-1487.

Liu, Y., A.H. Weerts, M. Clark, H.J. Hendricks Franssen, S. Kumar, H. Moradkhani, D.-J. Seo, D. Schwanenberg, P. Smith, A.I.J.M. van Dijk, N. van Velzen, M. He, H. Lee, S.J. Noh, O. Rakovec, P. and Restrepo (2012). "Advancing data assimilation in operational hydrologic forecasting: progresses, challenges, and emerging opportunities." *Hydrology and Earth System Sciences*, 16: 3863-3887.

McInerney, B., and C. Alvord (2007). "Assessing Water Supply Conditions for Utah." *Intermountain West Climate Summary (January 2007):* 23:24.

NASA (No Date). "MODIS Specifications." Accessed 7/19/2011. http://modis.gsfc.nasa.gov/about/specifications.php.

NASA (2011). "The Thematic Mapper". Accessed 8/7/2011. http://landsat.gsfc.nasa.gov/about/tm.html.

NASA (2011). "The Enhanced Thematic Mapper Plus". Accessed 8/7/2011. http://landsat.gsfc.nasa.gov/about/etm+.html.

NASA and USGS (2010). "The Landsat Data Continuity Mission." Accessed 7/19/2011. http://landsat.gsfc.nasa.gov/pdf_archive/20101119_LDCMbrochure.pdf

National Research Council. *Weather Services for the Nation: Becoming Second to None*. Washington, DC: The National Academies Press, 2012.

Nester, T., R. Kirnbauer, J. Parajka, and G. Blöschl (2012). "Evaluating the snow component of a flood forecasting model." *Hydrology Research*, 43.6: 762-779.

NWS (2004). "Initial Parameter Values for the HYDRO-17 Snow Model". Accessed 10/2/2012. http://www.nws.noaa.gov/oh/hrl/nwsrfs/users_manual/part4/_pdf/422snow17.pdf

NWS (2005). "HYDRO-17 Snow Model Operation.". Accessed 10/8/2012. http://www.nws.noaa.gov/oh/hrl/nwsrfs/users_manual/part5/_pdf/533snow17.pdf

NWS (2006). "National Weather Service River Forecast Verification Plan." Accessed 3/19/2012. http://www.nws.noaa.gov/oh/rfcdev/docs/Final_Verification_Report.pdf

National Weather Service/Office of Hydrologic Development (2012). "Fortran Codes for Research." Ver. 11/20/2012. Accessed 3/4/2013. ftp://hydrology.nws.noaa.gov/pub/CHPS/For_Software_Developers/fortranModels/FortranCodes4research.tar.gz.

Painter, T.H., K. Rittger, C. McKenzie, P. Slaughter, R. E. Davis, and J. Dozier (2009). "Retrieval of subpixel snow covered area, grain size, and albedo from MODIS." *Remote Sensing of Environment*,113: 868-879.

Painter, T. H., S. M. Skiles, J. S. Deems, A. C. Bryant, and C. C. Landry (2012). "Dust radiative forcing in snow of the Upper Colorado River Basin: 1. A 6 year record of energy balance, radiation, and dust concentrations." *Water Resources Research,* 48, W07521, doi:10.1029/2012WR011985.

Parajka, J. and G. Blöschl (2006). "Validation of snow cover images over Austria." *Hydrology and Earth System Sciences,* 10: 679-698.

Parajka, J. and G. Blöschl (2008). "The value of MODIS snow cover data in validating and calibrating conceptual hydrologic models." *Journal of Hydrology,* 358**:** 240-258.

Parajka, J., M. Pepe, A. Rampini, S. Rossi, and G. Blöschl (2010). "A regional snow-line method for estimating snow cover from MODIS during cloud cover." *Journal of Hydrology,* 381**:** 203-212.

Raleigh, M. S., K. Rittger, and J. D. Lundquist (2011). "What lies beneath? Comparing MODIS fractional snow covered area against ground-based observations under forest canopies and in meadows of the Sierra Nevada." Presented at the Western Snow Conference, Lake Tahoe/Stateline, Nevada, April 18-21, 2011.

Riggs, G., and D. Hall (2012). "Improved Snow Mapping Accuracy with Revised MODIS Snow Algorithm." Presented at the Eastern Snow Conference, Claryville, New York, June 5-7, 2012.

Riggs, G.A., D.K. Hall, and V.V. Salomonson (2006). *MODIS Snow Products User Guide to Collection 5.*

Rittger, K., T.H. Painter, and J. Dozier (2013). "Assessment of methods for mapping snow cover from MODIS." *Advances in Water Resources,* 51:367-380.

Riverside Technology, inc (RTi) (2011). "Using Snow Covered Area to Improve Snow Modeling and Water Supply Forecasts."

Rodell, M. and P.R. Houser (2004). "Updating a Land Surface Model with MODIS-Derived Snow Cover." *Journal of Hydrometeorology,* 5:1064-1075.

Salomonson, V.V. and I. Appel (2004). "Estimating fractional snow cover from MODIS using the normalized difference snow index." *Remote Sensing of Environment*, 89**:** 351-360.

Salomonson, V.V. and I. Appel (2006). "Development of the Aqua MODIS NDSI fractional snow cover algorithm and validation results." *IEEE Transactions on Geoscience and Remote Sensing,* 44(7): 1747-1756.

Serreze, M. C., M. P. Clark, R. L. Armstrong, D. A. McGinnis, and R. S. Pulwarty (1999). "Characteristics of the western United States snowpack from snowpack telemetry (SNOTEL) data." *Water Resources. Research,* 35(7): 2145–2160

Smith, M. B., D. P. Laurine, V. I. Koren, S. M. Reed, and Z. Zhang (2003). "Hydrologic Model calibration in the National Weather Service", in *Calibration of Watershed Models*, *Water Sci. Appl.*, vol. 6, edited by Q. Duan et al., pp. 133–152, AGU, Washington, D. C.

Tang, Q., and D.P. Lettenmaier (2010). "Use of satellite snow-cover data for streamflow prediction in the Feather River Basin, California." *International Journal of Remote Sensing,* 31: 3745-3762.

Turpin, O., R. Ferguson, and B. Johansson (1999). "Use of remote sensing to test and update simulated snow cover in hydrologic models." *Hydrological Processes,*13: 2067-2077.

Utah Division of Water Quality (2006). "Smith and Morehouse Reservoir." Accessed 5/27/2013. http://www.waterquality.utah.gov/watersheds/lakes/SMITHMOR.pdf.

Wilks, D. S. (1995). *Statistical Methods in the Atmospheric Sciences.* Academic Press Limited, London, UK. 467 pp.

Wood, A., and K. Werner (2011). "Development of a seasonal climate and streamflow forecasting testbed for the Colorado River Basin." Presented at the 36th NOAA Annual Climate Diagnostics and Prediction Workshop, Fort Worth, Texas, October 3-6, 2011.

Wright, R. (2011). "Reflectance spectroscopy: common Earth surface materials." Accessed 11/8/2011. http://www.higp.hawaii.edu/~wright/gg460_2011/lecture4.pdf.

Zhou, L. (2011). "Advances in Imagers from AVHRR to VIIRS." Presented at the Satellite Direct Readout Conference, Miami, Florida, April 4-8, 2011.

Zambrano-Bigiarin, M. (2013). "Goodness-of-fit functions for comparison of simulated and observed hydrological time series (hydroGOF)." Ver. 0.3-6. The Comprehensive R Network.